

ALMA MATER STUDIORUM
Universita' di Bologna

SCUOLA DI SCIENZE
DIPARTIMENTO DI FISICA ED ASTRONOMIA

LAUREA MAGISTRALE IN ASTROFISICA E COSMOLOGIA

Optical design of MAORY Laser Guide Star Objective

Relatore: Prof. Bruno Marano
Corelatore: Dott. Emiliano Diolaiti
Corelatore: Dott. Matteo Lombini
Corelatore: Dott. Mauro Patti

Laureanda: GIULIA SERENI

A.A. 2016 - 2017

To my family and love

Abstract

Without turbulence, a point size source would be imaged on the focal plane of the telescope as a sharp image with a dimension given by the diffraction limit, while for ground based observations a short exposure image is formed by many speckles having each the dimension of the diffraction limit images and evolving rapidly. On long exposure, the speckles pattern is blurred by the turbulence, producing a seeing disk. Hence the turbulence affects the angular resolution of images. Single Conjugate Adaptive optics, SCAO, is the simplest way to correct the atmospheric turbulence using a Natural Guide Star, NGS, but it has some limitations such as the anisoplanatism. Multi Conjugate Adaptive Optics, MCAO, is a technique which overcomes this issue by using as many NGSs, as Wavefront Sensors, WFSs. In order to increase the sky coverage, Laser Guide Stars, LGSs, are also used.

One of the first light instrument of the 40 meter European Extremely Large Telescope is MICADO, or the Multi-Adaptive Optics Imaging Camera for Deep Observations. It works with the post-focal MCAO relay, called MAORY, which uses six LGSs. A description of MAORY optical design is provided in this thesis. These LGSs suffer from aberrations and thus, after separating the light by a dichroic, an objective is designed to reduce these aberrations. In fact, since during sky tracking the zenith angle changes, the six LGSs launched at the Sodium layer vary their distances from the telescope primary mirror. As a consequence, the LGSs at different distances will focus on different positions along the optical axis. Through the procedure of optimization one can improve or modify the design in order to reduce or remove aberrations. Since no component can be perfectly manufactured and aligned, a tolerance analysis is important to ensure that the final, assembled instrument meets the requested performance.

All in all, the goal of this thesis is to optimize and perform the tolerance analysis for the LGS Objective of MAORY and show the results. The mechanical constraints and the variations of the aberrations with the zenith and azimuthal angle are taken into account. The number of optical surfaces has been minimized keeping the LGS Objective requirements satisfied. Moreover, the residual aberrations of the LGSs have been kept as small as possible in order to reach the performance requirements of MAORY. The software Zemax has been used for this purpose.

In detail, chapter one describes the AO and MCAO scheme, its main components, features and error sources. The second chapter explains the LGSs and the issues related to an AO or MCAO system using one or more LGSs. A brief introduction of the Seidel and Zernike aberrations, a guideline for optimization and tolerancing

is given in the third chapter. The fourth chapter deals with a description of MAORY optical design with its requirements, and the LGS Objective optical design with its interfaces. In the end, the results are reported in two sections: the aberrations analysis after optimizing the system and the tolerance analysis.

Sommario

Senza la presenza della turbolenza, l'immagine di una sorgente puntiforme che si forma sul piano focale del telescopio appare come un'immagine nitida e con una dimensione data dal limite di diffrazione. Invece per osservazioni da terra, un'immagine ottenuta a breve esposizione e' formata da molte macchioline (chiamate 'speckles'), ognuna avente la dimensione del limite di diffrazione dell'immagine. D'altra parte con esposizioni lunghe il campione di macchioline e' sfocato dalla turbolenza producendo cosi' un 'seeing disk'. Dunque la turbolenza influisce sulla risoluzione angolare delle immagini. Utilizzare le ottiche adattive come per esempio il 'Single Conjugated Adaptive Optics', SCAO, e' il modo piu' semplice per correggere la turbolenza atmosferica usando stelle guida naturali (Natural Guide Star, NGS), ma cio' comporta delle limitazioni tra cui l'anisoplanatismo. Diversamente, l'utilizzo di ottiche adattive multi coniugate (Multi Conjugated Adaptive Optics, MCAO) e' una tecnica che, usando tante NGSs quanti sensori di fronte d'onda (Wavefront Sensors, WFSs), supera questo problema. Inoltre per aumentare la copertura del cielo, vengono usate anche le stelle guida laser (Laser Guide Stars, LGSs).

Uno dei primi strumenti dell'European Extremely Large Telescope, il cui diametro e' di 40 metri, e' MICADO (Multi-Adaptive Optics Imaging Camera for Deep Observations). Questa camera lavora con MAORY (Multi conjugated Adaptive Optics RelaY) il quale utilizza sei LGSs per correggere la turbolenza atmosferica. Una descrizione del disegno ottico di MAORY viene fornita in questa tesi. Siccome queste LGSs soffrono di aberrazioni, e' stato progettato un obiettivo (chiamato 'LGS Objective of MAORY') per ridurre questi problemi. Infatti, durante il puntamento del cielo l'angolo zenitale cambia e dunque le sei LGSs lanciate verso lo strato di sodio variano la loro distanza dallo specchio primario del telescopio. Di conseguenza, le LGSs andranno a fuoco in differenti posizioni lungo l'asse ottico. Attraverso l'ottimizzazione del sistema ottico si puo' migliorare o modificare il progetto in modo da ridurre o rimuovere le aberrazioni. Dato che nessuna componente puo' essere perfettamente fabbricata ed allineata, e' importante fare un'analisi delle tolleranze per assicurarsi che lo strumento assemblato soddisfi la performance richiesta.

In sintesi, lo scopo di questa tesi e' di ottimizzare ed eseguire le analisi delle tolleranze per il 'LGS Objective of MAORY' e mostrarne i risultati. I vincoli meccanici e le variazioni delle aberrazioni con l'angolo zenitale e azimutale sono stati presi in considerazione; il numero di superfici ottiche e' stato minimizzato facendo in modo che i requisiti del 'LGS Objective of MAORY' siano soddisfatti; le aberrazioni residue delle LGSs sono state tenute piu' piccole possibili al fine di

raggiungere i requisiti di performance di MAORY; il software Zemax e' stato usato per questo scopo.

In dettaglio, il capitolo uno descrive l'ottica adattiva e multi coniugata, le loro principali caratteristiche e le sorgenti d'errore. Il secondo capitolo spiega le LGSs e i problemi legati all'ottica adattiva e multi coniugata usando una o piu' LGSs. Una breve introduzione delle aberrazioni di Seidel e Zernike, una guida per fare l'ottimizzazione e le tolleranze viene data nel terzo capitolo. Il quarto capitolo tratta di una descrizione del progetto ottico di MAORY, del 'LGS Objective of MAORY' e dei loro requisiti. Per ultimo vengono riportati i risultati in due sezioni: l'analisi delle aberrazioni dopo l'ottimizzazione del sistema e l'analisi delle tolleranze.

Acronyms

AO Adaptive Optics

BS Beam Splitter

DM Deformable Mirror

DOF Degree Of Freedom

E-ELT European Extremely Large Telescope

FoV Field of View

FWHM Full Width at Half Maximum

GS Guide Star

IR InfraRed

LA Lenslet Array

LGS Laser Guide Star

LOR Low Order and Reference

MAORY Multi conjugated Adaptive Optics Relay

MCAO Multi Conjugated Adaptive Optics

MICADO Muti-AO Imaging Camera for Deep Observations

NCPA Non-Common Path Aberration

NIR Near InfraRed

NGS Natural Guide Star

OPD Optical Path Difference

PDR Preliminary Design Review

PSF Point Spread Function

RON Read Out Noise

RTC Real Time Computer

RMS Root Mean Square

RSS Root Sum Square

SCAO Single Conjugated Adaptive Optics

SHWFS Shack-Hartmann Wavefront Sensor

S/N Signal to Noise

TBC To Be Confirmed

TT Tip Tilt

WF WaveFront

WFE WaveFront Error

WFS WaveFront Sensor

Contents

| | | |
|----------|---|-----------|
| 1 | Adaptive optics | 1 |
| 1.1 | Atmospheric wavefront distortion | 1 |
| 1.2 | AO scheme | 3 |
| 1.3 | Anisoplanatism | 5 |
| 1.4 | Strehl ratio | 6 |
| 1.5 | The coherence time | 8 |
| 1.6 | Wavefront corrector | 8 |
| 1.7 | Wavefront sensor | 10 |
| 1.8 | The MCAO concept | 12 |
| 1.9 | Error sources in AO | 13 |
| 2 | Laser guide stars | 16 |
| 2.1 | LSG issues | 18 |
| 2.1.1 | Fratricide effect | 18 |
| 2.1.2 | TT indetermination | 19 |
| 2.1.3 | Cone effect | 19 |
| 2.1.4 | LGS launching effect | 20 |
| 2.1.5 | Zenith angle effect | 21 |
| 2.1.6 | Perspective elongation | 21 |
| 2.1.7 | Sodium layer variability | 23 |
| 3 | How to optimize and tolerance | 25 |
| 3.1 | Seidel aberration | 25 |
| 3.1.1 | Spherical aberration | 26 |
| 3.1.2 | Coma | 28 |
| 3.1.3 | Astigmatism | 29 |
| 3.1.4 | Distortion | 30 |
| 3.1.5 | Spot diagrams | 31 |
| 3.2 | Zernike aberrations | 31 |
| 3.3 | Optimizing optical systems | 35 |
| 3.3.1 | Local minima: the damped least squares and Hammer algorithm | 35 |

| | | |
|----------|---|-----------|
| 3.3.2 | Optimizing: the last step | 36 |
| 3.3.3 | Analysis methods | 36 |
| 3.4 | Tolerancing optical system | 38 |
| 3.4.1 | Element tolerance | 39 |
| 3.4.2 | Sensitivity analysis | 41 |
| 3.4.3 | Monte Carlo simulation | 42 |
| 4 | MAORY | 43 |
| 4.1 | E-ELT | 43 |
| 4.2 | MAORY and its issues | 44 |
| 4.2.1 | MAORY requirements | 46 |
| 4.2.2 | MAORY post-focal relay optical design | 46 |
| 4.3 | The LGS Objective | 47 |
| 4.3.1 | Client requirements for the LGS Objective | 49 |
| 4.4 | LGS WFS | 50 |
| 4.4.1 | Sodium layer features and spot truncation: impact on MAORY performance | 51 |
| 5 | LGS Objective design | 52 |
| 5.1 | The LGS Objective optical design | 54 |
| 5.2 | Optimization | 55 |
| 5.3 | Aberrations analysis | 56 |
| 5.3.1 | Aberrations after the LGS Dichroic | 57 |
| 5.3.2 | Aberrations on the image plane | 62 |
| 5.3.3 | Distortion | 67 |
| 5.4 | Tolerance analysis | 71 |
| 6 | Results | 76 |
| 6.1 | Performance | 76 |
| 6.2 | Tolerance analysis | 79 |
| | APPENDICES | 84 |
| | A Worst Offenders | 85 |
| | Bibliography | i |

Chapter 1

Adaptive optics

Long telescope may cause Objects to appear brighter and larger than short ones can do, but they cannot be so formed as to take away that confusion of Rays which arises from the Tremors of the Atmosphere. The only Remedy is a most serene and quiet Air, such as may perhaps be found on the top of the highest Mountains above the grosser Clouds.

-Isaac Newton, Opticks, 1704

1.1 Atmospheric wavefront distortion

On the surface of the Earth, the turbulence, which causes dynamic density variations in the atmosphere, limits the resolving power of the telescopes. This loss of resolution is termed *seeing* and is measured as the angular FWHM of the image of a point source. In fact the index of refraction of air depends on its density. The solar heating drives convective cells in the lowest layer of the atmosphere, a region about 10 – 12 km thick called troposphere. Many cells are established, and the air tends to break up into ever smaller eddies and lumps of different density (i.e. temperature). This break-up of the flow is called *turbulence*. Therefore a plane WF passing through the Earth's turbulent atmosphere will be distorted. The statistical properties of turbulence were proposed by Kolmogorov (Tatarski, 1961).

Figure 1.1 shows how seeing affects an Earth-bound telescopes image in two different cases: short and long exposures.

- *On short exposures* turbulence moves the lumps of air around at high velocity so a particular speckle pattern has only a momentary existence, to be quickly replaced by a different pattern. In practice, one can 'freeze' the speckle pattern on very short exposures (below about 1/20 second). The number of speckles

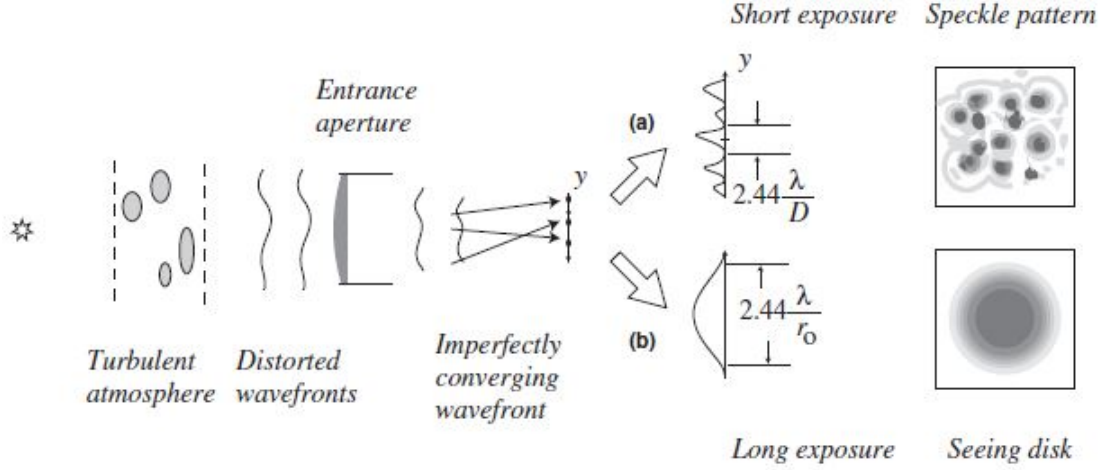


Figure 1.1: Astronomical seeing: image formation by a telescope in a turbulent atmosphere. (a) In a short exposure, WF distortions caused by variations in refractive index in the atmosphere produce interfering Airy patterns. In (b) turbulent motion in the atmosphere during a long exposure moves the individual maxima around the image plane to produce a large seeing disk.

in a single exposure depends on the typical diameter of an atmospheric lump, r_0 , also called turbulence coherence length (see Equation 1.2). It is approximately equal to $(D_{tel}/r_0)^2$ where D_{tel} is the telescope diameter. Each speckle has a dimension comparable to that of the diffraction-limited core (see Equation 1.4).

- *On long exposures*, the speckle pattern is blurred by turbulence, producing a seeing disk with diameter of:

$$\theta_{seeing}[rad] \simeq 2.44 \frac{\lambda}{r_{0,\lambda}} \quad (1.1)$$

A method for quantifying the WF distortion is the zeroth moment of turbulence, which is usually given in terms of the *Fried parameter*, $r_{0,\lambda}$, defined as:

$$r_{0,\lambda} = \left(0.423 \left(\frac{\lambda}{2\pi n} \right)^{-2} \sec \xi \int_0^\infty C_n^2(z) dz \right)^{-3/5} \quad (1.2)$$

Here C_n is the turbulence profile which determines the strength of the turbulence at different altitudes z (Figure 1.2), ξ is the zenith angle, that is the angle between the direction observed and the zenith. The Fried parameter is the scale length over which the RMS optical phase distortion σ_φ is 1 rad^2 , that is to say, it is usually

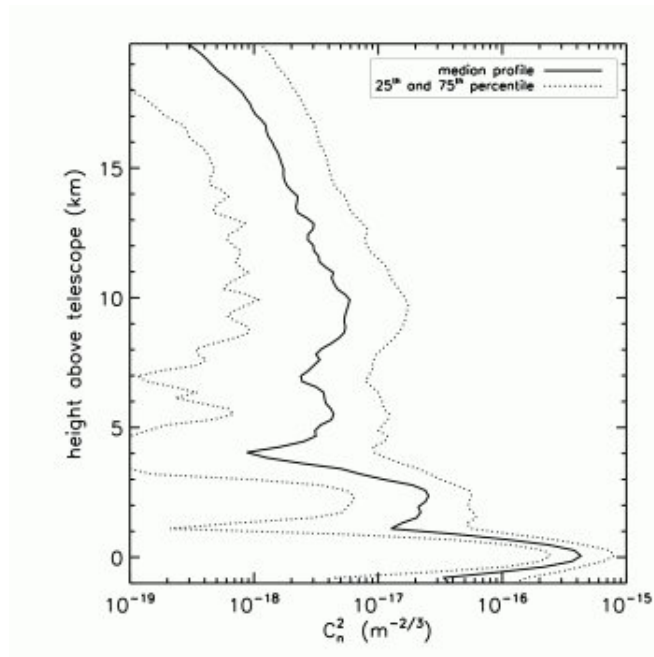


Figure 1.2: A C_n^2 profile shows the amount of air turbulences over height above the ground telescope in Mt. Graham. The strongest turbulences are close to the ground. (Figure by E. Masciadri, INAF)

used to describe the characteristic spatial extent of the WF aberrations. If this quantity becomes less than one square radian or, in other words, if this quantity becomes greater than $\lambda/2\pi\sigma_\varphi$ (about 1/6 of a wavelength), then the 2D patch of the front is no longer coherent.

By convention, if the diameter of the telescope is similar to $r_{0,\lambda}$, a Strehl ratio of about 40% is get (see Section 1.4). Whereas if the diameter is less than $r_{0,\lambda}$, a minor SR, that is a worse SR is obtained. Hence the Fried parameter can be seen as a good indicator of image quality.

In conclusion, advanced techniques called AO can correct WF distortions and sharpen blurred images on both short and long exposures.

1.2 AO scheme

AO corrects in real time, specifically at the timescale given by the coherence time (see Section 1.5), for the atmospheric turbulence which affects the spatial resolution of the astronomical images obtained by ground based telescopes. With such a system the resolution is set by the telescope aperture and an higher Strehl ratio (see Section 1.4) is achieved. The typical wavelength band observed is the

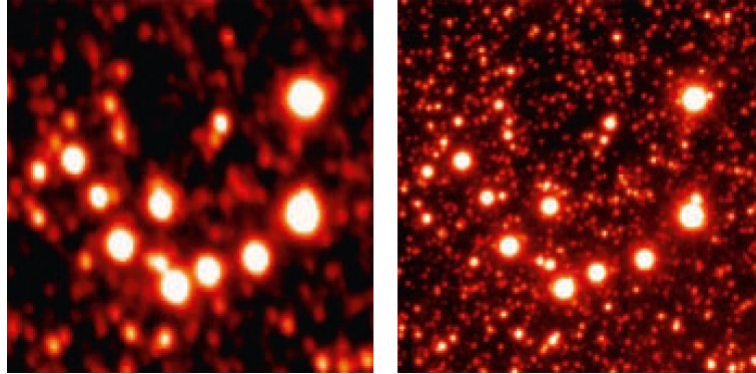


Figure 1.3: 20×20 arcseconds region nearby the centre of the globular cluster Omega Centauri. The image on the left was obtained in K-band by ISAAC and has an average FWHM of 0.6 arcseconds. The right-hand image was obtained at the same wavelength by MAD with MCAO correction. In the latter case the FWHM is often below 0.1 arcsecond, a remarkable value taking into account that the closest GS is $\simeq 1$ arcmin away.

NIR where it is easier to track the turbulence variation and the coherence time is greater with respect to shorter wavelength. The difference between an image obtained with and without AO is shown in Figure 1.3: it is evident that with AO a better resolution is reached.

The main components of an AO system are:

- a *Deformable Mirror*, DM
- a *Dichroic*
- a *WaveFront Sensor*, WFS
- a *Real Time Computer*, RTC

They will be explained in the following sections. In figure 1.4 a schematic view of the optical layout of an AO system is presented: the distorted beam of a GS (see Chapter 2) coming from the telescope is collimated onto a DM placed on the pupil plane image. The light is folded by the DM toward the dichroic where the shorter wavelength light is directed to the WFS while the longer wavelength beam is imaged by the scientific detector. The WFS measures the shape of the WF so that the RTC can compute the correction to be applied to the incoming beam by means of the DM. The AO system so described operates in closed loop, it means that the WFS measures the residual WF after the correction of the previous

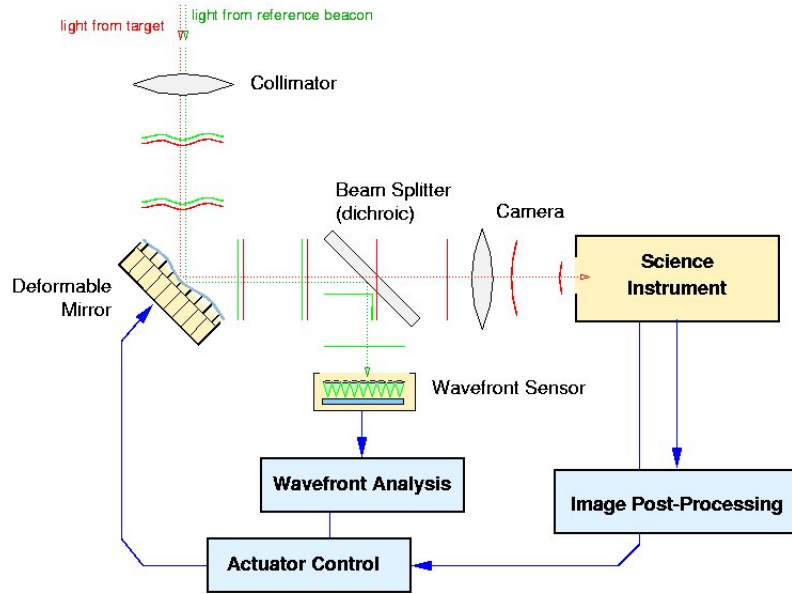


Figure 1.4: A schematic of a practical AO system.

cycle, whereas in an open loop the aberrated WF is detected in its raw state before reflecting off the DM.

In more detail a DM can be of several types, but all must have surface whose shape can quickly change to compensate for the sensed WF distortions. An example is a segmented mirror made up of many independent flat reflectors. The DM has to update its shape several hundred times in a second. During operation, the AO system senses the WF distortion, then very quickly positions each of the segments to null out the pathlength errors in each portion of the WF. Each hexagonal segment is a low-mass mirror that can execute three types of motion: piston, tip and tilt. The number of segments needed in a DM depends on the coherence length of the WF and it is proportional to D_{tel}/r_0^2 .

1.3 Anisoplanatism

In the single conjugated AO systems the FoV is very limited, typically a few arcseconds for images obtained at IR wavelengths. This limitation arises from the fact that the distorted WF is estimated by the WFS only in the direction of a sufficiently bright GS located near the observed astronomical object, and is corrected for this same direction by a DM. The direct consequence is that the images of the astronomical objects far from the GS are only partially corrected. This

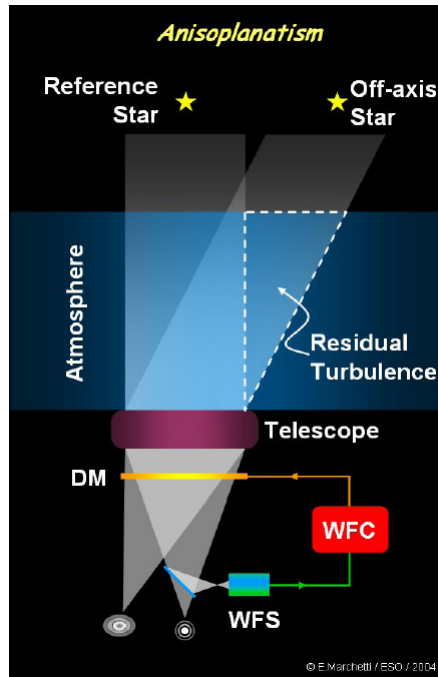


Figure 1.5: Anisoplanatism effect leading to a degradation of the correction.

phenomenon is called *atmospheric anisoplanatism* and a graphical representation is given in figure 1.5. This effect gets more important as the angular distance between science target and guide source increases. The degradation of the correction is due to the fact that the cylinder of atmosphere seen and measured by the WFS doesn't match perfectly the cylinder of atmosphere through which the science target beam propagates.

Therefore it is appropriate to introduce the definition of the *isoplanatic angle*, θ_0 , which is the largest angle for which the expected distortions differ by less than 1 rad^2 :

$$\theta_0[\text{rad}] = 0.314 \frac{r_0 \lambda \cos \xi}{\bar{h}} \quad (1.3)$$

Since turbulence generally occurs at different heights, \bar{h} represents a weighted mean height.

1.4 Strehl ratio

Because of diffraction from the system stop, an aberration-free optical system does not image a point to a point. An *Airy disk* is produced having a bright

central core surrounded by diffraction rings. The angular diameter of the Airy disk (diameter to the first zero) containing 84% of the light is:

$$\Theta_{Airy}[rad] = 2.44 \frac{\lambda}{D_{tel}} \quad (1.4)$$

The Rayleigh resolution criterion states that two point objects can be resolved if the peak of one falls on the first zero of the other. The angular resolution of such a system is given by:

$$R[rad] = 1.22 \frac{\lambda f_{\#}}{f} \quad (1.5)$$

where f is the focal length of the system and $f_{\#}$ is the so called *f-number* defined by f/D_{tel} . Rayleighs criterion is a good predictor of the performance of space telescopes.

However, with ground-based telescopes we must deal with seeing which limits the resolving power. When turbulence is compensated by AO, part of the energy is transferred from the seeing disk or halo to the central core of the image, which starts to appear when the residual WFE, σ_W , (see Section 1.9) has been reduced to about 2 rad RMS. The process of WF compensation alters the shape of the image intensity distribution, but does not significantly change their respective diameters. Therefore a better measure of the performance of an AO system is the *Strehl ratio*, SR. It is defined as the ratio of the peak intensity of an aberrated image profile of a point source I_{PSF} to the peak intensity of a perfect diffraction-limited image I_{Airy} for the same optical system:

$$SR = \frac{I_{PSF}}{I_{Airy}} \quad (1.6)$$

Therefore it can be used to assess the image quality of any image. The best image is obtained when $SR = 1$, while a lower value corresponds to worse images because of the Earth's atmosphere, optical aberrations, mechanical misalignments and vibrations. For $\sigma \leq 2 \text{ rad}$, the Strehl ratio is closely approximated by:

$$SR \simeq e^{-\sigma^2} \quad (1.7)$$

The equation 1.7 is known as the Maréchal formula, where σ^2 is the mean-square WFE (the variance) expressed in rad. In order to transform the mean-square WFE expressed in unit of λ to unit of radians, one can use the following equation:

$$\sigma_{\varphi}[rad] = \frac{2\pi}{\lambda} (\sigma_W[\lambda]) \quad (1.8)$$

The minimum σ_φ , which is considered the best one, corresponds to about $\lambda/14$, that is $\pi/7$. In conclusion, by using equation 1.7, the minimum acceptable value for the SR is 0.8 meaning that the system is well enough corrected only if SR has a value greater than 0.8.

1.5 The coherence time

The maximum delay between sensing the WF and adjusting the DM that can be tolerated is called the *coherence time* (or Greenwood time delay), τ_0 :

$$\tau_0 = 0.057 \left(\lambda^{-2} \text{sec} \xi \int C_n^2(z) v(z)^{5/3} dz \right)^{-3/5} \quad (1.9)$$

where $v(z)$ is the velocity of turbulence layer depending on altitude z . In a quantitative way, equation 1.9 describes the time after which the changes in the WF aberrations amount to 1 rad^2 . For typical values of the parameters, the Greenwood time delay is several milliseconds. The wavelength dependence of τ_0 is one reason why AO is easier at longer wavelengths: τ_0 is longer in the IR than in the optical. Moreover since exposure time for the WFS (see Section 1.7) must be less than the Greenwood time, the GS (see Chapter 2) must be bright.

1.6 Wavefront corrector

The E-ELT M4 adaptive unit is a fundamental part of the E-ELT: it provides the AO correction that compensates the WF distortion induced by atmospheric turbulence and partially corrects the structural deformations caused by wind.

The unit is based on the contactless, voice-coil technology and a schematic view is shown in figure 1.6 (R.Biasi and D.Gallieni). It features a 2.4 m diameter flat mirror, controlled by 5910 actuators and divided in six segments. The reference body, which defines a reference surface for the back of the thin shell, is a thick optical piece, lightweighted, with hole patterns to allow the passage of the 5910 voice coil actuators. These are mounted on the cold plate and apply forces on 1170 corresponding magnets glued on the back face of the thin shell. Being the actuators contactless, only magnetic forces are transferred to the mirror. The voice-coil based, contactless adaptive mirror has been conceived by Piero Salinari in 1993 (P.Salinari, C. Del Vecchio and V.Biliotti).

Since we are employing force motors, but ultimately the actuators have to be commanded in position, we need a measurement of the shell position, co-located with the actuator. Metallic coatings on the shell back face and the front face of the reference body act as capacitive sensors used to measure the gap between the

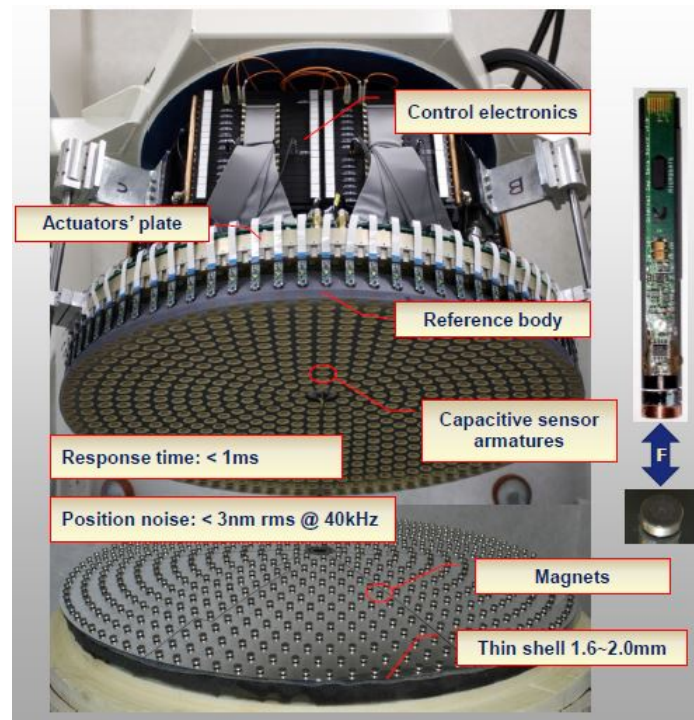


Figure 1.6: Contactless DM.

thin shell and the massive and stiff reference body.

The description of some particularly challenging performance requirement for the M4 unit are listed below:

- The AO temporal error verification through simulation to assess the system performance in terms of residual WFE: for instance the M4 must guarantee static and dynamic performance in the correction of optical aberrations.
- The E-ELT M4 long-term stability. This is one of the most challenging aspects of the project, which mainly affects the capacitive sensor design.
- The position of the M4 unit in the telescope induces stringent requirements in term of thermal uniformity and cooling reliability. Any temperature gradient at the level of the intermediate focal plane creates some aberrations on the optical path. The risk of liquid leakage on M1, M5 or M3 (see Section 4.1) must be avoided. Therefore a new cooling design has been developed, where the concept was to substitute the glycol with a liquefied gas.

1.7 Wavefront sensor

In general, the basic principle of an AO system is to reconstruct the WF once the WFS has measured the WF distortions which has to be applied to the DM.

The most widespread sensor is the *Shack-Hartmann sensor* which is the baseline WFS for MAORY (see Chapter 4). It is placed on a pupil plane, so it measures the same WF arriving to the telescope aperture, but degraded by the aberrations produced by the optics. These non-common path aberration, NCPA, between the imaging and WF sensing channel, are calibrated apart and then these corrections are applied before compensating for the atmosphere. The SHWFS is an array of square or hexagonal lenses followed by the detector in the focal plane of the lenses as shown in figure 1.7:

- In the upper sketch a perfect plane propagates through the LA, which separates the rays from each segment of the WF into isolated bundles, called *sub-apertures*, each of which is brought to a different focus on a detector array. In this case all images are located in a regular grid defined by the LA geometry.
- In the lower figure the WF is distorted. The distortion causes local changes in the WF slope and corresponding changes in directions of the rays. Each bundle of rays now comes to a focus displaced from their nominal positions and the shifts of the image centroids in two orthogonal directions are proportional to the local average WF slopes over the sub-apertures. At the end, in order to reconstruct the original WF (not distorted by atmosphere) the computer must convert the array of slopes for each sub-aperture into the actual shape of the distorted WF. For a large number of sub-apertures, this requires a very fast computer, since adaptive corrections must be made within τ_0 .

The performance of the Shack-Hartmann sensor depends on how well the displacement of the spot is estimated. The *dimension of the spot*, d , on a distinct region of pixels coming from a single lenslet is given by:

$$d = \frac{f_l \lambda}{D_l} \quad (1.10)$$

where f_l and D_l are the focal length and the diameter of a single lenslet (the sub-aperture size) respectively. The *resolution of SHWFS* is equal to D_l and, so, depends on the number of the sub-apertures. Moreover, the sub-aperture size is proportional to the turbulence coherence length r_0 of the observing wavelength in the science channel and it does not depend on the telescope diameter:

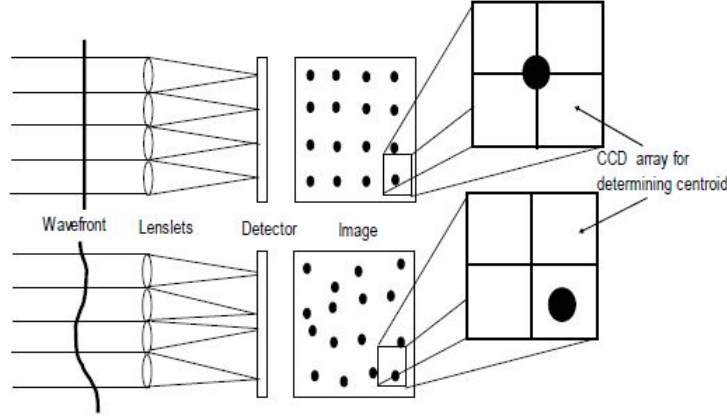


Figure 1.7: The Shack Hartmann sensor.

$$R_{SHWFS} = D_l \propto r_0 \quad (1.11)$$

Coming back to the performance of SHWFS, one of the approach to estimate the displacements of the image centroid, is the Centre of Gravity (CoG) approach. The slopes x and y are so calculated:

$$x = \frac{\sum_{i,j} x_{i,j} I_{i,j}}{\sum_{i,j} I_{i,j}} \quad (1.12)$$

$$y = \frac{\sum_{i,j} y_{i,j} I_{i,j}}{\sum_{i,j} I_{i,j}} \quad (1.13)$$

where $I_{i,j}$ are the intensities of light on the detector pixels. It is assumed that x , y coordinates are expressed in radians. This is the optimal estimator for the case where the spot is Gaussian distributed and the noise is Poisson. It has some limitations when using a real spot (diffraction or seeing limited) and in presence of RON.

Rousset (1999) shows that for a Gaussian spot, the RON contributions to phase variance, σ_φ^2 is proportional to N_s^4 , that is the total number of pixels used in the CoG calculation. So the RON contribution can be decreased by using the smallest number of pixels N_s^2 possible in the CoG calculation. This leads to the quad cell (QC) method, which is another estimator of spot positions. The QC is the specific case of the CoG for a 2×2 pixels array ($N_s^2 = 4$). In this case, the FoV is given by the pixel size and by definition the spot is undersampled. QC is widely used in astronomical AO systems because the weak signal from GSs is better detected against RON and because, with a small number of pixels, the RON can be further

reduced by a slow CCD readout. A QC algorithm calculates the centroid x_{QC} in each direction:

$$x_{QC} = \pi\gamma \frac{I_l - I_r}{I_l + I_r} \quad (1.14)$$

where I_l and I_r are the intensities, respectively, on the left and the right halves of the detector and γ is the coefficient, given in pixels, translating intensity ratio into displacement, depending on the spot shape and size.

Nowadays, detectors in SHWFS can be photon-noise limited. In that case, the error variance of QC is 1.57 times greater than that of the simple CoG. In conclusion, using QC centroiding is only efficient for a noisy detector under low-flux conditions. For accurate WF measurement and photon-noise limited detectors other CoG methods are better.

1.8 The MCAO concept

MCAO tries to overcome the limitation of anisoplanatism by sensing and correcting for the whole atmospheric volume probed by the observed FoV (Beckers 1988). A graphic representation of MCAO is given in figure 1.8. The process of implementing MCAO correction consists of three main steps.

- To measure the deformation of the WF due to the atmospheric turbulence along different directions in the FoV. This is performed with several WFSs looking at different GSs in the FoV.
- To reconstruct the vertical distribution of the atmospheric turbulence at different locations of the field, in order to obtain a three-dimensional mapping of the turbulence above the telescope. This step is called *atmospheric tomography*.
- To apply the WF correction to the whole FoV and not only in a specified direction. This is achievable by using several DMs which are optically conjugated to different altitudes in the atmosphere above the telescope. So in this way they tune the correction depending on the location in the field.

The atmospheric turbulence has a continuous vertical structure which induces a systematic error in the WF correction, due to the fact that, for technical reasons, the number of conjugation altitudes at which the DMs can be placed is limited. What in practice is done for an MCAO system is to optimise the correction to be given to each DM in order to minimise the uncorrected turbulence, both along the vertical of the telescope and in the scientific FoV.

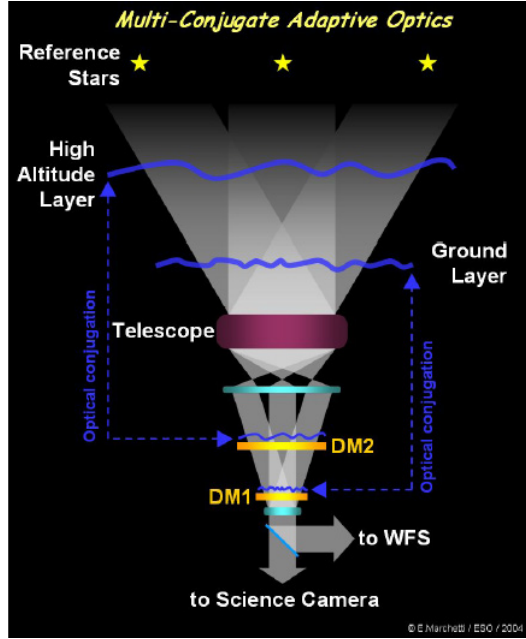


Figure 1.8: The principle of MCAO. Several WFSs and DMs are combined in order to optimize the adaptive correction in a larger FoV.

1.9 Error sources in AO

In AO systems there are many sources that limits the image quality, its performance. The main factors are listed below.

- *Fitting errors* comes from insufficient approximation of the WF. In other word, the fitting error is the residual error due to the instability of the WF compensator to correct the WF exactly. The mean-square fitting error can be defined as:

$$\sigma_{fit}^2 = \langle (W_t(x) - W_c)^2 \rangle \quad (1.15)$$

where W_t is the turbulent WF, W_c the WF corrector function and x the position vector. It may also be expressed as:

$$\sigma_{fit}^2 \simeq 0.3 \left(\frac{a}{r_0} \right)^{5/3} \quad (1.16)$$

where a is the sub-aperture size of the DM. Hence the fitting error can be reduced by using a small value of a , that is by using more actuators. Since

r_0 increases with wavelength (see Section 1.2), σ_{fit} is inversely proportional to wavelength.

- *Temporal errors* is caused by the time delay between measurement and correction of turbulence. The equation can be written like:

$$\sigma_{temp}^2 \simeq \left(\frac{\Delta t}{\tau_0} \right)^{5/3} \quad (1.17)$$

where Δt is the delay time.

- *Anisoplanatic error* is a consequence of sampling different lines of sight through the atmosphere. In fact when the reference source used for WF measurement is displaced angularly from the science object, the turbulence sampled by WFS is different from that in the imaging path. So the mean-square anisoplanatic error at an angle θ is expressed in terms of isoplanatic angle θ_0 :

$$\sigma_{aniso}^2 \simeq \left(\frac{\theta}{\theta_0} \right)^{5/3} \propto \lambda^{-2} \quad (1.18)$$

By remembering the definition of the anisoplanatic angle, the anisoplanatic error varies as λ^{-2} .

- *Photon error* is produced by random noise in the WFS (from reference source, background and detection noise):

$$\sigma_{ph}^2 \propto \frac{1}{\sqrt{N_{ph}}} \quad (1.19)$$

where N_{ph} is the number of photon counted. WFS usually operates with a small amount of light from LGSs, so the photon error is typically a large component of the error budget. It can be reduced by increasing the integration time at the expense of the temporal error. Therefore a trade-off must be made to determine the optimum value.

- *Calibration errors* are due to the NCPA between sensing and imaging channel.
- *Measurement errors* come from the WFS:

$$\sigma_{measure}^2 \propto S/N \quad (1.20)$$

The overall performance of an AO system is estimated by summing the individual error terms σ_i^2 . If these sources are uncorrelated, the residual WFE is given by the sum of their variances:

$$\sigma^2 = \Sigma\sigma_i^2 \quad (1.21)$$

Many of the parameters are interrelated, so it is necessary to perform trade-offs in order to optimize the overall performance (i.e. all terms should be of about equal magnitude). Once the total WFE variance is calculated, the Strehl ratio is computed from the equation 1.7.

Chapter 2

Laser guide stars

Another serious limitation for AO arises from the obvious condition that AO only works if it can sense the distortions of the WF. This WF is usually from a point source, the GS, but because of the angular anisoplanatism the area over which compensation is effective is restricted to a small radius surrounding the reference source. So AO systems using NGSs to measure the WFs impose a severe restriction on the choice of targets. GSs must be selected within the isoplanatic patch θ_0 of the target. For a given distance θ between the GS and target, the residual WFE due to anisoplanatism is estimated as Equation 1.18. On the other hand, the photon noise error is inversely proportional to the photon flux, which is related to the stellar magnitude m :

$$\sigma_{phot}^2 \propto \lambda^{-3.6} 10^{-0.4m} \quad (2.1)$$

To maximize the value of image compensation in observational astronomy, the probability to find suitable GSs, called *sky coverage*, must be high. In the above formula, it is clear that the sky coverage is a strong function of λ : at visible wavelengths, the isoplanatic angle (see Section 1.5) is about 2 arc seconds for average conditions, and the required reference source magnitude needed to measure WFs is about $m_v = 10$. Using NGSs the sky coverage is limited to about 1/100000 of the hemisphere. Whereas at infrared wavelengths, r_0 , θ_0 are larger than in visible wavelengths and the reference source with $m_v = 14$ is required to compensate images at $2.2\mu m$. The isoplanatic angle increases to about 10 arc seconds, giving a sky coverage of about 1/1000 of the hemisphere. Therefore the AO is easier in the infrared than in the optical, even though the sky coverage is still small. In Figure and Table 2.1 from the Roddier book (1999) the typical magnitudes of GSs and their distances from the object as restricted by anisoplanatism are plotted for various photometric bands. Note that both the required photon flux and the isoplanatic patch size depend on the turbulence profile.

| Image spectral band | R | I | J | H | K |
|---|------|------|------|------|------|
| Wavelength (for imaging) | 0.65 | 0.85 | 1.22 | 1.65 | 2.2 |
| Maximum guide star mag (at 0.63 μm) | 13.1 | 14.0 | 15.2 | 16.3 | 17.3 |
| Maximum angular distance (arcsec) | 13.4 | 18.6 | 28.6 | 41.1 | 58.1 |

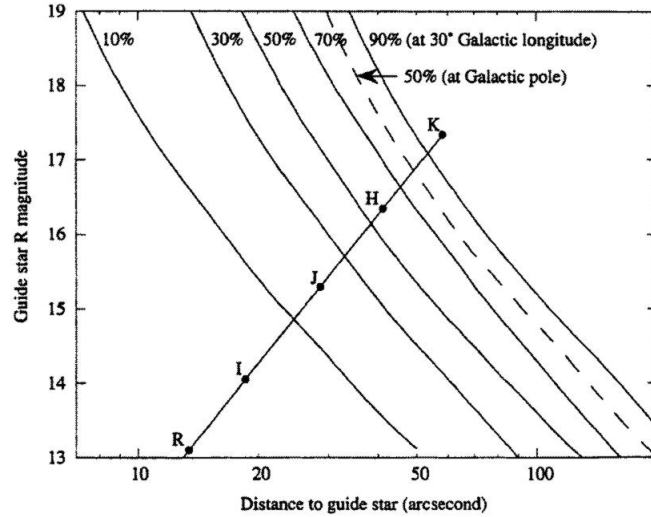


Figure 2.1: The typical magnitudes of GSs and their distances from the object as restricted by anisoplanatism for various photometric bands. The labeled curves show the probability to find a suitable GS at medium Galactic latitude, while dashed line at Galactic pole.

Though it is difficult to find a suitable NGS. In fact the probability to find it is estimated by combining AO parameters with the model of star density in the sky which decreases away from the Milky way, i.e. with increasing Galactic latitude (Bahcall and Soneira, 1981). Stellar density at low galactic latitudes is at least a factor of 2 higher than at Galactic pole. The problem is that even though there may be hundreds of thousands or even a million stars bright enough to be GSs, they only cover a small fraction of the sky. For instance, if the science source is faint, and if there is no NGS of sufficient brightness closer to it than the isoplanatic angle, then AO cannot compensate the image of the source.

One possible solution to the problem of the sky coverage is to use the *laser guide star*, LGS. The existing two types of LGS use either the Rayleigh scattering from air molecules or the fluorescence of sodium atoms in the mesosphere, and are called Rayleigh and sodium LGSs, respectively. The basic idea of Sodium LGSs is to use a laser to illuminate a spot in the upper atmosphere well above the turbulence layer as figure 2.2 describes. In fact, at about 90 km of altitude there is a 10

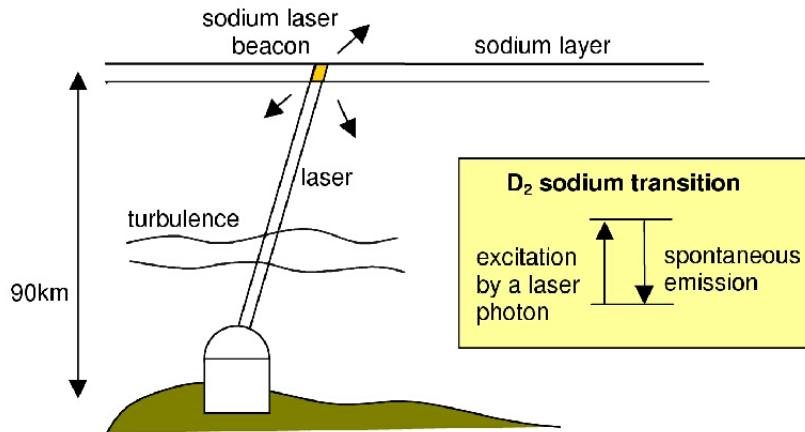


Figure 2.2: The operating principle of the LGS.

km thick layer in the mesosphere with an unusually high concentration of neutral sodium and potassium atoms, probably of meteoritic origin. A laser on the ground near the telescope is tuned to the sodium D_2 lines ($\lambda \simeq 588.99$ nm) and fired to pass through the mesospheric layer at the desired position. The laser light excites sodium atoms, which in turn emit line radiation by spontaneous emission (after about 10^{-8} seconds), with most of the emission concentrated in the sodium layer and the same wavelength of the laser. In conclusion, the systems, which produce and utilize a laser beacon, are expensive and difficult to implement, but they do allow AO and MCAO to operate where NGSs are unavailable.

2.1 LSG issues

During WF sensing there are several problems that must be taken into account when using one or more LGSs in an AO system, respect to the use of NGSs. These features are essentially due to the finite distance of the Sodium layer and the temporal variability of its density vertical distribution, causing an increase of the WFE. These issues are described in the following subsections.

2.1.1 Fratricide effect

When the LGSs are launched from behind the secondary mirror, the beam lying below the LGSs is produced by the Rayleigh scatter. This is the case of Gemini South Observatory (D'orgeville et al., 2008). During the measuring of WF, the SHWFS sub-apertures are contaminated by the foreground light of the up going laser beams from the other LGSs. This causes a reduction of the image SNR.

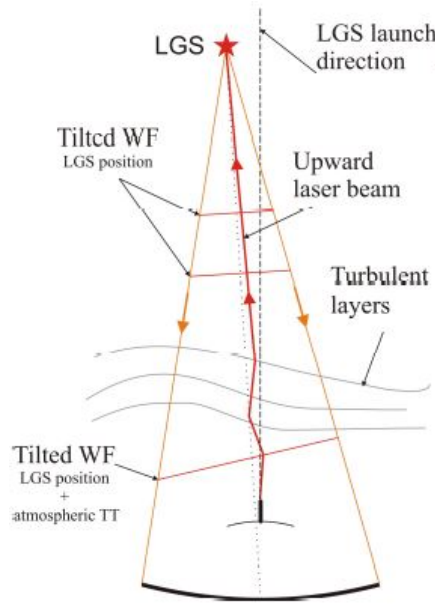


Figure 2.3: TT indetermination.

2.1.2 TT indetermination

Because of the lower atmosphere, that is the part of the turbulence which causes the WF aberration, even the TT indetermination has to be taken into account. In Figure 2.3 the laser beam wanders on both the upward and downward trips through the same atmospheric turbulence. If the laser was projected by the full telescope aperture no tilt signal would be measured. When the laser is launched by a small telescope at the side of the primary mirror or behind the secondary obstruction, the TT contributions from the LGS actual position and the atmospheric turbulence can not be disentangled. So NGSs are needed to measure the global TT that must be removed (Rigaut & Gendron, 1992).

2.1.3 Cone effect

LGS does not sample the higher layers of the atmosphere because the footprint of the LGS is smaller than the telescope diameter (see Figure 2.4(a)). As a consequence, a mismatch between the volume of atmosphere sensed with the LGS and the volume corrected for the science target causes what is called cone effect. The footprint diameter is:

$$D_f = D (1 - H_l/H_s) \quad (2.2)$$

where H_s is the Sodium layer height. The WF reconstruction using a single

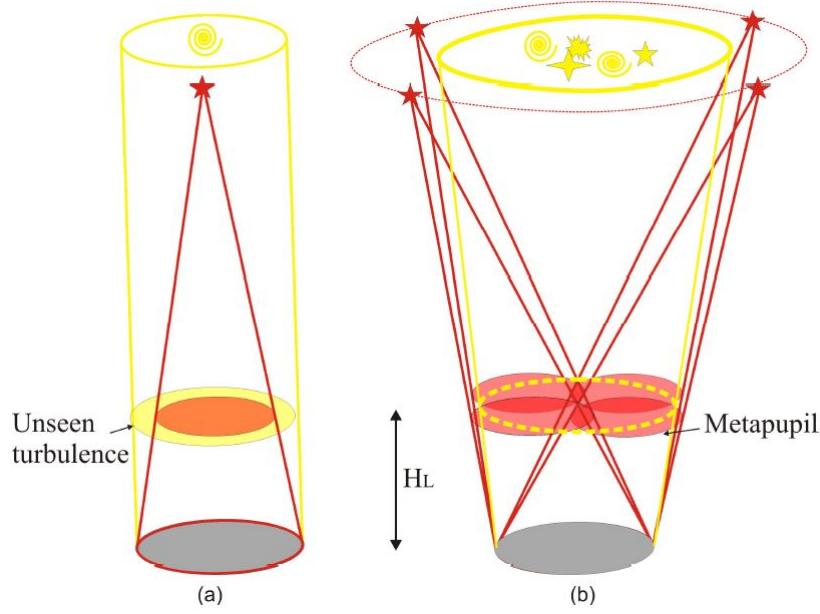


Figure 2.4: (a) Cone effect, (b) MCAO with LGSs

LGS results clearly less effective respect to an NGS in the same direction and with the same received flux, since part of the turbulence volume is not sensed. The tomographic reconstruction of the atmospheric turbulence requires more LGSs, respect to NGSs, to sample the same metapupil area at a given altitude (see Figure 2.4(b)). The cone effect is the main reason for the impossibility of using Rayleigh LGS for MCAO. These artificial stars are tuned on only at low altitudes, hence their footprints at the high turbulence layers are very small, requiring a big number of stars (and of course of WFSs) to have a proper metapupil coverage ¹.

2.1.4 LGS launching effect

The scientific FoV 2α and the technical one defined by the incoming LGS light mean angle 2β , are different:

$$\beta = \text{atan} \left(\frac{D/2 + H_s \text{atan}(\alpha)}{H_s} \right) \quad (2.3)$$

where H_s is the Sodium layer height.

¹For a finite FoV of a radius θ , the diameter of the second DM, called metapupil, must be larger than the telescope pupil D by at least $2\theta H_2$, where H_2 is the conjugation height of the second DM. A beam of some GS illuminates only a portion of the meta-pupil: the beam footprint diameter is smaller than D for an LGS or equal to D for an NGS.

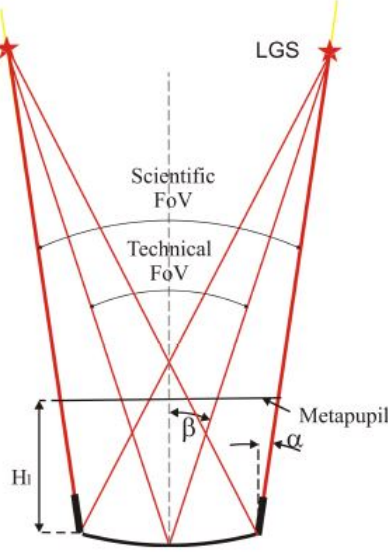


Figure 2.5: The launching angle.

The technical FoV is the angle for the LGS to sample the *metapupil* at a given height H_t (turbulent layer height) for a scientific FoV. The LGS launching angle coincides with β in case of projection from behind the secondary mirror and α in case of side launch scheme as Figure 2.5 illustrates. The LGS launching angle can have an impact on the MCAO modules where the optics dimension are defined by β in order not to vignette the incoming light of the LGSs.

2.1.5 Zenith angle effect

The different zenith angle ξ between observations and its variation during the sky tracking changes the Sodium layer mean distance respect to the telescope by a factor depending on the cosine of ξ . Consequently the LGS image shifts along the optical axis. Therefore the WFS design must foresee some compensation device to follow the LGS image position and possibly reduce the $f_{\#}$ of the beams entering the LGS channel since this effect is proportional to it. In case of multiple LGSs, the different azimuthal angles of the LGSs respect to the optical axis, make the star to be formed at different distances from the Sodium layer to the telescope and thus a predictable defocus signal whose intensity is given by equation 2.6.

2.1.6 Perspective elongation

The LGS is seen by the off-axis sub-apertures of a SHWFS with a given FoV as an extended source due to parallactic effect as Figure 2.5 shows. On the detector the

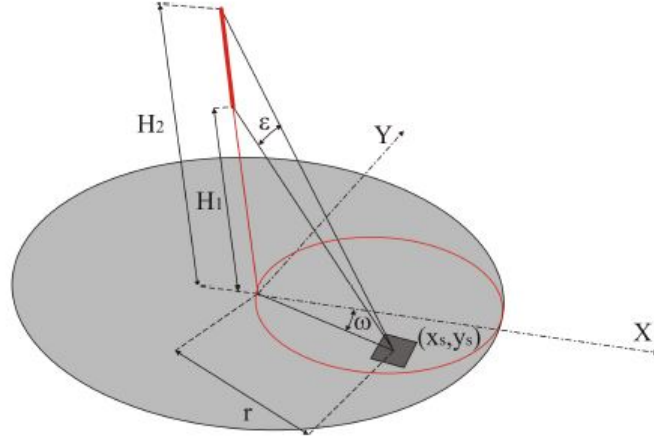


Figure 2.6: The description of the LGS parallactic effect on the off-axis sub-apertures of a SHWS, the red circle indicates a telescope with side launch of the LGS.

spots appear elongated by an angular dimension ε , proportional to the sub-aperture distance r from the LGS launcher:

$$\varepsilon = \cos(\xi)r \left(\frac{1}{H_1} - \frac{1}{H_2} \right) \simeq \cos(\xi)r \frac{(H_2 - H_1)}{H_m^2} \quad (2.4)$$

where ξ is the zenith angle, H_1 e H_2 are the LGS height edges and H_m is the LGS mean altitude. Because of the dependence of ε on r in Equation 2.4, in case of side launch of the LGSs, a doubled maximum elongation respect to the central launch scheme occurs. In other words, looking at Figure 2.7, two sub-apertures having the same FoV, centered at H_m and placed at different distances r and r' from the laser launcher, see different segments of the LGS vertical extension.

The spot elongation orientation ω is always directed toward the laser launcher and is defined as:

$$\omega = \text{atan} \left(\frac{y_l - y_s}{x_l - x_s} \right) \quad (2.5)$$

where (x_l, y_l) are the laser launcher coordinates and (x_s, y_s) the sub-aperture center coordinates.

For a Gaussian intensity profile of the LGS the spot elongation would be asymmetric, with a longer tail from the lower part of the LGS. This effect causes a spots off-set proportional to the distance of the sub-aperture from the laser launcher. The choice of the sub-apertures FoV depends on the sampling of elongated images and it is a trade-off between the number of pixels per sub-aperture and the spot

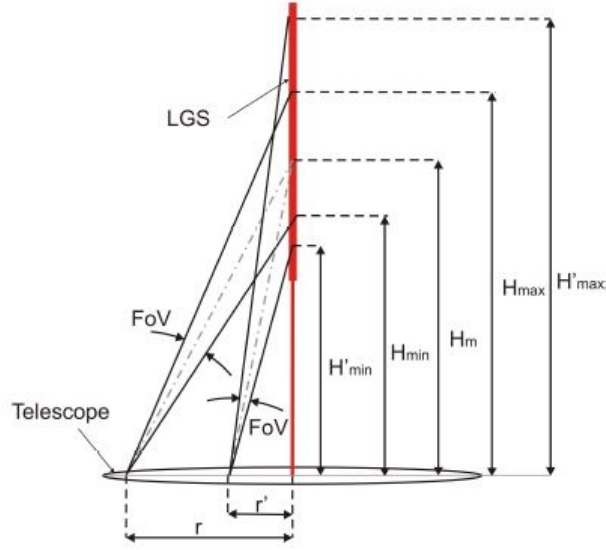


Figure 2.7: Parallactic effect: a sub-aperture with a given FoV at a distance r from the laser launcher and centered at H_m , sees the LGS inside two edge heights H_{min} and H_{max} that are at different distances from H_m .

centroiding WFE. A reasonable value of the FoV is ~ 12 arcsec for E-ELT and the side launch scheme of LGS.

2.1.7 Sodium layer variability

The concentration of the Sodium layer varies significantly with latitude and also temporally (Figure 2.8), even sporadic events can cause variations in the Sodium layer on a very short timescale. The mean Sodium altitude variation can be of the order of hundreds of meters or even kilometers. This variation in time, in addition to the predictable shift of the focal plane due to the changing zenith angle during the observation, leads to a *defocus term* on the LGS WFS. This term must not be applied by the DM because the science images are not affected by this aberration. The RMS WFE σ_{def} from Sodium layer defocus is:

$$\sigma_{def} = \frac{1}{16\sqrt{3}} \frac{D_{tel}^2}{H^2} \Delta H \quad (2.6)$$

where H is the height of the sodium layer (variable) and ΔH is the variation of the LGS height. It is evident that with a large telescope the WFE increases too much. For instance, given D_{tel} of about 40 m and H of 90 km, σ_{def} is 7 nm for each meter of ΔH . Therefore a NGS is necessary to overcome this problem by measuring the defocus signal.

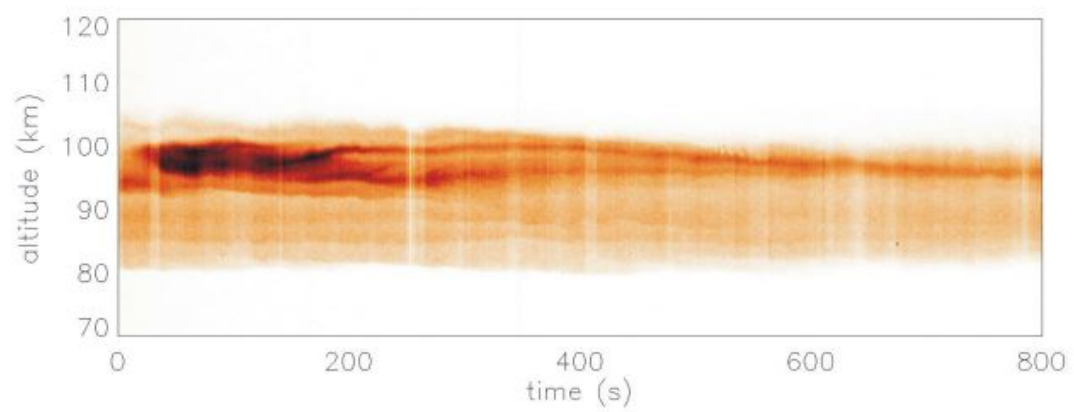


Figure 2.8: Sodium layer profile in function of time. (Paul Hickson, Department of Physics and Astronomy, University of British Columbia.)

Chapter 3

How to optimize and tolerance

No perfect optical design exists. In fact imaging with an optical system is influenced by aberrations generated by the components it consists of. Through the procedure of optimization one can improve or modify the design in order to reduce or remove aberrations. Since no component cannot be perfectly manufactured, stating a reasonable acceptable range for the optical specifics is important to ensure that the final, assembled instrument meets the requested performance.

This is the reason why a brief introduction of the aberrations is written in the first section. The second part explains how optimization is implemented and the last section deals with tolerancing.

3.1 Seidel aberration

Third-order aberration theory is a much more accurate computation of where rays travel than the one given by paraxial theory. In the third-order treatment, one can show that the optical path difference between the test ray and the chief ray (see Figure 3.1) takes the form:

$$\Delta W = C_1\rho^4 + C_2\rho^3b \cos \phi + C_3\rho^2b^2 \cos^2 \phi + C_4\rho^2b^2 + C_5\rho b^3 \cos \phi \quad (3.1)$$

where the C_i values depend on the shapes of the optical surfaces and (if refractions are involved) indices of refraction, b is the image height $b = R \sin \theta$ (R is the lens radius) and the circular coordinates ϕ and ρ locate the intersection of the test ray and the aperture. Since each of the terms in Equation 3.1 has a different functional dependence, we distinguish five monochromatic third-order aberrations, also known as the Seidel aberrations.

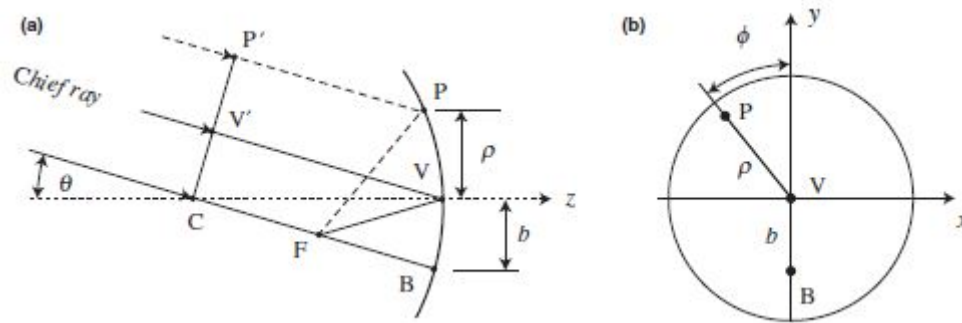


Figure 3.1: Diagram (a) shows rays through the center of curvature and vertex V. Diagram (b) locates points P, V, and B in the plane of the aperture when looking down the optical axis. In this diagram, the distance b is related to the angle θ ($b = R \sin \theta$), that is, it measures how far the source is from the axis. The circular coordinates ϕ and ρ locate the intersection of the test ray and the aperture.

| Aberration | Functional dependence |
|---------------------------|--------------------------|
| Spherical aberration (SA) | ρ^4 |
| Coma | $\rho^3 b \cos \phi$ |
| Astigmatism | $\rho^2 b^2 \cos^2 \phi$ |
| Curvature of field | $\rho^2 b^2$ |
| Distortion | $\rho b^3 \cos \phi$ |

Figure 3.2: Third-order monochromatic aberrations.

Table 3.2 lists the aberrations in order of importance for large telescopes, where the exponent on ρ is crucial. This is also in the order in which they are usually corrected. Astigmatism, for example, is only corrected after both coma and spherical aberration have been eliminated. In the following sections spherical aberration, coma, astigmatism and distortion will be described in more details providing solutions for each aberrations.

3.1.1 Spherical aberration

As the ray height at the lens increases, the position of the ray intersection with the optical axis moves further and further from the paraxial focus. That is called spherical aberration, SA. In figure 3.3 *longitudinal and transverse spherical aberration* LA_R and TA_R are sketched. "R" refers to the ray through the margin of the lens aperture. The transverse measure of an aberration is directly related to the size of the image blur.

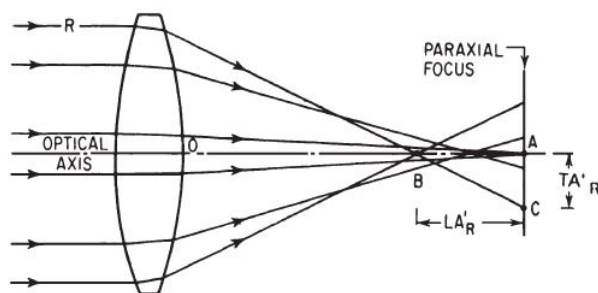


Figure 3.3: A simple converging lens with undercorrected SA. The rays farther from the axis are brought to a focus nearer the lens.

When the marginal focus is closer to the lens than the axial focus, such as exhibited by the positive element in Figure 3.3, one speaks of undercorrected SA. Conversely, when the marginal focus is located beyond the axial focus the lens is said to suffer from overcorrected SA. In general, a positive, converging lens or surface will contribute undercorrected SA to a system, and a negative lens or divergent surface, the reverse, although there are certain exceptions to this.

The image of a point formed by a lens with SA is usually a bright dot surrounded by a halo of light, while the effect on an extended image is to soften the contrast of the image and to blur its details.

A way to measure the aberration is by means of OPD, or WF deformation, the departure of the actual WF from a perfect reference sphere centered on the ideal image point. It is the most useful measure of image quality for well-corrected systems.

For a given aperture and focal length, the amount of SA in a simple lens is a function of object position and the shape, or bending, of the lens. So in order to reduce the SA one can use:

- A plano convex with the convex surface toward the object and the object at infinity or an equiconvex lens with object and image with the same size.
- Any lens with a large enough focal ratio will approach the paraxial case closely enough that the blur due to SA can be reduced to the size of the seeing disk. Since a large focal ratio also minimizes chromatic aberration, very early (1608-1670) refracting telescope designs tended to have modest apertures and large focal lengths. The problem with these designs was reduced image brightness and, for large apertures, unwieldy telescope length.
- An achromatic doublet can be designed to minimize both spherical and chromatic aberration.

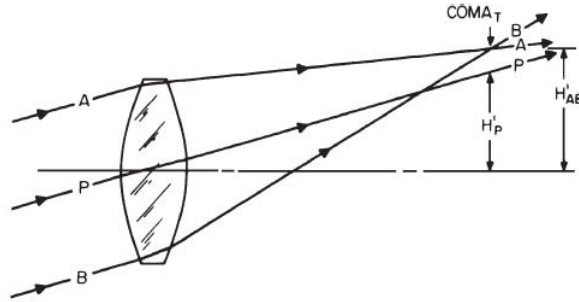


Figure 3.4: In the presence of coma, the rays through the outer portions of the lens focus at a different height than the rays through the center of the lens.

In addition, other strategies, which are able to remove the SA, are listed below.

- A negative power lens can remove the SA of a positive lens of a different index.
- A mirror with parabolic shape.
- A transparent corrector plate placed in front of a spherical mirror. It can lengthen the optical path for rays of different ρ by the appropriate amount, whatever their direction. An example is the Schmidt telescopes.

3.1.2 Coma

Of the four off-axis aberrations, only coma and astigmatism actually degrade the image resolution, while the other two only alter the image position. In figure 3.4 the marginal rays A and B intersect the image plane above the ray P which passes through the center of the lens. The distance from P to the intersection of A and B is called *tangential coma* of the lens. the aberration is named after the comet shape of the image. Unlike SA, coma increases with object distance from the axis.

Coma is a particularly disturbing aberration since its flare is nonsymmetrical. Its presence is very detrimental to accurate determination of the image position since it is much more difficult to locate the center of gravity of a coma patch than for a circular blur such as that produced by SA. In an axially symmetrical system there is no coma on the optical axis. An optical system with neither SA nor coma is called aplanatic, but no single element aplanatic telescope is possible, either in a refractor or reflector. Aplanatic reflecting telescope designs require two mirrors.

Coma varies with the shape of the lens element and also with the position of any aperture or diaphragms.

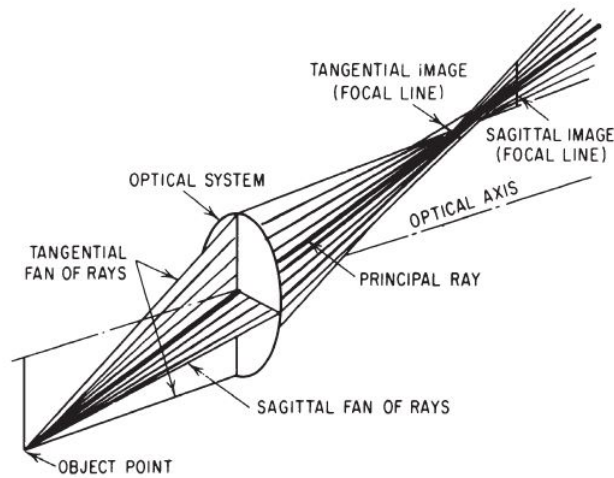


Figure 3.5: Astigmatism: tangential and sagittal image.

What reduce coma is listed below:

- Large focal ratios. Unfortunately, it imposes penalties in image brightness and telescope length.
- A system of lenses and achromatic doublet or triplet designs in refracting systems minimize both SA and coma.
- A correcting lens system (usually with zero power) in a single-mirror telescope. Such correcting optics may also aim to correct additional aberrations, but must take care to avoid introducing chromatic aberration.

3.1.3 Astigmatism

Astigmatism is the aberration that occurs when rays from an off-axis object that strike in different planes are imaged at different distances.

The image of a point source formed by an oblique fan of rays in the tangential plane will be a line image. This line, called the *tangential image*, is perpendicular to the tangential plane, it means that it lies in the sagittal plane. Moving beyond this line, the meridional rays spread out again and the sagittal rays converge creating the image of a line in the meridional plane called the *sagittal image*. Hence astigmatism occurs when the tangential and sagittal images do not coincide.

The difference between these focal lengths becomes greater as the object moves further off axis. Between the astigmatic foci the image is an elliptical or circular blur. When there is primary astigmatism in a lens system, the images lie on curved

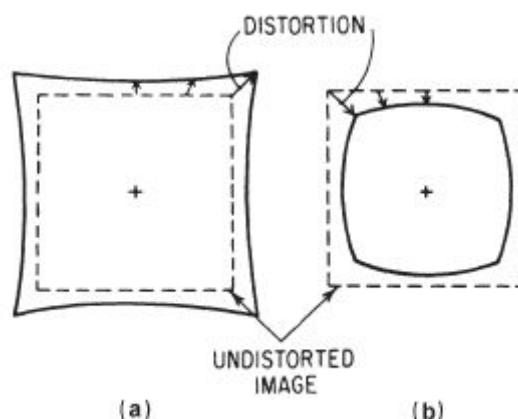


Figure 3.6: (a) Pincushion distortion of an object that has a square outline centered on the optical axis. (b) Barrel distortion of the same object. The sides of the image are curved because the amount of distortion varies as the cube of the distance from the axis. Thus, in the case of a square, the corners are distorted $2\sqrt{2}$ as much as the center of the sides.

surfaces which are paraboloid in shape.

The amount of astigmatism in a lens is a function of the power and shape of the lens and its distance from the aperture or diaphragm which limits the size of the bundle of rays passing through the lens. There is no astigmatism when an axial point is imaged. All uncorrected refractors and all practical two-mirror reflectors suffer from astigmatism.

In many cases a corrector lens or plate removes the astigmatism. If a telescope design is free from astigmatism, coma, and SA, it is called an anastigmatic aplanat. For large anastigmatic telescopes, the correction plate is usually located near the focal plane. An example of small anastigmatic telescopes is the Schmidt-Cassegrain, a two-mirror telescope with a corrector plate located at the aperture.

3.1.4 Distortion

Distortion relocates images in the focal plane so that the colinearity requirement is violated: straight lines on the sky become curved lines in the focal plane. There is no image blur. Figure 3.6 illustrates two kinds of distortion, "barrel" and "pincushion" distortion, either of which will increase more rapidly with distance from the axis than do the other Seidel aberrations. In fact the distortion itself usually increases as the cube of the image height.

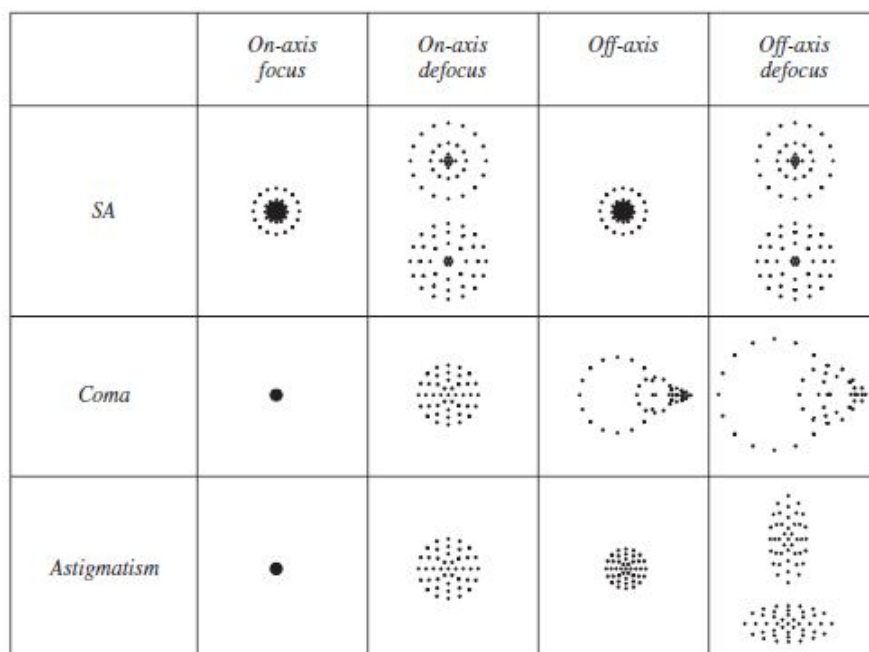


Figure 3.7: Qualitative appearance of images of a point source in optical systems with a single aberration present. In the diagram, "focus" means the best compromise on-axis focus, which may differ from the Gaussian focus.

3.1.5 Spot diagrams

Figure 3.7 gives a qualitative summary of the distortions in the image of a point source that are introduced by SA, coma and astigmatism. Since more than one aberration may be present in an actual optical system, its image-forming behavior will generally exhibit some combination of the effects illustrated. The figure shows spot diagrams for each aberration. Each spot is the focal-plane location of a single ray traced through the system. Rays are chosen to sample the entrance aperture in a uniform fashion, so the density of spots gives an indication of the brightness distribution of the final image.

3.2 Zernike aberrations

The Zernike polynomials are a mathematical description of several aberrations entering in an optical system, both in a simple and complex one. Specifically, they are a polynomial expansion of the WF function, $W(\theta, \rho)$, defined over a unit circle. Since the Zernike polynomial are orthogonal, we can express them with the product of a radial part and an angular one, like:

$$Z_n^m = \sqrt{n+1} R_n^m \begin{cases} \sqrt{2} \cos(m\theta) & \text{if } m > 0 \\ \sqrt{2} \sin(m\theta) & \text{if } m < 0 \\ 1 & \text{if } m = 0 \end{cases}$$

where,

$$R_n^m(\rho) = \sum_{s=0}^{(n-m)/2} \frac{(-1)^s (n-s)!}{s! \left(\frac{n+m}{2} - s\right)! \left(\frac{n-m}{2} - s\right)!} \rho^{n-2m} \quad (3.2)$$

The radial portion of the polynomial is defined by two indices, n and m . The n index defines the order of the radial power; so an n value of 5 would indicate all polynomials whose maximum radial power was ρ^5 . Only certain values for m , the azimuthal frequency, are allowed once n is chosen; $n+m$ must be even, and $0 \leq m \leq n$. This method is used in the design of optical systems for balancing the various aberrations in order to obtain the best image.

The first 27 plots of Zernike polynomials, ordered vertically by radial degree and horizontally by azimuthal degree are shown in the Zernike pyramid 3.8, whereas the optical aberrations up to the sixth order coefficients are listed in Table 3.9.

The practical consequence of the orthogonality is that any aberration terms, like tilt or defocusing, or any other, may be added or subtracted from $W(\theta, \rho)$ without losing the best fit to the data point. So any continuous $W(\theta, \rho)$ may be represented by a linear combination of the Zernike polynomials, Z_n^m , as follows:

$$W(\theta, \rho) = \sum_n \sum_{m=-n}^n a_n^m(\rho) Z_n^m \quad (3.3)$$

where a corresponds to the aberration coefficient (the weight).

It is generally meaningful to specify WF quality using the RMS WFE, σ . Equation 3.4 defines it for a circular pupil as well as the variance σ^2 . It is commonly expressed in units of wavelength. $\Delta W(\rho, \theta)$ is the OPD value measured with respect to the best fit spherical wave and it generally has the units of waves. $\overline{\Delta W}$ is the mean WF OPD.

$$\sigma_W^2 = \frac{1}{\pi} \int_0^{2\pi} \int_0^1 (\Delta W(\rho, \theta) - \overline{\Delta W}(\rho, \theta))^2 \rho \delta \rho \delta \theta = \overline{\Delta W(\rho, \theta)^2} - \overline{\Delta W}(\rho, \theta)^2 \quad (3.4)$$

In addition, the orthogonality permits also to calculate the total variance of the WF, σ_W^2 , as the sum of the single component of the variance.

$$\sigma_W^2 = \sum_{n,m} \sigma_W^2(Z_n^m) \quad (3.5)$$

where $\sigma_W(Z_n^m)$ are the variance relative to a specific Zernike coefficient. The Strehl ratio is computed using this RMS and equation 1.7.

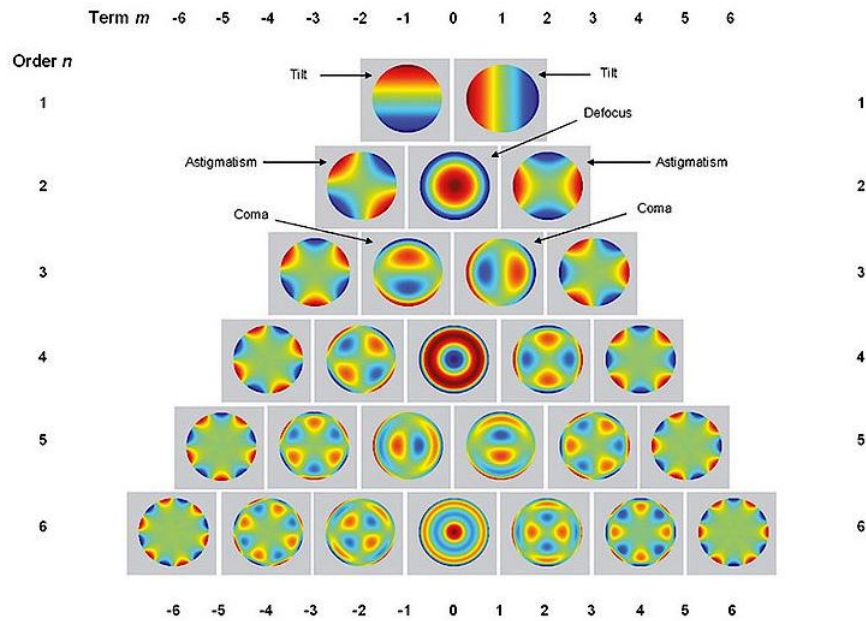


Figure 3.8: Two dimensional plots of Zernike polynomials.

An important feature in the normalized Zernike expansion consists of the existent direct proportionality between the coefficient of every polinomy and its relative contribute to the total WFE. That is said, it does not mean that the aberration with a coefficient higher degrades even more the vision, as it is not always true that more the total WFE grows, more the image quality worsens. Applegate has indeed demonstrated that a different combination of aberrations can even lead to a better optic quality of the image, but only when the aberrations have got the same sign, same angular frequency, m and they are distant of two radial orders n . (Applegate, 2004)

| Zernike coefficient | Radial Order | Angular frequency | Optical aberration |
|---------------------|--------------|-------------------|--------------------------------|
| 0 | 0 | 0 | Piston |
| 1 | 1 | -1 | Tip, Tilt (Prism) |
| 2 | 1 | 1 | Tip, Tilt (Prism) |
| 3 | 2 | -2 | Astigmatism |
| 4 | 2 | 0 | Defocus |
| 5 | 2 | 2 | Astigmatism |
| 6 | 3 | -3 | Trefoil |
| 7 | 3 | -1 | Coma (vertical) |
| 8 | 3 | 1 | Coma (horizontal) |
| 9 | 3 | 3 | Trefoil |
| 10 | 4 | -4 | 4-fold |
| 11 | 4 | -2 | Astigmatism |
| 12 | 4 | 0 | Spherical aberration |
| 13 | 4 | 2 | Astigmatism |
| 14 | 4 | 4 | 4-fold |
| 15 | 5 | -5 | 5-fold |
| 16 | 5 | -3 | 3-fold |
| 17 | 5 | -1 | Secondary coma (vertical) |
| 18 | 5 | 1 | Secondary coma (horizontal) |
| 19 | 5 | 3 | 3-fold |
| 20 | 5 | 5 | 5-fold |
| 21 | 6 | -6 | 6-fold |
| 22 | 6 | -4 | 4-fold |
| 23 | 6 | -2 | Astigmatism |
| 24 | 6 | 0 | Secondary spherical aberration |
| 25 | 6 | 2 | Astigmatism |
| 26 | 6 | 4 | 4-fold |
| 27 | 6 | 6 | 6-fold |

Figure 3.9: Double-index Zernike polynomial describing optical aberrations up to the sixth order coefficients.

3.3 Optimizing optical systems

Optimization capability is the most important feature of modern optical design software. Given a starting system, the software changes automatically the system parameters in order to lead to the required quality.

The main steps for automatic optimization are:

1. To specify a *starting system Configuration* with its *aperture* and *Field*, that is where the object is placed.
2. To define a function of the system parameters that measures the quality of the system at each stage, called *Merit function*, *MT*, or error function (see subsection 3.3.3).
3. To define a subset of system parameters that are automatically changed during optimization. Examples of *optimization variables* are the surface curvatures (or, alternatively, the corresponding radii), glass thickness, air spaces, or aspheric coefficients, the refractive index and dispersion or gradient index coefficients.
4. To add a set of *constraints* or boundary conditions in the MT function that limits the variation domain of the optimization variables.

Optimization is implemented as a numerical algorithm that attempt to find iteratively the local minimum of the non linear MT function that depends on the defined variables. Then the designer must check if the results evolves toward the envisaged goal, otherwise he makes changes in the optimization parameters.

3.3.1 Local minima: the damped least squares and Hammer algorithm

For simplicity, consider the case when there are no constraints. A point in the solution space is described by the vector $x = (x_1, x_2, \dots, x_N)$, whose components are the N optimization variables. Determining the minimum that can be reached from a given starting configuration without ever increasing the error function is called local optimization. Starting from the initial configuration, a local optimization algorithm reduces the value of the error function f by changing the vector x until the solution arrives at (or comes close enough to) a minimum of f. There, the gradient of f vanishes and small changes of the optimization variables can only lead to an increase of f. When multiple local minima exist, the attempt to find the best among the local minima is called global optimization. Because in optical design the error function can be highly nonlinear, multiple local minima often exist.

The result of local optimization is then critically dependent on the choice of the initial configuration. Poor choices of starting configurations most often lead to poor quality solutions.

There are different algorithms to implement optimization. The conventional means of optimizing lenses has for decades been the use of the *damped least squares algorithm*, *DLS*. It uses numerically computed derivatives to determine a direction in solution space which produces a design with a lower merit function. DLS has many attractive features; it is efficient, and it is very good at finding the "local" minimum of the merit function. The problem with this method is that once you have arrived at the local minimum, there is no known way to determine if there is not a better, lower minimum somewhere else. Moreover, to try out every possible configuration to see which is best will require too much time with such an algorithm.

However, given a sufficiently long time, some algorithms can find solutions that are considerably better than those found by local optimization. For instance a global optimization algorithm provided in ZEMAX is the *Hammer algorithm*. It is used for exhaustively searching for the optimum solution once a reasonably good starting point is found. Although the global optimization algorithms are extremely useful, it is important to realize that there is no guarantee that the true global optimum will always, or even occasionally be found. Of course, there is no way to even determine if any solution is the global optimum, even if it is the best you have ever found. In addition it requires extensive computational effort to be effective.

3.3.2 Optimizing: the last step

The order in which the system parameters are freed as optimization variables can also determine toward which local minimum the solution will converge. The designers may choose to free only a limited number of variables in the first stage of optimization, hoping that the solution will go toward the desired minimum. The remaining variables are then freed only in a later stage. Freeing all variables simultaneously may lead to a different result.

3.3.3 Analysis methods

A brief description of each of the analysis features which ZEMAX supports is given below. This includes aberrations, spot diagrams, and many other computations. Analysis in this context means any graphical or text data computed from data defining the optical components.

- The correct choice of the *MT function* is essential for a successful design. The error function defines the goal to be achieved. So it is important that the designer ensure that the error function accurately reflects the actual design requirements. First, a number of system characteristics must be defined (e.g. lens parameters), called *operands*, and the corresponding *target values* to be held within certain limits. Since not all operands reach their target values exactly, it is necessary to minimize the merit function.

The Merit function is defined as:

$$f(x) = \sqrt{\frac{\sum w_i (a_i(x) - \tilde{a}_i)^2}{\sum w_i}} \quad (3.6)$$

where a_i is the operand, w_i is the *corresponding weight*, and the tilde denotes the target values for the corresponding operands. Obviously, in an ideal situation where all operands are equal to their targets, the value of f would be zero. If the optimization does not behave as expected, the designer should inspect the behaviour of the individual operands or changing operands and/or their weights to solve the problem.

- In the *Spot diagram* (see Section 3.1.5) the RMS radius is the root-mean-square radial size. The distance between each ray and the reference point is squared, and averaged over all the rays, and then the square root is taken. The GEO spot radius which is the radius of the circle centered at the reference point which encloses all the rays. While the RMS spot radius gives a rough idea of the spread of the rays, since it depends upon every ray, the GEO spot radius only gives information about the one ray which is farthest from the reference point.
- The *RMS WFE* is a statistical OPD deviation averaged over entire WF expressed in linear units, commonly in units of wavelength. A visual and mathematical representation of this concept is given in Figure 3.10 and Equation 3.3.3.

$$\sigma = \sqrt{\frac{\sum_{i=1}^N (OPD)^2}{N}} = \sqrt{\frac{\int (OPD)^2 dx dy}{\int dx dy}} \quad (3.7)$$

where N is the number of points sketched in Figure 3.10

- The *Zernike coefficients* are a mathematical way to point out the different types of aberration.

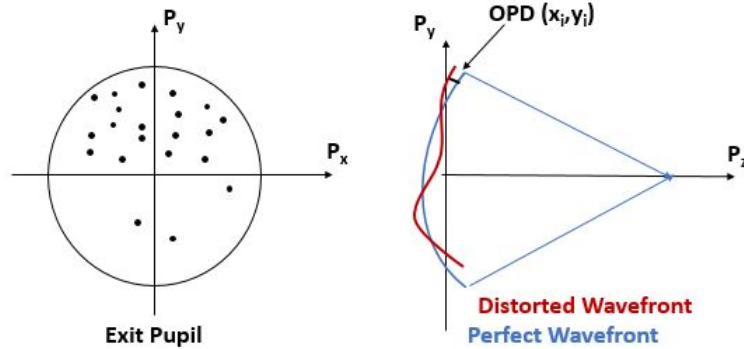


Figure 3.10: Representation of the RMS WFE.

3.4 Tolerancing optical system

Once the optimization procedure is done, the tolerance analysis is necessary because fabrication and mounting errors affect the design performance. For instance, surface radius, glass index and decenter of a real lens will be always different from the designed elements. Therefore setting a maximum acceptable range for every error, within the specifications of the elements can vary, is useful to still reach a good performance. There are two requirements that limit the allowable changes of opto-mechanical parameters: the RMS WFE and the optical distortion.

Some lens elements are more sensitive to the errors than other lens elements. Hence, the tolerance analysis allows to identify these parameters. Generally speaking, elements with short surface radii or with large incident/exit ray angles are more sensitive to fabrication and mounting errors. In addition, for a spherical element, decentering and tilt between the two surfaces of the same element are actually the same thing, while for an aspheric element, the decentering and wedge between the two surfaces are not necessary the same thing. Note that these errors refers to fabrication errors. The decentering and tilt referring to the mounting error are not the same neither for a spheric lens nor for an aspheric one.

The basic procedure of optical system tolerancing consists of the following steps:

1. Define an appropriate set of *tolerances* for optical elements, allowable errors (the main tolerances are described in the next section).
2. Add *compensators* and set allowable ranges for the compensators: they can be adjusted to minimize the WFE. The default compensator is the back focal distance, which controls the position of the image surface. In fact the main effect of all tolerance adding up is defocusing. Another way to compensate

for the tolerance-caused defocusing is to change the spacing between two lens elements.

3. Select an appropriate criterion, such as RMS spot radius, WFE, MT function, or boresight error. The criterion is what Zemax looks at when it does the tolerancing.
4. Select the desired mode, either *sensitivity* or *inverse sensitivity*.
5. Perform an analysis of the tolerances.
6. Review the data, the Worst Offenders ¹ generated by the tolerance analysis, and consider the budgeting of tolerances. If required, adjust tolerances, balance cost and schedule with performance and repeat the analysis.

The design process consists of modelling the errors generated by each component and then making the necessary trade-offs and compromises to achieve the required overall performance. The best way is to start with loose tolerance ranges and gradually tighten (loosen) the ranges of the tolerances that more (less) affect the performance (see Subsection 3.4.2). Generally speaking, one should avoid two cases: design a lens with on-paper performance barely meeting the specifications, and rely on extremely tight lens element fabrication and mounting tolerance to make the real lens performance meet specifications. Secondly avoid to design a lens with on-paper performance well above the specifications.

3.4.1 Element tolerance

The main element fabrication tolerances are radius tolerance, thickness, tilt x and y (equivalent to decenter) and S + A Irregularity.

- The *radius* tolerance is usually specified by Fringes because they can be directly measured using a test plate. Fringes corresponds to a change in sag given by $N\lambda/2$, where N is the number of fringes and λ is the test laser wavelength. In Figure 3.11 the definition of sagitta is presented: SAG stands for sagitta, R radius of curvature and D the lens diameter. The below equation is accurate for all spheres:

$$SAG = R - \sqrt{R^2 - \left(\frac{D}{2}\right)^2} \quad (3.8)$$

¹The Worst Offenders are those tolerances that contribute more than other tolerances to the drop of the MT function value

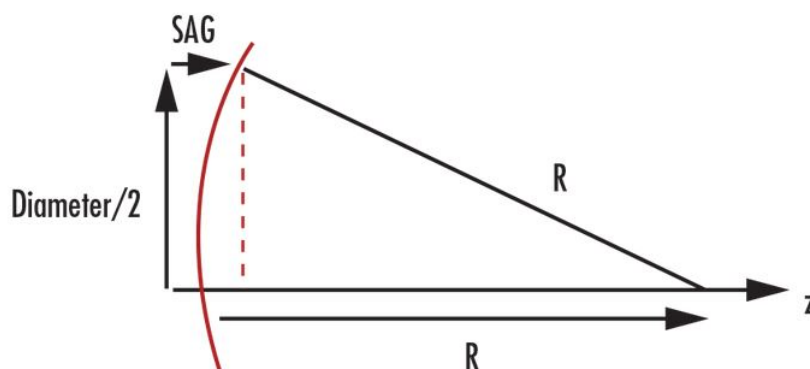


Figure 3.11: Sagitta.

- The *thickness* between two surfaces.
- For the *tilt* tolerance, sag difference between a known radius and the surface under test is usually used with the unit millimeter.
- The *Wedge angle* is measured in degree. It is the tilt between two faces of a lens.
- For *S + A Irregularity* a 0.5 wave is common.

As regards the lens mounting tolerance, decenter x, decenter y, tilt x and tilt y are the most important; they are two different issues in this case.

Other important tolerances are:

- The *glass index* tolerance.
- The *Abbe number* which is in term of percentuage and it is defined as:

$$V = \frac{n_D - 1}{n_F - n_C} \quad (3.9)$$

where n_D , n_F and n_C are the refractive indices of the material at the wavelengths of the Fraunhofer D-, F- and C- spectral lines (589.3 nm, 486.1 nm and 656.3 nm respectively).

Table 3.12 shows the allowable errors for each element tolerance, both for commercial, precision and high precision quality. It is usually calledd rule of thumbs.

| Attribute | Commercial | Precision | High Precision |
|---|------------------------|-------------------------|----------------------|
| Glass Material (n_d, v_d) | $\pm 0.001, \pm 0.8\%$ | $\pm 0.0005, \pm 0.5\%$ | Melt Data |
| Diameter (mm) | $\pm 0.00/-0.10$ | $+0.000/-0.025$ | $+0.000/-0.015$ |
| Center Thickness (mm) | ± 0.150 | ± 0.050 | ± 0.025 |
| SAG (mm) | ± 0.050 | ± 0.025 | ± 0.015 |
| Clear Aperture | 80% | 90% | 90% |
| Radius (larger of two) | $\pm 0.2\%$ or 5 fr | $\pm 0.1\%$ or 3 fr | $\pm 0.05\%$ or 1 fr |
| Irregularity - Interferometer (fringes) | 2 | 0.5 | 0.2 |

Figure 3.12: The tolerance guidelines for prototype optics.

3.4.2 Sensitivity analysis

Once a list of parameters (x_1, x_2, \dots) and tolerances Δx_i is defined, the sensitivity analysis is used to evaluate independently each tolerance. In other words, a small perturbation Δx_i should be applied to each parameter x_i in order to find the corresponding change in the criterion. ZEMAX uses a RSS assumption or a linear difference for computing the estimated changes in the performance. If the Change is computed using RSS Difference, the change due to a tolerance is computed as:

$$\Delta \simeq (P - N)\sqrt{|P^2 - N^2|} \quad (3.10)$$

P is the perturbed criterion and N is the nominal criterion.

The total change can then be computed from a sum over all tolerances of the averaged squared values as follows:

$$C^2 = \sum_i \frac{\Delta_{i,min}^2 + \Delta_{i,max}^2}{2} \quad (3.11)$$

Then the final performance is:

$$F = \sqrt{N^2 + C^2} \quad (3.12)$$

From these information, the sensitivities can be calculated by dividing the change in the criteria by the perturbation.

During Sensitivity analysis, Zemax reports the magnitude of the individual perturbation P, and the corresponding change to the system criterion Δ . The value of the sensitivity analysis is that the tolerances which are too loose will, in general, have greater contributions to the increase in the criterion than other tolerances. This technique allows to identify surfaces which are highly sensitive to certain errors. In conclusion, the sensitivity analysis aids in identification of which tolerances need to be tightened, and which might be loosened. It is also valuable for finding the optimum (and minimum) number of compensators, and the required range of adjustment.

3.4.3 Monte Carlo simulation

Since all the tolerance errors are statistic, the tolerance analysis is done mainly using Monte Carlo analysis. The Monte Carlo simulation generates a set of random error numbers for all the tolerances based on the defined tolerance ranges and the error distribution pattern selected by us. The available distributions are: the normal, uniform, parabolic and user defined statistical distribution. Unlike the sensitivity analysis, the Monte Carlo analysis simulates the effect of all perturbations simultaneously. For each cycle, the compensators are adjusted and then the criterion value, the change in the system performance and compensator values are printed. The Monte Carlo analysis is useful because it indicates the probability that the estimated yield of lenses will meet the required specification.

Chapter 4

MAORY

4.1 E-ELT

E-ELT is the largest optical/near-infrared Nasmyth telescope in the world. First light is targeted for 2024. It will allow to study high redshift galaxies, super-massive black holes, star formation, exoplanets, protoplanetary systems and to make a direct measurement of the acceleration of the Universe expansion.

The diameter of the segmented primary mirror is approximately 39 metres. The wide FoV is 10 arcmin. It is planned to be built by the European Southern Observatory (ESO) on a mountain top in Cerro Armazone, in Chile (the altitude is 3060 meter). The E-ELT optical design (see Figure 4.1) differs from other ELT designs mostly by including adaptive optics into the telescope and providing high spatial resolution. It consists of three mirror on-axis anastigmat (M1, M2, M3) with two flat folding mirrors (M4, M5) providing the AO. M1 is an elliptical $f/0.93$ segmented mirror of 39 m diameter and a 11.1 m central obstruction. The 4.2 m secondary mirror (M2) is convex, the 3.8 m tertiary mirror is mildly aspheric concave. The AO system consists of the 2380×2340 mm quaternary flat adaptive mirror (M4) supported by up to 5910 actuators. M5 is a flat mirror, elliptical in contour, it allows for the final image correction and steers the beam toward the Nasmyth focus. The output beam at $f/17.48$ is very nearly diffraction limited over the entire 10 arcmin FoV.

Two Nasmyth platforms are accommodated by the structure, at either side of the rotatable telescope. Each platform can host several instruments: one of these is MAORY.

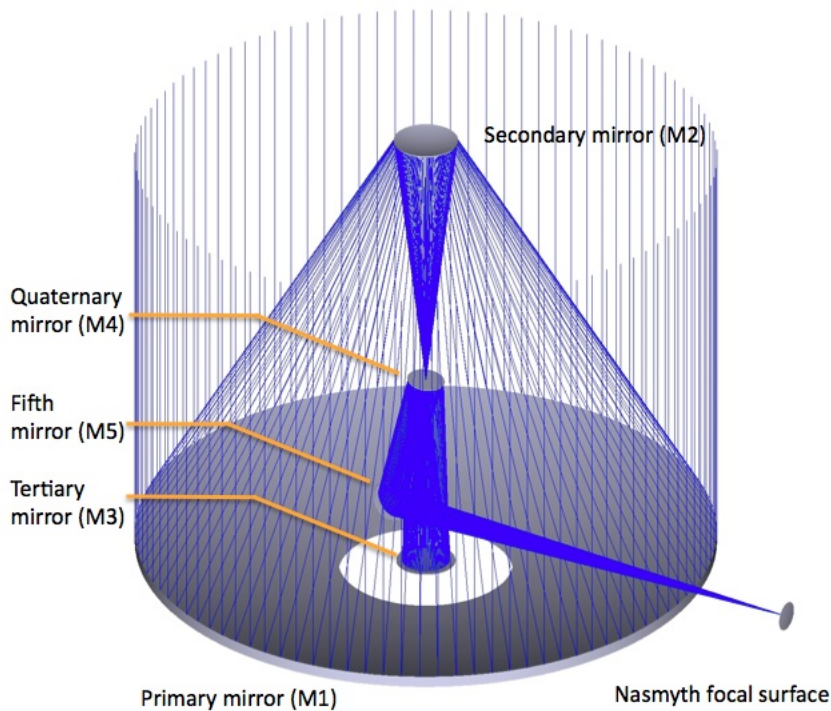


Figure 4.1: Nasmyth configuration of E-ELT.

4.2 MAORY and its issues

MAORY is a first light instrument providing a corrected FoV of up to two arcmin diameter over the wavelength range $0.8\text{-}2.4 \mu\text{m}$.

MAORY Phase A study was carried out by a Consortium led by the OABo, including the Astronomy department of UniBo, OAPd, ONERA and sponsored by ESO. It is a feasibility study. The estimated performance of MAORY at the end of this phase is shown in Figure 4.2: it is expressed in terms of Strehl ratio for different wavelengths and is expected to be approximately 50% at central wavelength of the Ks band ($2.16\mu\text{m}$) averiging over a 1 arcmin field. Phase A concluded in december 2009 and assessed that there were possibilities for some simplification of the optical design. Right now Phase B, that is the preliminary design of MAORY, is carring on and is going to be finish in februar 2018. Then Phase C will consist in the final design review.

MAORY is a post-focal MCAO module for the E-ELT. The instrument will be installed on the E-ELT Nasmyth platform A on the straight-through port and contains an optical relay to re-image the telescope focal plane at the instrument port.

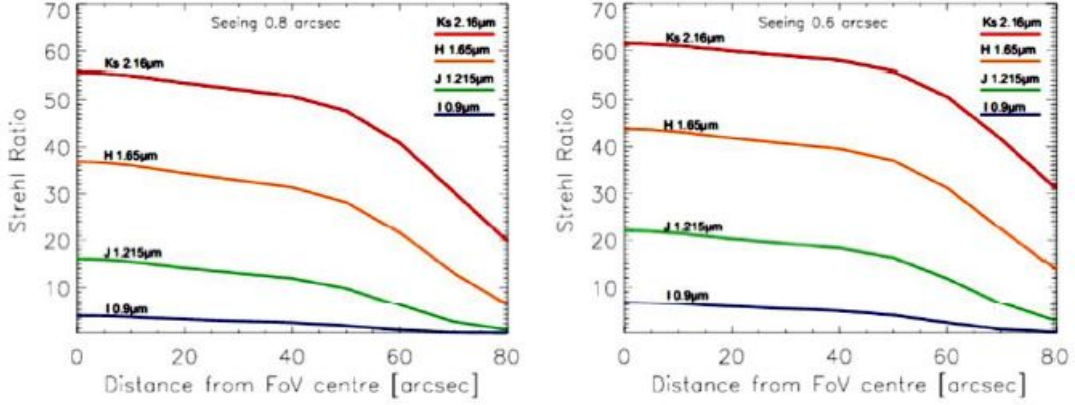


Figure 4.2: The Strehl ratio value as a function of the off-axis for two different seeing values. Data are shown for different wavelength.

The E-ELT high angular resolution camera MICADO (Davies et al., 2010) is a client instrument of MAORY and requires an image correction of high quality and uniformity to perform high accurate photometry and astrometry (Origlia et al., 2010). MAORY has to provide two AO modes to support the NIR camera MICADO:

- The *MCAO mode* is required to achieve uniform AO compensation over the full MICADO FoV. The WF compensation is reached by up to two DMs in MAORY conjugated to different altitudes in the atmosphere, which work together with the telescope adaptive and TT mirrors M4 and M5 respectively. The MCAO technique was successfully demonstrated on-sky by the Multi conjugate Adaptive optics Demonstrator (MAD) on the Very Large Telescope.
- The *SCAO mode* is required for peak performance, rather than uniformity over the field, when a suitable NGS is available. WF distortions are measured by a single NGS WFS and compensated by the telescope M4 and M5 mirrors while the DMs inside MAORY are kept flat.

Moreover, the MCAO mode of MAORY is based on the use of six LGSs for WF sensing and three NGSs detected by SHWFSs. The six LGSs are assumed to be launched from the side of the telescope primary mirror and projected from around the circumference of the telescope primary mirror. This scheme increases the re-imaged spot sizes in the off-axis sub-apertures due to the perspective elongation (see Subsection 2.1.6) but it avoids the so called fraticide effect (see Subsection 2.1.1). MCAO is also the solution to the cone effect (see Subsection 2.1.3). However the

zenith angle effect (see Subsection 2.1.5) is not removed and hence the global shift of the image along the optical axis is compensated by a motion of all six LGS WFSs together. The use of three NGSs are indispensable to solve intrinsic limitations of artificial beacons, such as TT, anisoplanatism and defocus (see Subsections 2.1.2 and 2.1.7).

4.2.1 MAORY requirements

Some MAORY requirements [16] applicable to the LGS Objective design are reported below:

- To deliver the performance required by the MICADO science case, MAORY uses six LGS WFSs and three NGS WFSs.
- Operational range of zenith angles: MAORY shall be capable of observing at zenith angles greater than 1.5° and smaller than 70° .
- The volume of the instrument elements located on the Nasmyth platform shall not exceed the design volume specified in AD5 (Applicable Document: "Standard Coordinate Systems and Basic Conventions" Number ESO-193058 Version 6).

4.2.2 MAORY post-focal relay optical design

In Figure 4.3 MAORY post-focal relay optical design illustrates how the rays propagate through the optical elements: the light comes in from the E-ELT focal plane and is propagated through the MAORY common path optics and the post-focal DMs inside the MCAO module. A dichroic, placed after the post-focal DMs, transmits the LGS light to the WFS ($0.589 \mu m$) and reflects the science light at wavelength longer than $0.589 \mu m$ to MICADO. The WF measurements performed by the LGS and LOR WFSs in the MCAO mode are processed by the MAORY RTC, which drives in closed loop the MAORY post-focal DMs and, through the telescope central control system, the actuators in the telescope.

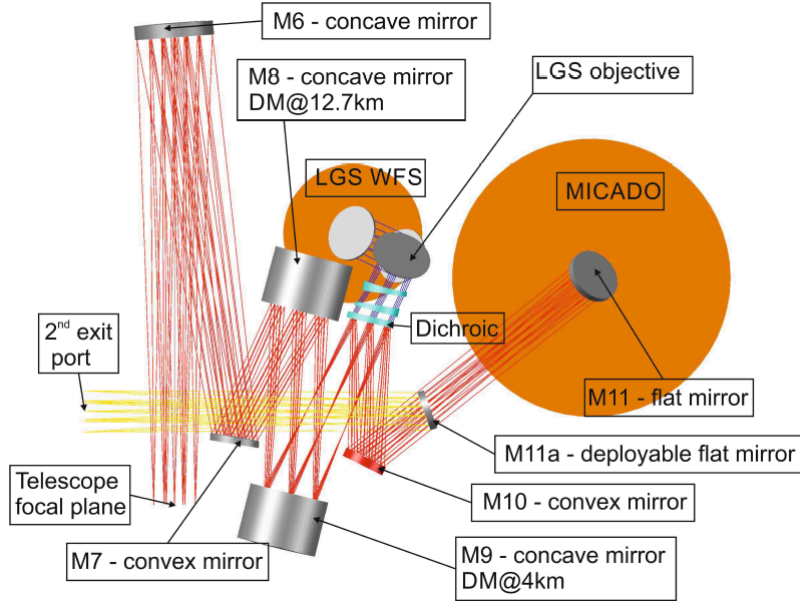


Figure 4.3: MAORY post-focal relay optical design. Red rays: optical beam from telescope focal plane to exit port for MICADO, for scientific purpose. The orange circles are the projection of the design volumes for the LGS WFS and for MICADO.

4.3 The LGS Objective

The LGSs light transmitted by the dichroic ($\lambda < 600 \text{ nm}$) is affected by aberrations introduced by the MAORY mirrors (M6, M7, M8 and M9, see Figure 4.3). Moreover, since during sky tracking the zenith angle changes, the six LGSs launched at the Sodium layer varies their distances from the telescope primary mirror, so the LGSs footprint dimension on the mirrors changes as the zenith angles. As a consequence, the six LGSs at a specific altitude will focus on different points respect to LGSs located at other distances. Those with a shorter focal length will have a greater aberration, those with a longer one, the reverse. These are the reason why an optical system is necessary to correct for aberrations.

The maximum allowable zenith angle of the telescope for MAORY will be 70° and the distances of the LGSs from the telescope primiry mirror, at which they will be launched, scale as the cosin (see Figure 4.4):

$$\cos\xi_{13} = \frac{h_1}{h_3} \quad (4.1)$$

These height range from an altitude of 80 km to one of 240 km . This roto-traslational motion of the LGSs launched in the Sodium layer is illustrated in Figure 4.5: ξ is the zenith angle and the z-axis represents the altitude.

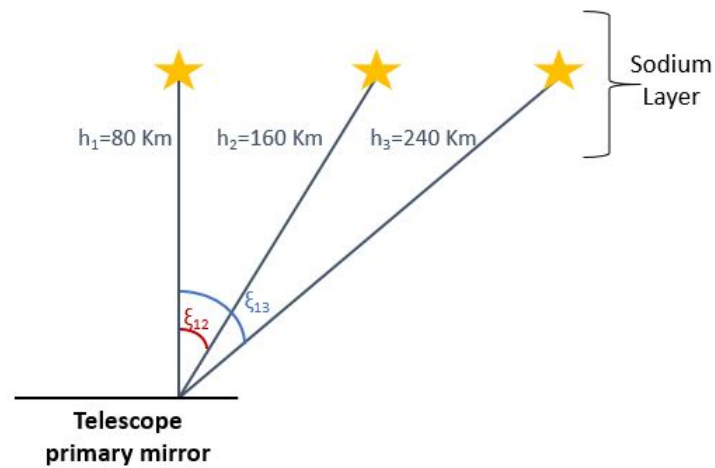


Figure 4.4: A schematic view of a LGS launched in the Sodium layer at different zenith angle, that is, at different distances from the telescope primary mirror. The minimum distance is 80 km, the maximum allowable one is 240 km.

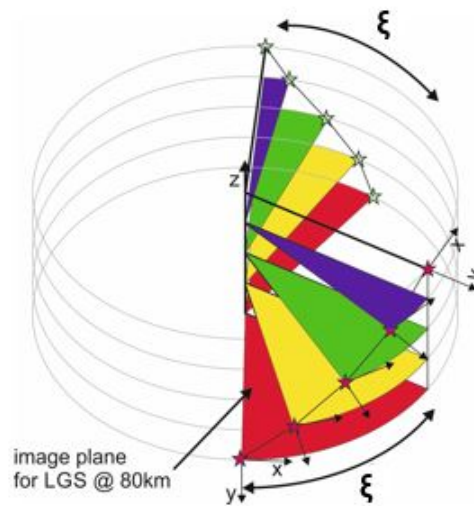


Figure 4.5: The roto-translational motion of the LGSs launched in the Sodium layer: ξ is the zenith angle and the z-axis represents the altitude.

As a result of some simulations in median conditions, it has been noticed that the best AO performance is achieved over a radius of $45''$ FoV. This is the reason why the six LGSs will be launched over a $45''$ FoV.

Hence the LGS Objective for MAORY (see Figure 4.3) is being designed to correct for aberrations.

As is known, on a large diameter telescope the mean Sodium altitude variation has an important effect on the WFE. In the case of the 40 meter telescope every meter of change of the Sodium layer mean altitude translates into $\sim 7nm$ of defocus (RMS WFE). Furthermore, if the laser is launched by the telescope no tilt signal would be measured because the TT contribution due to the LGS actual position can not be disentangled from the TT contribution due to the atmospheric turbulence. Hence a fast NGS WFS measuring the low-order aberration, that is, TT, Defocus and also Astigmatism is required (Schreiber L. et al). Once the measure is done then the corrections are applied to the DMs together with the correction given by the LGSs. Interesting techniques have been proposed to mix the focus measurements provided by LGS and NGS (G. Herriot et al).

4.3.1 Client requirements for the LGS Objective

The client requirements¹ decided inside MAORY consortium are listed below:

- $f/5$ to reduce LGS focus range variation and reduce the motion of the WFSs. It means that the focus aperture must be $1/5$ rad. In fact the focus range varies quadratically with the $f_{\#}$.
- Exit pupil at infinity to avoid pupil diameter variations with zenith angle.
- Exit pupil quality to avoid reducing AO performance: the image must be round. The rule of thumbs states that the exit pupil must be $1/10$ of D_t .
- Reduction of aberrations.

The optical design will be discussed in the next chapter.

¹A client requirement is different from a customer requirement. The last one is decided by ESO.

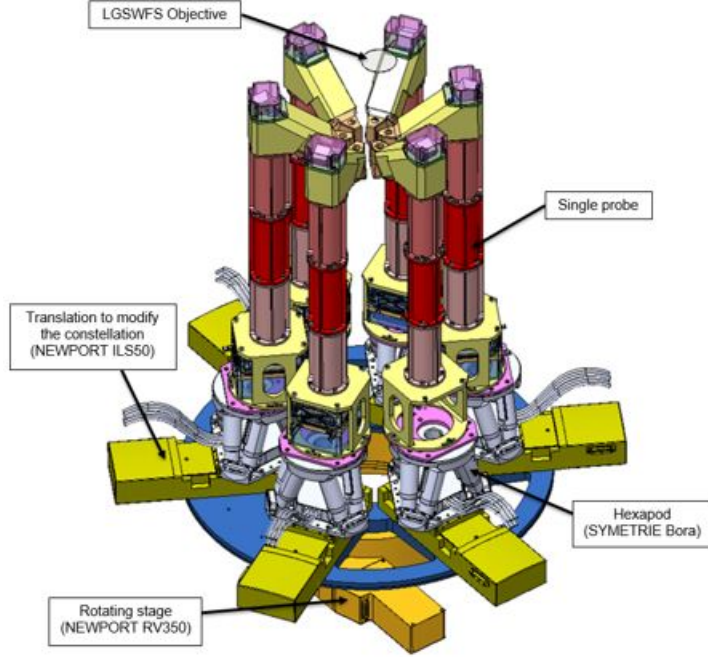


Figure 4.6: LGS WFS baseline current design.

4.4 LGS WFS

The LGS WFS measures the WF aberrations due to atmospheric turbulence and other effects. Because of well-known limitations of LGSs, measurements from NGSs are required as well: these additional measurements are provided by the NGS WFS. The data produced by the cameras of the LGS WFS and of the NGS WFS are collected by the MAORY RTCs, which drives the DMs (i.e. the telescopes M4/M5 adaptive/TT mirrors) and two post-focal DMs inside MAORY itself. All the WFSs in MAORY are placed downstream the DMs ensuring optical feedback.

The operational wavelength is $0.589\mu\text{m}$. The WFS type is the SHWFS (see Section 1.7). The 6 LGSWFS units are in on-sky hexagonal geometry. Figure 4.6 shows the current mechanical design for LGS WFS. The global shift of the image along the optical axis, due to the variation of the Sodium layer distance with the Zenith angle, is compensated by a motion of all six LGS WFSs together.

The current choice of the LGS WFS FoV is $15''$. The detector size is 800×800 pixels, the pixel size is $24\mu\text{m}$, the number of sub-apertures is 80×80 , the number of pixels per sub-aperture is 10×10 and the E-ELT sub-aperture size is 0.482 m . An $8 \times 8/10 \times 10$ sub-apertures WFS running at $0.2/0.1$ frame per second seems to

lead to an acceptable WFE, already allocated in the global MAORY error budget (reference). The choice of $\geq 10''$ LGS WFS FoV implies the need of sub-sampling the LGS image and so to foresee some trick to recover a good spot resolution for slope measurement.

4.4.1 Sodium layer features and spot truncation: impact on MAORY performance

Since the Sodium layer is characterized by non-negligible thickness, the artificial reference source looks elongated, especially when observed from the edge of a large aperture. Considering a circular aperture of diameter $D=38.542$ m and a SH having 80 sub-apertures across the diameter, the worst case in terms of elongation is represented by the sub-aperture at ~ 19 m from the pupil center and the Laser Launching Facility positioned at $(21.5+2)$ m along the diameter aligned with the SH sub-apertures.

The image elongation spans a range that could exceed $20''$. In order to avoid severe spot truncation, the LGS image in a sub-aperture at the edge of the pupil needs a FoV of at least $10''$. This FoV implies anyway spot truncation that has an impact on the MAORY performance. In the current baseline, this impact is mitigated by the Reference channel in the NGS Low Order & Reference WFS.

The combination of the dynamics of the sodium layer both regarding its centroid altitude variation and its thickness/profile variation including sporadic events with the truncation of the LGS images on the LGS WFS due to the finite SH sub-apertures FoV, may cause the introduction of spurious WF aberrations only due to the Sodium layer and that have no relation with the WF aberrations due to atmospheric turbulence that the AO system should compensate.

In this context, the trade-off among detector size, detector alignment (respect to LGS launching angle), LGS image sampling, LGS WFS FoV and opto-mechanical LGS WFS design complexity and performance, need to be carefully assessed. (L. Schreiber)

Chapter 5

LGS Objective design

The goal of this thesis is to design the LGS Objective, optimize and perform the tolerance analysis for the LGS Objective of MAORY. The mechanical constraints and the variations of the aberrations with the zenith and azimuthal angle are taken into account. The number of optical surfaces has been minimized keeping the LGS Objective client requirements satisfied (see Subsection 4.3.1). Moreover, the residual aberrations of the LGSs have been kept as small as possible in order to reach the performance requirements of MAORY (see Subsections 4.2.1). The procedure, which has led to this, has been divided in four different parts and will be discussed in the next sections:

1. LGS Objective design.
2. LGS Objective local and global optimization.
3. The aberrations analysis of the LGS Objective.
4. LGS Objective tolerancing.

The software Zemax has been used for this purpose.

Three Configurations and several Fields for each Configuration have been chosen. From here on "Configuration 1" indicated that the six LGSs are at an altitude of 80 km from the telescope primary mirror, "Configuration 2" at an altitude of 160 km and "Configuration 3" at an altitude of 240 km (see Section 4.3). In other words Configuration 1 means that the LGSs are launched at a zenith angle of 0° , Configuration 2 at a zenith angle of about 60° and Configuration 3 at a zenith angle of about 70° .

As regards the Fields ¹, they cover a circumference of maximum radius of about 0.0167° , which corresponds to $1'$. The dimensions of the optical components have been designed for these Fields, giving more weight to $45''$ where the AO performance over the full MICADO FoV is better (see Section 4.3).

Table 5.1 describes the X and Y-Field angles which have been used during optimization and tolerancing.

A wavelength of $0.589 \mu m$ has been used.

| Field | α_x [deg] | α_y [deg] |
|-------|------------------|------------------|
| 1 | 0 | 0 |
| 2 | 0.0125 | 0 |
| 3 | 0.008833 | 0.008833 |
| 4 | 0 | 0.0125 |
| 5 | -0.008833 | 0.008833 |
| 6 | -0.0125 | 0 |
| 7 | -0.0088 | -0.0083 |
| 8 | 0 | -0.0125 |
| 9 | 0.0083 | -0.0083 |
| 10 | 0 | -0.0167 |
| 11 | 0 | -0.0167 |
| 12 | -0.0167 | 0 |

Table 5.1: Normalized Field angles: α_x is the X-Field angle and α_y is the Y-Field angle, being the Z-axis the optical axis. Field 1 corresponds to the centre of the normalized coordinate field, Fields 2, 3, 4, 5, 6, 7, 8 and 9 cover a circumference of radius $45''$ (0.0125°) and Fields 10, 11 and 12 cover a circumference of radius $1'$ (0.0167°) giving to them a minor weight respect to the other fields during optimization.

¹Field points are specified as angles in degrees. The angles are measured with respect to the object space and the paraxial entrance pupil position on the object space. Positive field angles imply positive slope for the ray in that direction, and thus refer to negative coordinates on distant objects.

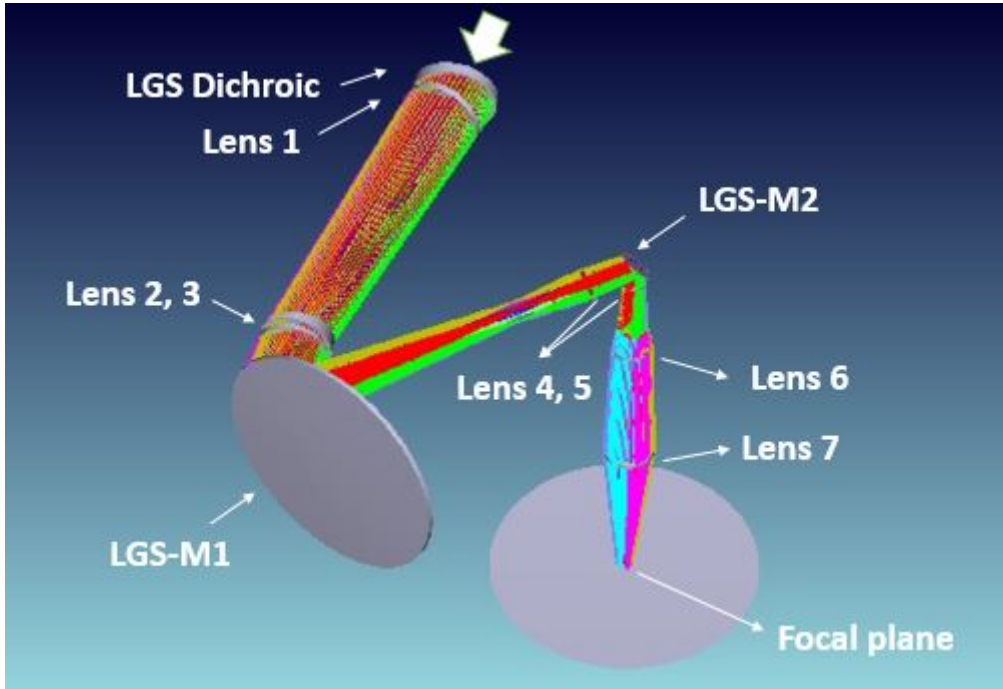


Figure 5.1: The optical design of the LGS Objective. Table 5.2 describes the specifics of each elements.

5.1 The LGS Objective optical design

Coming back to Section 4.3, the reason why the LGS Objective is being designed is to correct for aberrations introduced by the MAORY mirrors (M6, M7, M8 and M9) and by the variation of the LGSs distances from the primary mirror as the zenith angle changes.

The LGS Objective is intended to focus the light of the LGS for the LGS WFSs. Figure 5.1 illustrates the optical design of the LGS Objective. It consists of mirrors, lenses and a dichroic beam-splitter (hereafter Dichroic) for separation of the LGS light. The LGS light transmitted by the LGS Dichroic propagates through the LGS path optics and then to the LGS WFSs (see Section 4.4). The WFSs are not part of this study.

As regards the LGS path optics, a detailed description of the refractive and reflective elements with their specifications is reported in Table 5.2. It has been designed by taking into account the client requirements and the cost. However, the introduction of refracting elements may solve one problem but at the expense of arising others. The material for the refractive elements is BK7.

| ID | Diameter [mm] | Thickness [mm] | Shape [mm] | Conic constant [1] | Wedged |
|-------------------------|------------------|-------------------|--------------------|--------------------------|--------|
| LGS Dichroic | 600 | 89 | flat | - | yes |
| Lens 1 | 600 | 67 | plano- convex | - hyperbolic | yes |
| Lens 2 | 550 | 59 | plano- concave | - spherical | yes |
| Lens 3 | 520 | 57 | convex- plano | elliptical - | yes |
| LGS-M1 | 530 | - | concave | spherical | - |
| Lens 4 | 340 | 40 | convex- convex | spherical hyperbolic | yes |
| LGS-M2 | 380 | - | flat | - | - |
| Lens 5 | 170 | 20 | convex- concave | elliptical elliptical | - |
| Lens 6 | 280 | 48 | concave- convex | spherical elliptical | - |
| Lens 7 | 380 | 63 | convex- convex | hyperbolic hyperbolic | - |

Table 5.2: The specifics of the LGS Objective refractive elements. When two values are contained inside a single row, they refer to the front and rear surface of the optical element.

5.2 Optimization

First of all, local and then global optimization using DLS algorithm (see Subsection 3.3.1) has been made for these three Configurations to improve or modify the design in order to meet specific conditions. So a MT function (see Subsection 3.3.3) has been specified for some components during the implementation of the Objective:

- The admitted space and the clearance between the optical elements.
- The curvature radius of the optical components, $\frac{1}{R}$: greater than $\frac{4}{5}$ in order to be feasible and less costly.
- The thickness value: between $\frac{1}{10}$ and $\frac{1}{7}$ of the element diameter for manufacturing reasons.

- The conic value: between 0 and -10. The conic constant is less than -1 for hyperbolas, -1 for parabolas, between -1 and 0 for ellipses, 0 for spheres, and greater than 0 for oblate ellipsoids. The last one has to be avoided because it is much more difficult to be tested than the other one.
- The focal aperture: $f/5$ to reduce LGS focus range variation and reduce the motion of the six WFSs. It means that the focus aperture must be $1/5$ rad. In fact the focus range varies quadratically with the $f_{\#}$.
- The exit pupil shape: round to avoid reducing AO performance. In fact the WFS will be calibrated with a circular shape. The rule of thumbs states that the exit pupil must be $1/10$ of D_l (D_l is the diameter of the sub-aperture).
- Exit pupil: at infinity to avoid pupil diameter variations with zenith angle.

These constraints and some parameters of LGS Objective, such as thickness, conic, curvature radius of elements, has been freed in order to run optimization.

Optimization has been executed several times until the client requirements of the LGS Objective and the MAORY requirements have been reached.

Exit pupil

Referring to the client requirements in Subsection 4.3.1, the roundness of the exit pupil has been verified with the software Zemax. Since the exit pupil is at infinity, the $f_{\#}$ is the same for all the Configurations and the roundness of a Configuration is the same of the other one. The reason why such a choice has been made is to measure correctly the whole and the same WF. By using normalized Field coordinates on a unit circle, it has been checked that a round image is formed within $1/10$ of sub-aperture.

5.3 Aberrations analysis

It is important to remember that the aberrations increase as $f_{\#}$ decreases. Since the science path takes priority over the LGS Objective, its requirement is an $f/17$, which is very different from the LGS path one, $f/5$. The aberrations of the science path are corrected by means of a mirror, whereas those of the LGS path are corrected by locating specific types of lenses or mirrors after the LGS Dichroic as already shown in Table 5.2. Hence after the Dichroic, in the LGS path, the aberrations introduced by the MAORY mirrors (M6, M7, M8 and M9) are still very high. In the following sections the RMS WFE and the Zernike coefficients after the Dichroic will be shown. The reduction of these aberrations is one of the

LGS Objective purpose, so a study of the RMS WFE and the Zernike coefficients on the image plane will be also presented.

5.3.1 Aberrations after the LGS Dichroic

The analysis of the aberrations has been carried out for each Configuration. Firstly, the aberrations after the LGS Dichroic has been taken under study, which is the starting point of the LGS Objective design. So a paraxial lens has been placed after the LGS Dichroic to focus the rays coming from each Configuration.

If all the rays were well within the Airy disk, then the system would be said to be "diffraction limited". But, in all the Configurations the RMS spot radius (see subsection 3.1.5) is significantly larger than the Airy disk radius, then the system is not diffraction limited. In fact in the first Configuration the Airy disk is $1.296 \mu m$, in the second one is $1.322 \mu m$ and in the third one is $1.331 \mu m$, while the RMS spot radius of all three Configurations is larger than these values (the spot diagrams are not reported).

RMS WFE

In Figures 5.2, 5.3 and 5.4 the RMS WFE is plotted in function of the Y-Field for each of the three Configurations respectively. For Configuration 1 (80 km) the mean value of the RMS WFE over all the Fields is about 67.84 wave (39961.84 nm) with a standard deviation of 0.57 wave, for Configuration 2 (160 km) is about 56.87 wave (33495.32 nm) with a standard deviation of 0.53 wave, for Configuration 3 (240 km) is about 52.86 wave (31131.89 nm) with a standard deviation of 0.48 wave.

The RMS WFE value after the LGS Dichroic is very high over all the Fields. It decreases as the fields angle increases.

Zernike coefficients

The Zernike coefficients for each Field (see Table 5.1) and Configurations are shown in Tables 5.3, 5.4 and 5.5.

It is evident that astigmatism is the main aberration introduced after the LGS Dichroic. Configuration 1 (80 km) shows more astigmatism than the other two. All the three Configurations suffer from SA, coma, defocus and astigmatism as one can better see in the Zernike coefficients below.

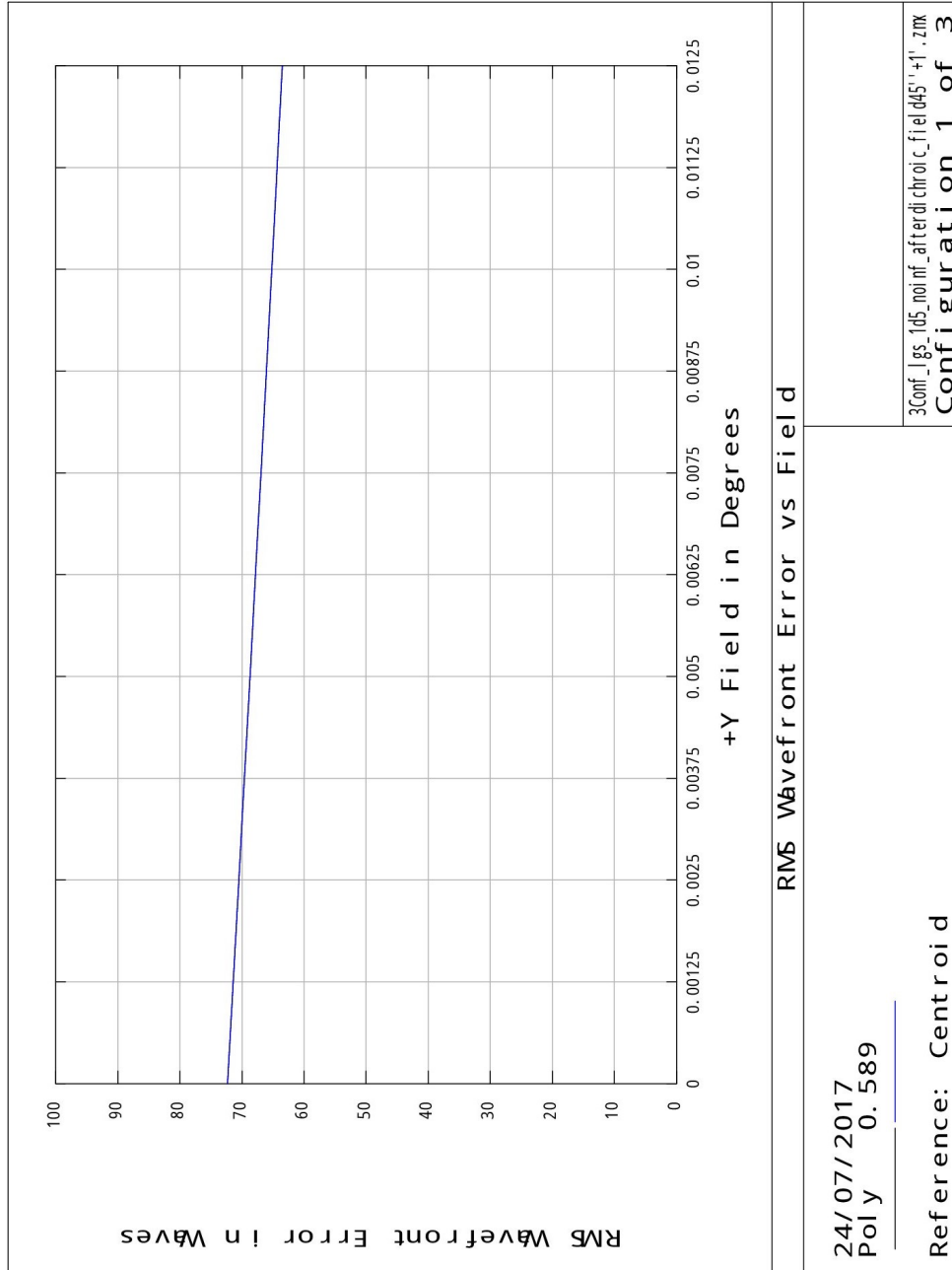


Figure 5.2: The RMS WFE vs. Field after the LGS Dichroic for Configuration 1.

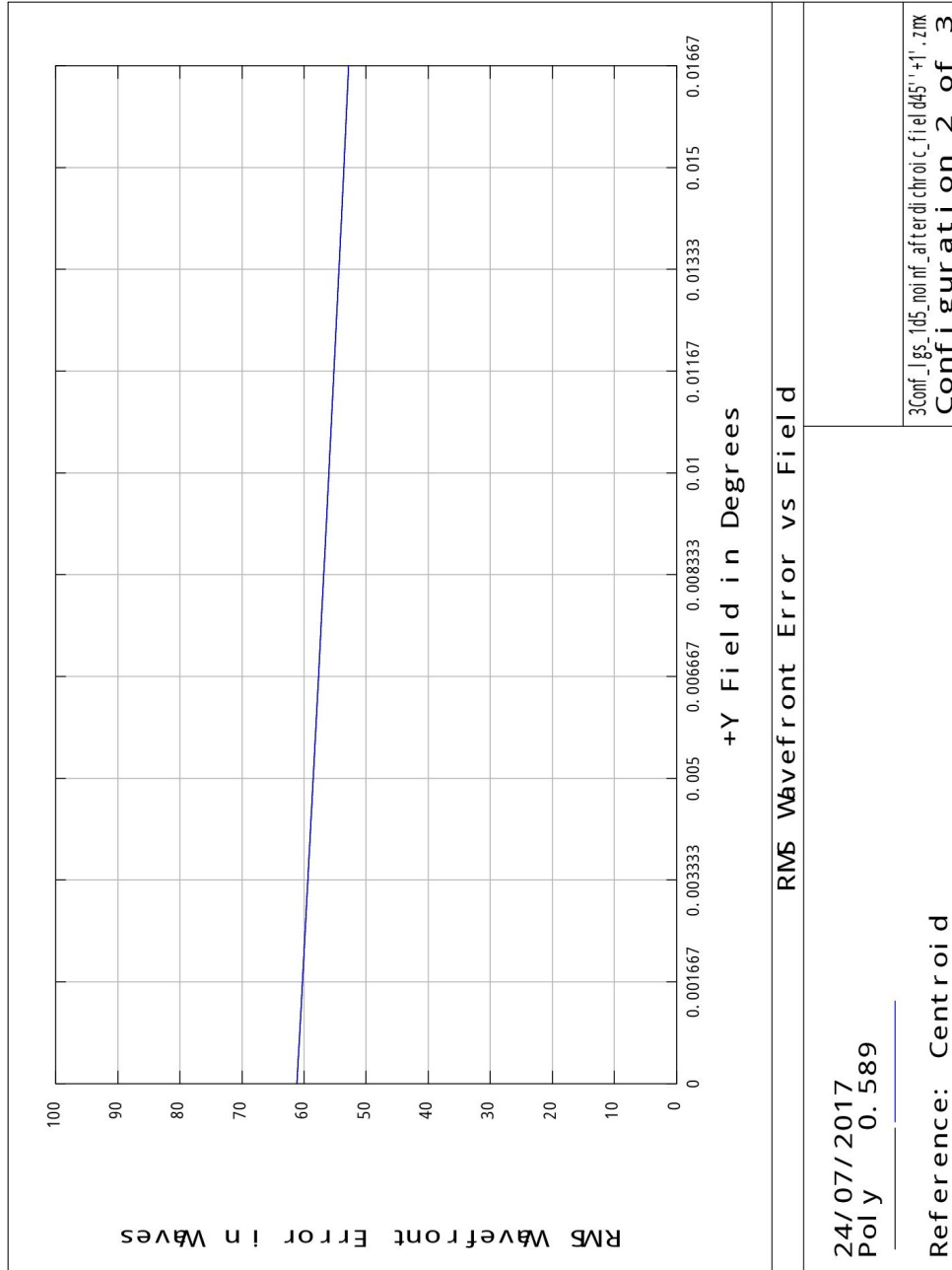


Figure 5.3: The RMS WFE vs. Field after the LGS Dichroic for Configuration 2.

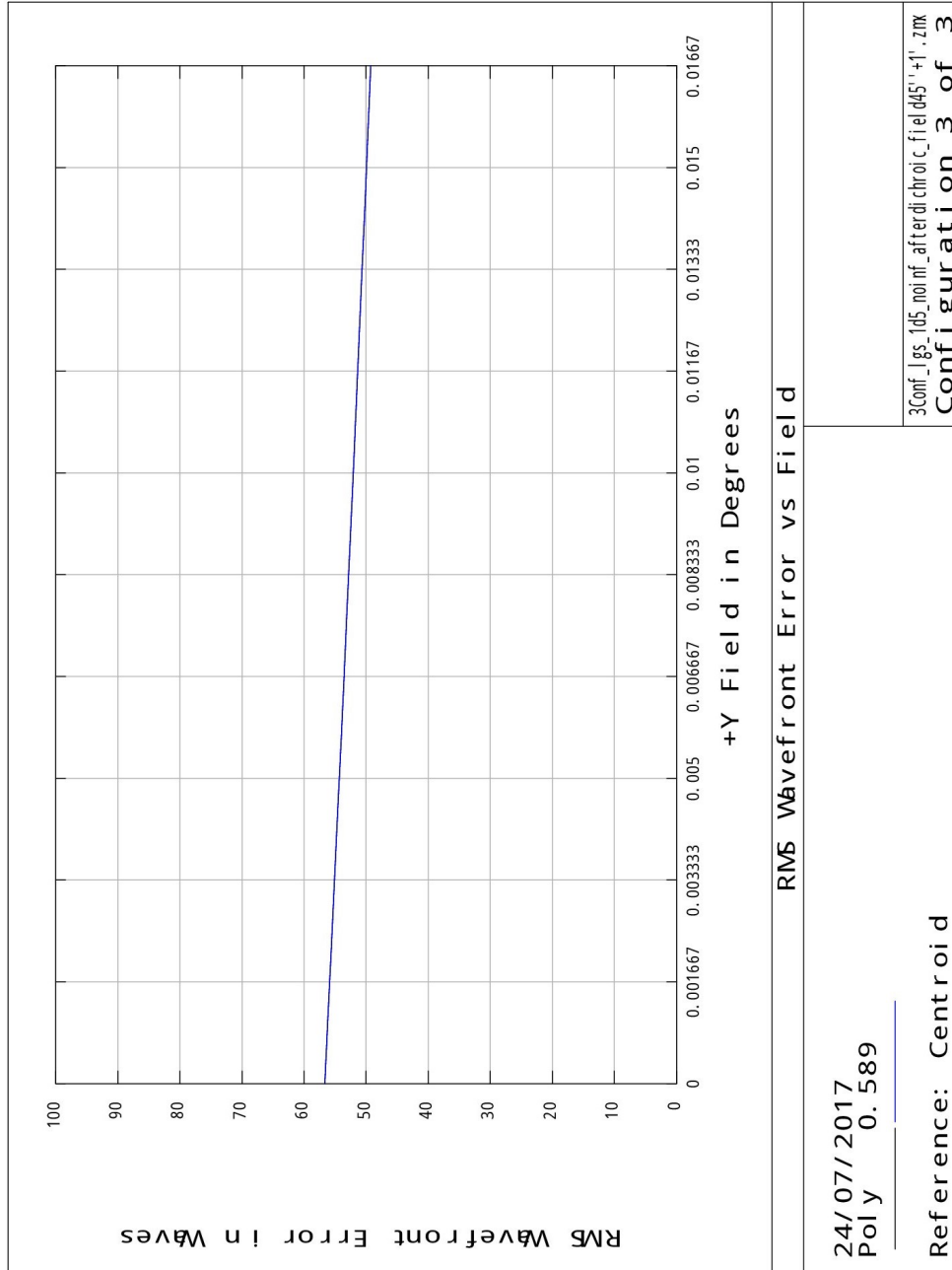


Figure 5.4: The RMS WFE vs. Field after the LGS Dichroic for Configuration 3.

| Configuration 1 | | | | | | | |
|------------------------|---------|------------|---------|------------|---------|---------|---------|
| Field | Z_2^2 | Z_3^{-1} | Z_3^1 | Z_3^{-3} | Z_3^3 | Z_4^0 | Z_4^2 |
| 1 | -72.258 | -3.072 | 0 | 0.232 | 0 | 0.420 | 0.79 |
| 2 | -71.954 | -3.062 | 0.568 | 0.244 | 0.088 | 0.419 | 0.786 |
| 3 | -65.803 | -2.762 | 0.397 | 0.277 | 0.050 | 0.416 | 0.716 |
| 4 | -63.449 | -2.639 | 0 | 0.285 | 0 | 0.415 | 0.689 |
| 5 | -65.804 | -2.762 | -0.397 | 0.277 | -0.051 | 0.416 | 0.716 |
| 6 | -71.954 | -3.062 | -0.568 | 0.244 | -0.088 | 0.419 | 0.786 |
| 7 | -78.397 | -3.351 | -0.406 | 0.189 | -0.075 | 0.422 | 0.861 |
| 8 | -81.821 | -3.497 | 0 | 0.153 | 0 | 0.424 | 0.901 |
| 9 | -78.414 | -3.352 | 0.383 | 0.188 | 0.071 | 0.422 | 0.861 |
| 10 | -85.177 | -3.636 | 0 | 0.12 | 0 | 0.425 | 0.94 |
| 11 | -71.717 | -3.054 | 0.757 | 0.253 | 0.116 | 0.419 | 0.783 |
| 12 | -71.717 | -3.054 | -0.757 | 0.253 | -0.116 | 0.419 | 0.783 |

Table 5.3: The Zernike coefficients after the LGS Dichroic for each Field and Configuration 1 of the LGS Objective. See Tables 3.9 and 5.1 for an explanation of the Zernike coefficients and for the correspondence between the field angles and the field numbers.

| Configuration 2 | | | | | | | |
|------------------------|---------|------------|---------|------------|---------|---------|---------|
| Field | Z_2^2 | Z_3^{-1} | Z_3^1 | Z_3^{-3} | Z_3^3 | Z_4^0 | Z_4^2 |
| 1 | -61.099 | -1.180 | 0 | 0.053 | 0 | 0.262 | 0.646 |
| 2 | -60.827 | -1.172 | 0.367 | 0.0629 | 0.098 | 0.262 | 0.643 |
| 3 | -56.656 | -1.028 | 0.256 | 0.112 | 0.061 | 0.259 | 0.597 |
| 4 | -54.754 | -0.957 | 0 | 0.132 | 0 | 0.258 | 0.577 |
| 5 | -56.407 | -1.019 | -0.256 | 0.115 | -0.061 | 0.259 | 0.595 |
| 6 | -60.827 | -1.172 | -0.367 | 0.063 | -0.098 | 0.262 | 0.643 |
| 7 | -65.579 | -1.323 | -0.262 | -0.004 | -0.079 | 0.264 | 0.694 |
| 8 | -68.139 | -1.399 | 0 | -0.044 | 0 | 0.266 | 0.722 |
| 9 | -65.881 | -1.332 | 0.247 | -0.008 | 0.075 | 0.265 | 0.698 |
| 10 | -52.792 | -0.883 | 0 | 0.155 | 0 | 0.256 | 0.555 |
| 11 | -60.615 | -1.166 | 0.488 | 0.070 | 0.130 | 0.262 | 0.641 |
| 12 | -60.615 | -1.166 | -0.488 | 0.070 | -0.130 | 0.262 | 0.641 |

Table 5.4: The Zernike coefficients after the LGS Dichroic for each Field and Configuration 2 of the LGS Objective. See Tables 3.9 and 5.1 for an explanation of the Zernike coefficients and for the correspondence between the field angles and the field numbers.

| Configuration 3 | | | | | | | |
|------------------------|---------|------------|---------|------------|---------|---------|---------|
| Field | Z_2^2 | Z_3^{-1} | Z_3^1 | Z_3^{-3} | Z_3^3 | Z_4^0 | Z_4^2 |
| 1 | -56.621 | -0.732 | 0 | 0.003 | 0 | 0.221 | 0.589 |
| 2 | -56.378 | -0.725 | 0.316 | 0.012 | 0.098 | 0.221 | 0.587 |
| 3 | -52.665 | -0.614 | 0.221 | 0.0644 | 0.0617 | 0.219 | 0.547 |
| 4 | -50.974 | -0.56 | 0 | 0.087 | 0 | 0.217 | 0.528 |
| 5 | -52.444 | -0.607 | -0.22 | 0.068 | -0.061 | 0.218 | 0.544 |
| 6 | -56.378 | -0.725 | -0.316 | 0.012 | -0.098 | 0.221 | 0.587 |
| 7 | -60.615 | -0.841 | -0.225 | -0.057 | -0.078 | 0.223 | 0.631 |
| 8 | -62.81 | -0.9 | 0 | -0.098 | 0 | 0.224 | 0.655 |
| 9 | -60.884 | -0.848 | 0.213 | -0.062 | 0.075 | 0.223 | 0.634 |
| 10 | -49.228 | -0.502 | 0 | 0.112 | 0 | 0.216 | 0.509 |
| 11 | -56.189 | -0.719 | 0.420 | 0.019 | 0.130 | 0.221 | 0.585 |
| 12 | -56.189 | -0.719 | -0.420 | 0.019 | -0.130 | 0.221 | 0.585 |

Table 5.5: The Zernike coefficients after the LGS Dichroic for each Field and Configuration 3 of the LGS Objective. See Tables 3.9 and 5.1 for an explanation of the Zernike coefficients and for the correspondence between the field angles and the field numbers.

5.3.2 Aberrations on the image plane

The LGS Objective is intended to reduce aberrations. So an analysis of the aberrations on the LGS Objective focus plane is discussed now in order to highlight that this goal is reached.

RMS WFE

In Figures 5.5, 5.6 and 5.7 the RMS WFE (see Section 1.9) is plotted in function of all the Fields (see Table 5.1) for Configuration 1, 2 and 3 respectively.

By comparing the RMS WFE after the Dichroic with that on the image plane of the LGS Objective, one can see that now the system is nearly diffraction limited and the RMS WFE value is decreased. For Configuration 1 the mean value of the RMS WFE over all the Fields is about 0.345 wave (203 nm) with a standard deviation of 6e-3 wave, for Configuration 2 is about 0.206 wave (121 nm) with a standard deviation of 0.013 wave, for Configuration 3 is about 0.263 wave (155 nm) with a standard deviation of 0.018 wave.

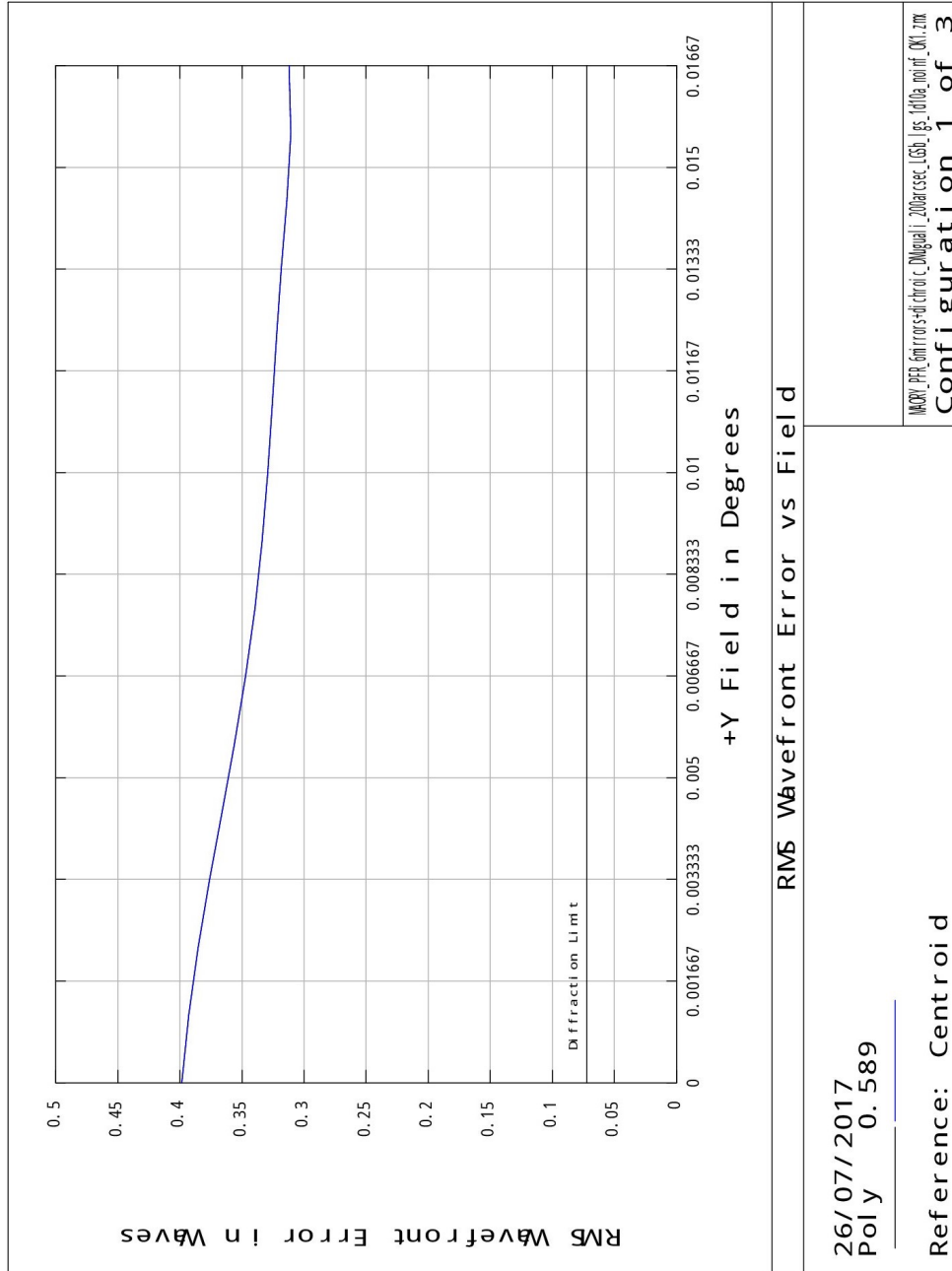


Figure 5.5: The RMS WFE vs. Field in the focal plane of Configuration 1.

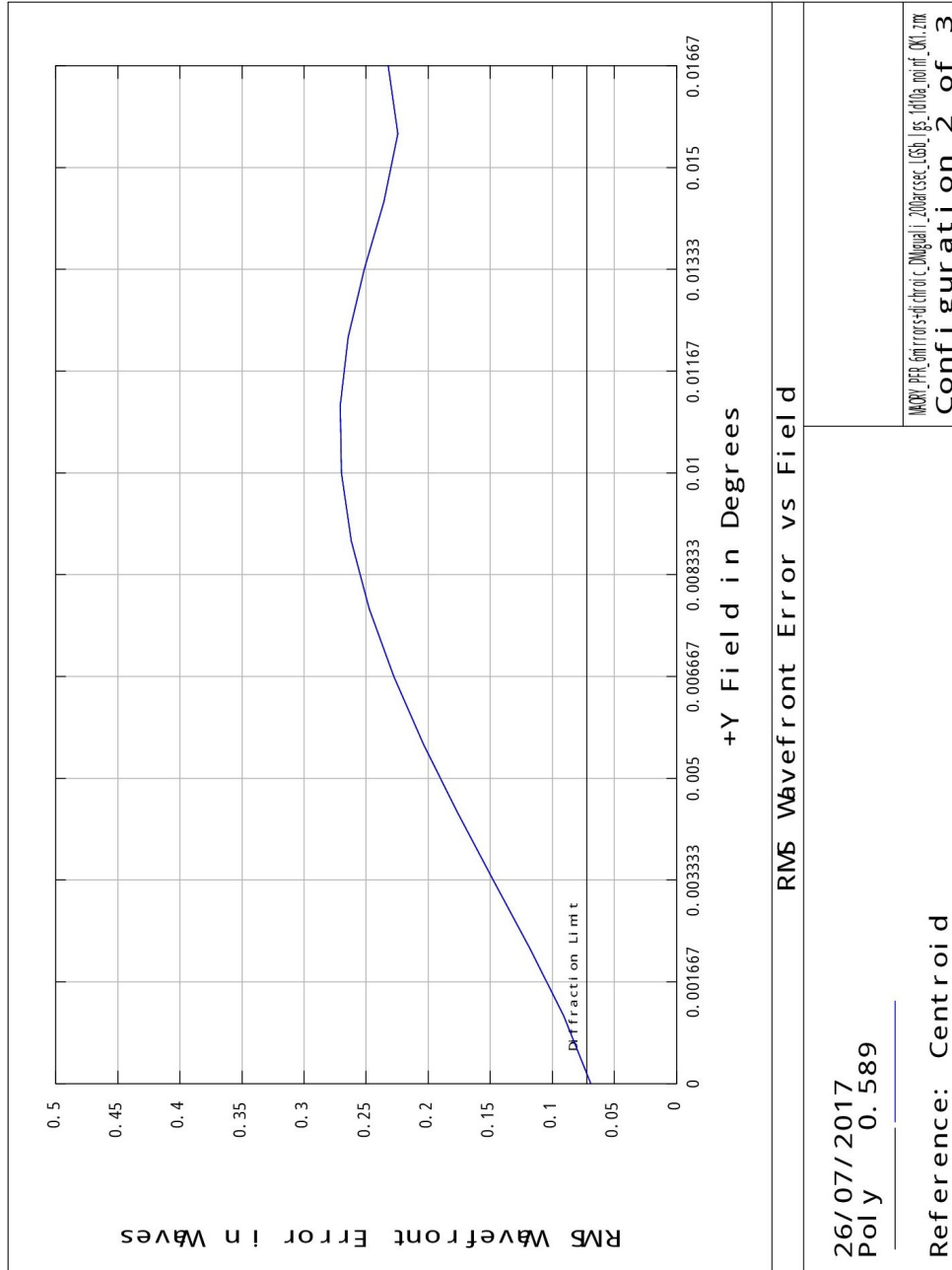


Figure 5.6: The RMS WFE vs. Field in the focal plane of Configuration 2.

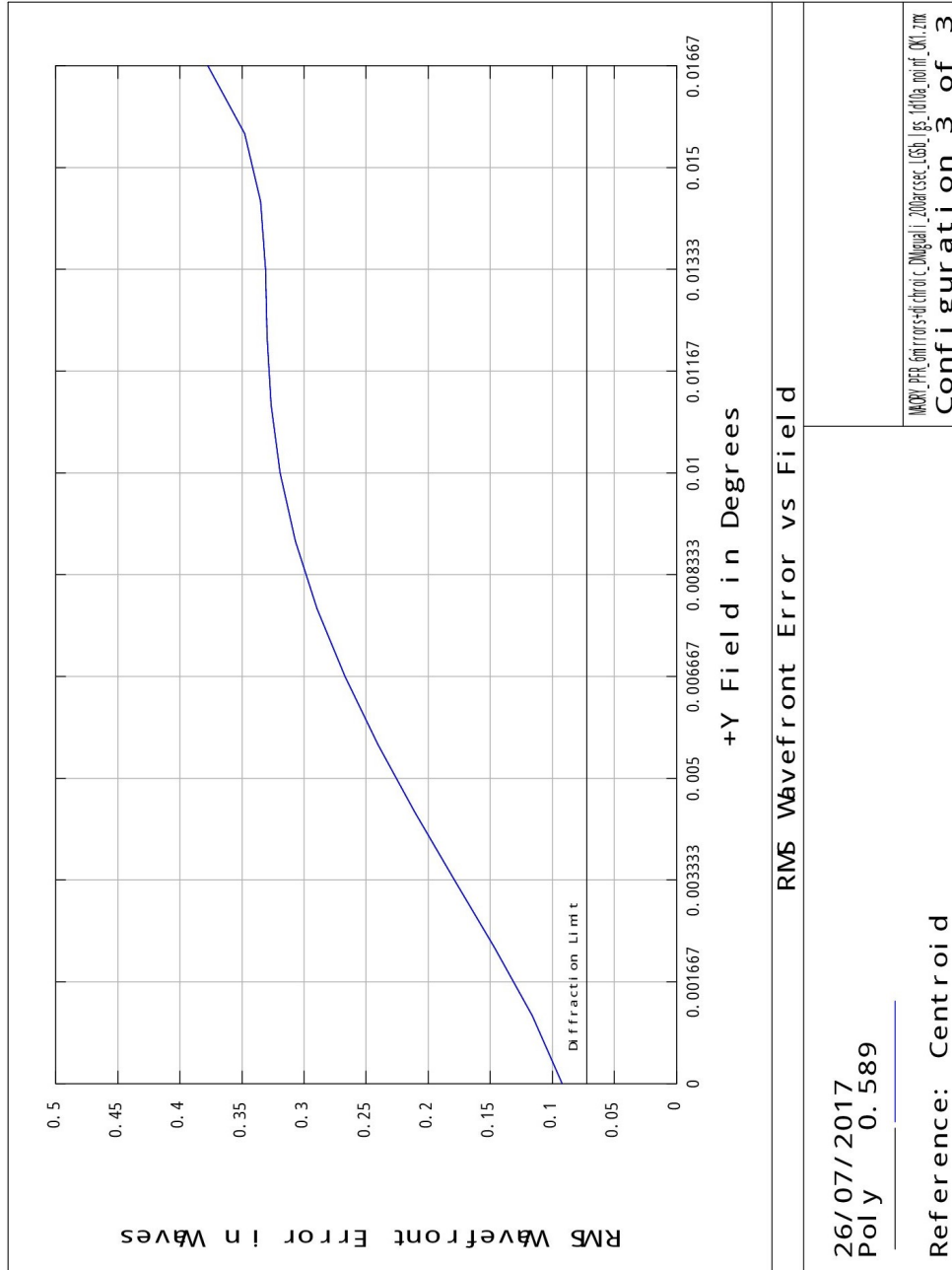


Figure 5.7: The RMS WFE vs. Field in the focal plane of Configuration 3.

Zernike coefficients

Table 5.8 lists the Zernike coefficients of the LGS Objective on the image plane. The main result is that astigmatism has been reduced. Hence, the client requirement discussed in Subsection 4.3.1 is achieved.

| Configuration 1 | | | | | | | |
|------------------------|---------|------------|---------|------------|---------|---------|---------|
| Field | Z_2^2 | Z_3^{-1} | Z_3^1 | Z_3^{-3} | Z_3^3 | Z_4^0 | Z_4^2 |
| 1 | 0.15 | 0.014 | 0 | 0.015 | 0 | 0.353 | 0.017 |
| 2 | 0.035 | 0.007 | -0.045 | 0.008 | -0.055 | 0.291 | 0.093 |
| 3 | 0.01 | 0.076 | 0.04 | 0.012 | 0.002 | 0.286 | 0.024 |
| 4 | -0.011 | -0.114 | 0 | 0.039 | 0 | 0.279 | -0.054 |
| 5 | 0.002 | -0.078 | 0.037 | -0.012 | -0.006 | 0.283 | 0.02 |
| 6 | 0.035 | 0.007 | 0.046 | 0.008 | 0.055 | 0.291 | 0.093 |
| 7 | 0.052 | 0.092 | 0.029 | 0.033 | 0.0028 | 0.297 | 0.015 |
| 8 | 0.048 | 0.129 | 0 | -0.012 | 0 | 0.299 | -0.06 |
| 9 | 0.065 | 0.095 | -0.034 | 0.0303 | -0.005 | 0.301 | 0.015 |
| 10 | 0.001 | -0.083 | 0 | 0.092 | 0 | 0.261 | -0.139 |
| 11 | -0.1567 | 0.001 | 0.02 | 0.002 | -0.117 | 0.277 | 0.18 |
| 12 | -0.157 | 0.001 | -0.02 | 0.002 | 0.117 | 0.277 | 0.18 |

Table 5.6: The Zernike coefficients for each Field and Configuration 1 of the LGS Objective. See Tables 3.9 and 5.1 for an explanation of the Zernike coefficients and for the correspondence between the field angles and the field numbers.

| Configuration 2 | | | | | | | |
|------------------------|---------|------------|---------|------------|---------|---------|---------|
| Field | Z_2^2 | Z_3^{-1} | Z_3^1 | Z_3^{-3} | Z_3^3 | Z_4^0 | Z_4^2 |
| 1 | 0.023 | -0.042 | 0 | 0.022 | 0 | 0.049 | -0.001 |
| 2 | -0.036 | -0.035 | -0.083 | 0.03 | 0.012 | -0.082 | 0.054 |
| 3 | -0.055 | -0.157 | -0.056 | 0.041 | 0.006 | -0.086 | 0.006 |
| 4 | -0.045 | -0.203 | 0 | 0.05 | 0 | -0.095 | -0.05 |
| 5 | -0.058 | -0.156 | 0.053 | 0.041 | -0.006 | -0.091 | 0.004 |
| 6 | -0.036 | -0.035 | 0.083 | 0.03 | -0.012 | -0.082 | 0.054 |
| 7 | 0.012 | 0.101 | 0.066 | 0.001 | -0.021 | -0.074 | -0.005 |
| 8 | 0.026 | 0.162 | 0 | -0.022 | 0 | -0.07 | -0.061 |
| 9 | 0.016 | 0.105 | -0.075 | 0.002 | 0.018 | -0.064 | -0.005 |
| 10 | 0.048 | -0.089 | 0 | 0.083 | 0 | -0.136 | -0.145 |
| 11 | -0.18 | -0.031 | 0.053 | 0.035 | -0.009 | -0.121 | 0.15 |
| 12 | -0.18 | -0.031 | -0.053 | 0.035 | 0.009 | -0.121 | 0.15 |

Table 5.7: The Zernike coefficients for each Field and Configuration 2 of the LGS Objective.

| Configuration 3 | | | | | | | |
|------------------------|---------|------------|---------|------------|---------|---------|---------|
| Field | Z_2^2 | Z_3^{-1} | Z_3^1 | Z_3^{-3} | Z_3^3 | Z_4^0 | Z_4^2 |
| 1 | 0.06 | -0.045 | 0 | 0.019 | 0 | -0.048 | -0.008 |
| 2 | 0.039 | -0.033 | -0.083 | 0.033 | 0.021 | -0.204 | 0.038 |
| 3 | 0.0482 | -0.152 | -0.056 | 0.046 | 0.003 | -0.209 | 0.001 |
| 4 | 0.068 | -0.193 | 0 | 0.045 | 0 | -0.22 | -0.046 |
| 5 | 0.049 | -0.15 | 0.048 | 0.046 | -0.003 | -0.215 | -0.001 |
| 6 | 0.039 | -0.033 | 0.083 | 0.033 | -0.021 | -0.204 | 0.038 |
| 7 | 0.019 | 0.107 | 0.07 | -0.008 | -0.027 | -0.192 | -0.014 |
| 8 | -0.01 | 0.172 | 0 | -0.03 | 0 | -0.187 | -0.063 |
| 9 | 0.025 | 0.111 | -0.080 | -0.007 | 0.024 | -0.181 | -0.014 |
| 10 | 0.177 | -0.057 | 0 | 0.073 | 0 | -0.270 | -0.143 |
| 11 | -0.055 | -0.0245 | 0.065 | 0.042 | 0.007 | -0.252 | 0.136 |
| 12 | -0.055 | -0.0245 | -0.065 | 0.042 | -0.007 | -0.252 | 0.136 |

Table 5.8: The Zernike coefficients for each Field and Configuration 3 of the LGS Objective. See Tables 3.9 and 5.1 for an explanation of the Zernike coefficients and for the correspondence between the field angles and the field numbers.

5.3.3 Distortion

If the lenses were on-axis, one would see an axis-symmetric distortion of the image. Actually, looking at Figures 5.8, 5.9 and 5.10 which have been taken from the focal plane of the LGS Objective, one can notice an asymmetric distortion. This distortion depends on the off-axis of the lenses and causes an image displacement (see Figure 6.3). Figure 5.8, 5.9 and 5.10 are obtained with Configuration 1 (80 km), 2 (160 km), 3 (240 km) respectively and Field 1. The six LGSs launched at a distance of 240 km from the primary mirror show more distortion than those launched at a distance of 80 km and 160 km. In fact distortion increases as the object height respect to the optical axis increases.

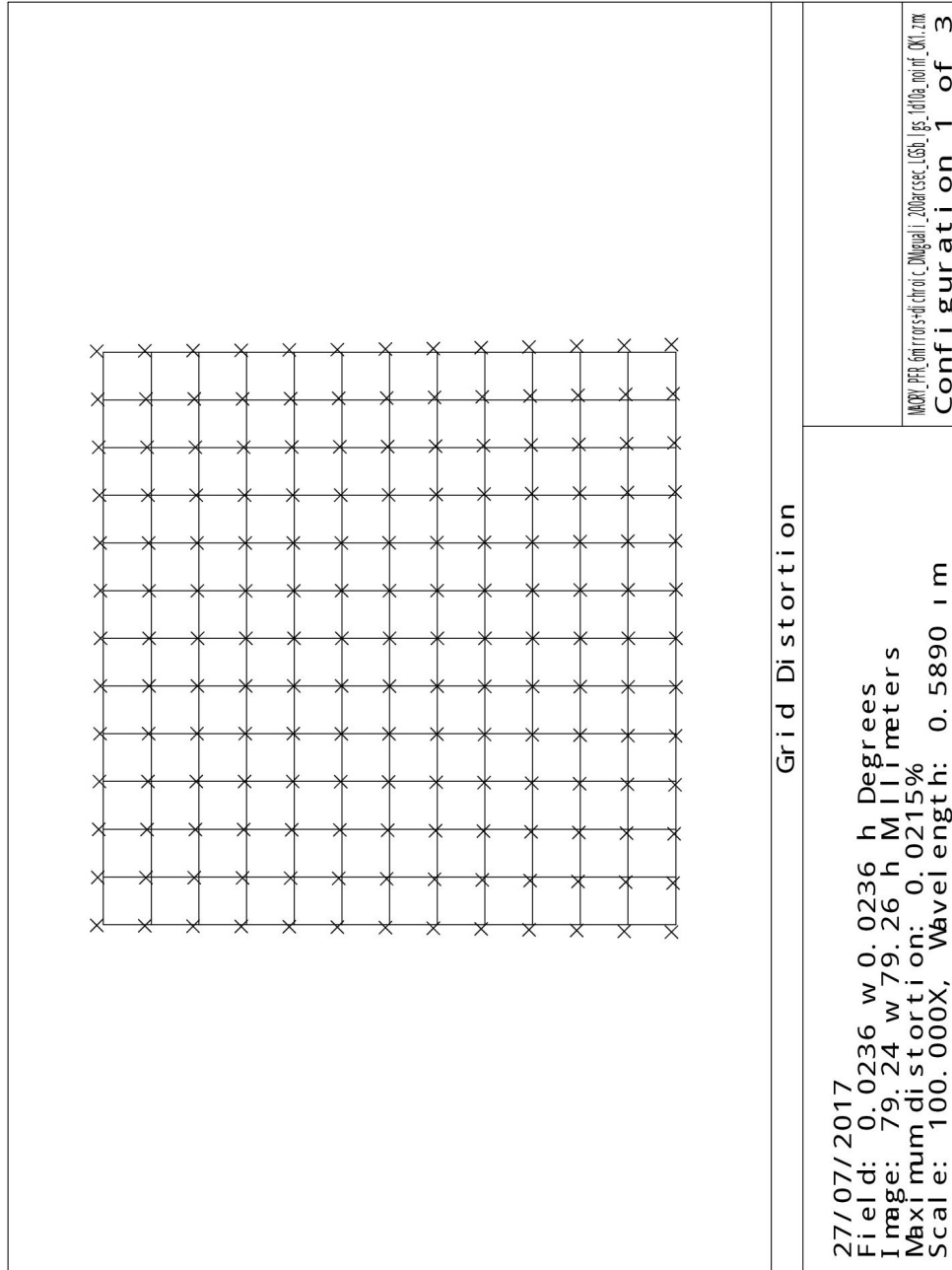


Figure 5.8: Distortion at the focal plane of the LGS Objective for Configuration 1 (80 km or zenith angle of 0°) and Field 1 ((0,0)deg). The scale is 100x for a better visualisation.

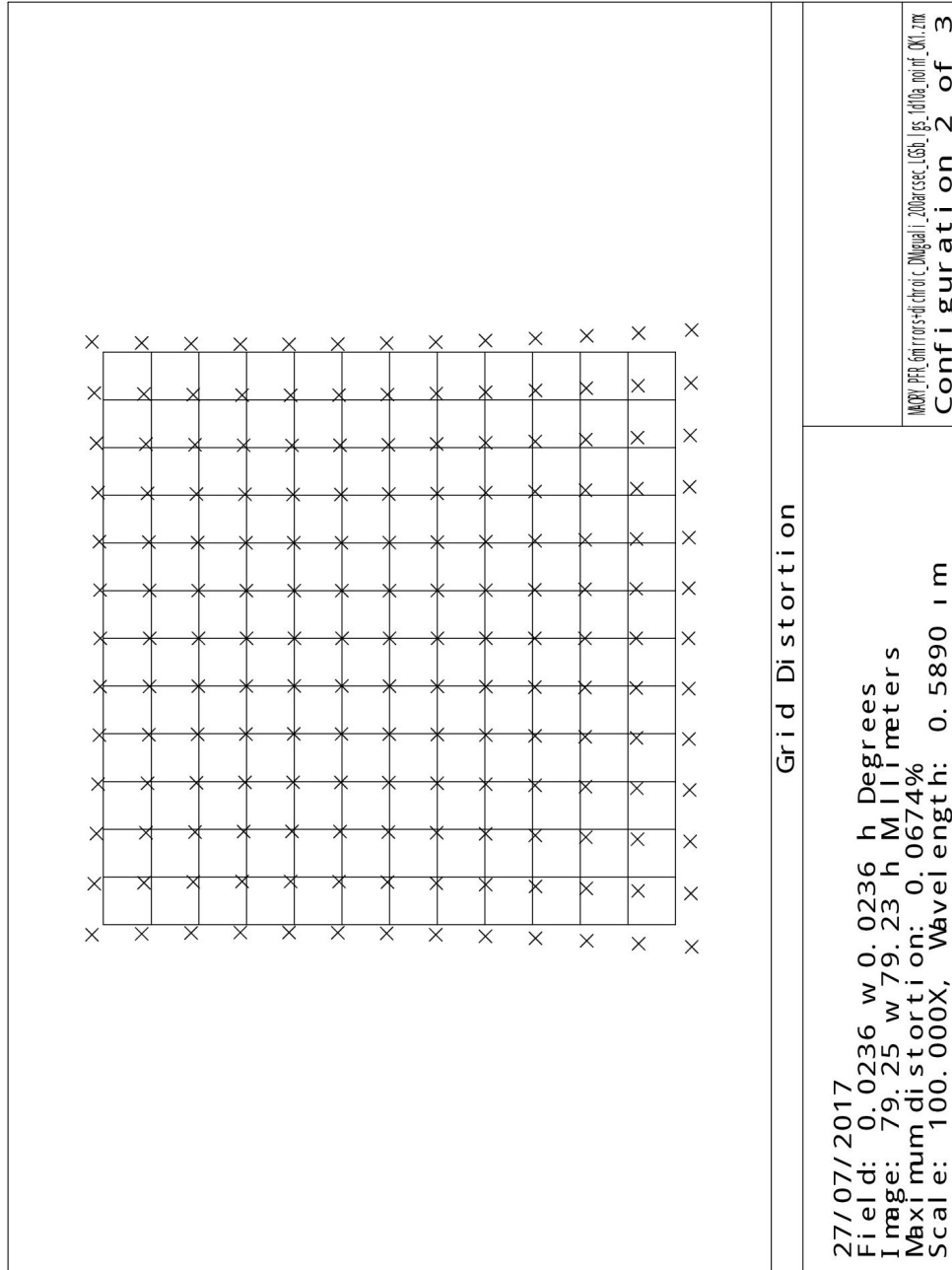


Figure 5.9: Distortion at the focal plane of the LGS Objective for Configuration 2 (160 km or zenith angle of 60°) and Field 1 ((0,0)deg). The scale is 100x for a better visualisation.

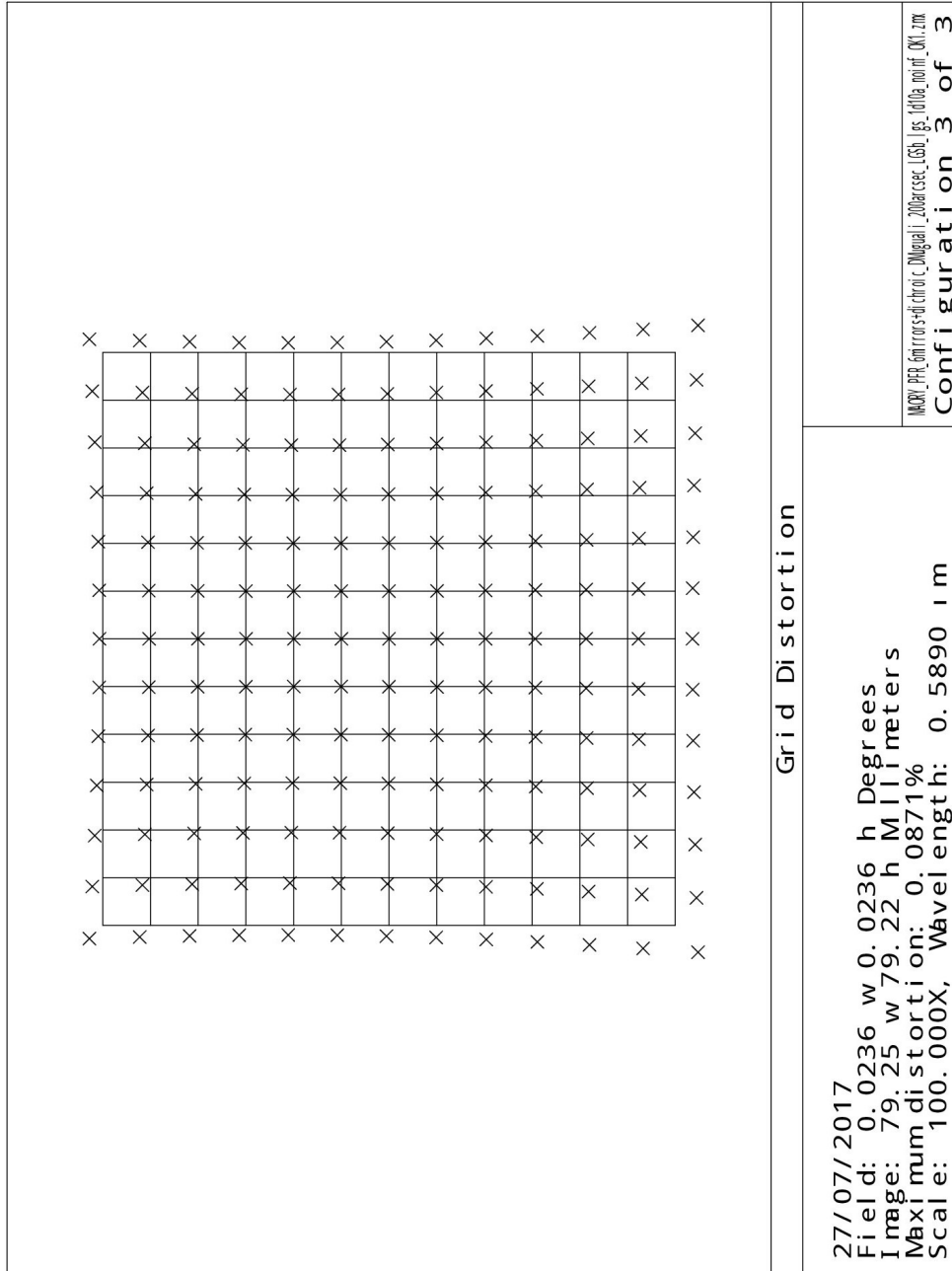


Figure 5.10: Distortion at the focal plane of the LGS Objective for Configuration 3 (240 km or zenith angle of 70°) and Field 1 ((0,0)deg). The scale is 100x for a better visualisation.

5.4 Tolerance analysis

The process of setting the tolerancing is described in Section 3.4. Tolerances has been computed by using the sensitivity analysis, Root Sum Square (RSS) assumption for computing the estimated Changes, C, in the performance and "RMS WFE" has been selected as the Criterion. Then the tolerance analysis has been performed with the current Fields (they cover a ring of maximum radius of 1' FoV and minimum radius of 45" FoV) and the paraxial focus compensator.

Since the variation of the DOF respect to the nominal position of the optical components (see Section 3.4.1) introduces different types of aberration, choosing the most effective mounting parameters as compensators is very important. It can also amplify the existing aberrations. So in order to find them, a set of *DOF tolerances*, also called mounting tolerances, have been applied to all refractive elements in the LGS Objective. They are listed in Table 5.9.

| Parameter | Tolerance |
|------------------|-----------------|
| Tilt X and Y | ± 0.005 deg |
| Decenter X and Y | ± 0.1 mm |
| Center thickness | ± 0.1 mm |

Table 5.9: The LGS Objective optical elements mounting tolerances.

After having run tolerances with these starting conditions the Worst Offenders have been obtained and shown in Appendix Table A.1. Some of these Worst Offenders are negligible since their nominal value is zero, while those (DOFs), which the system is more sensitive to, have been chosen as compensators (see Table 5.10).

Some definition of the tolerance operands, which have been used, are reported below.

- TRAD: Tolerance on radius of curvature in millimeter unit.
- TFRN: Tolerance on curvature in fringes or millimeter.
- TTHI: Tolerance on thickness in millimeter unit.
- TCON: Tolerance on conic.
- TIND: Tolerance on index of refraction.
- TABB: Tolerance on Abbe number.
- TUTX: Tolerance on user surface tilt (degrees) around the x-axis.

- TUTY: Tolerance on user surface tilt (degrees) around the y-axis.
- TUDX: Tolerance on user surface decenter (millimeter) around the x-axis.
- TUDY: Tolerance on user surface decenter (millimeter) around the y-axis.

| Compensators: | | | |
|----------------------|--------------------|--------------|------------------|
| Type | Surface | Value | Tolerance |
| TTHI [mm] | Lens 7-Image plane | -692.403 | ± 20 |
| TTHI [mm] | Lens 5-Lens 6 | -90.049 | ± 20 |
| TUTX [deg] | Lens 1 | -12.601 | ± 0.005 |
| TUTX [deg] | Lens 2 | 17.678 | ± 0.005 |

Table 5.10: The Compensators used for tolerancing. "Surface" refers to the optical design in Figure 5.1.

Then tolerancing on manufacturing elements has been computed with all these compensators excluding those which have not been used as variables during optimization. The manufacturing tolerance applied to the optical elements are listed in Table 5.11.

| Parameter | Tolerance |
|----------------------|-------------------------------------|
| Curvature radius | $\pm 0.2\%$ |
| Center thickness | $\pm 0.15mm$ |
| Conic constant | $\pm 0.08\%$ |
| Sag of flat surfaces | $\pm 0.35\mu m$ |
| Wedge | ± 100 micro-rad ($5.7e-3$ deg) |

Table 5.11: The LGS Objective optical elements manufacturing tolerances. Commercial tolerances.

The material for the LGS Dichroic and Lenses is BK7. The following tolerances have been applied to the optical components.

| Parameter | Tolerance |
|------------------------|------------------|
| Glass refractive index | $\pm 1e-3$ |
| Glass Abbe number | $\pm 1\%$ |

Table 5.12: The LGS Objective optical elements material tolerances.

The analysis result of the sensitivity shows that the Nominal MT function value, N , also called Nominal RMS WFE (in fact the chosen criterion is the RMS WFE), is 0.165 wave, while the Estimated RMS WFE, E , with the current tolerances set is 1.906 wave. The residual RMS WFE is calculated as:

$$WFE_{res}[nm] = (N - E) * \lambda[nm] \quad (5.1)$$

where λ is the used wavelength (589 nm). The allowable residual RMS WFE is the 30% of the nominal value, which is about 29 nm. So the total RMS WFE is about 126 nm (by summing up the nominal value and its 30%). Since the TT and Defocus term are excluded, the WFE_{res} could be greater than 30 nm. Indeed the tolerance has been made respect to the cendroid, that is to say that the TT is automatically removed while the defocus is calculated. In order to exclude the defocus, which is an aberration of the system itself, during the Monte Carlo realizations the Zernike are extracted and the defocus is removed.

Since the sensitivity analysis evaluates only the extreme values of the tolerances, the estimated performance is lower than that obtained with the Monte Carlo analysis, which generates realizations randomly (normal distribution) giving values for each probability ranges and takes the median value of the distribution (see Section 3.4.3). So one can also use the Monte Carlo statistics which includes the 90% probability result and put this value, $\tilde{E}=1.324$ wave, in the above equation. The 90% probability result is the 90% chance the optical system have a MT function value lower than \tilde{E} . The 10% has a greater value and so a lower performance. By this criterion, our current tolerance ranges are too loose. The 30% of WFE with this tolerances is about 683 nm.

Tolerancing has been iterated several times, by tighten the Worst Offenders (show Appendix A) and loosen the parameter which are less sensitive to the tolerances. Hence, after this procedure, the final estimated WFE is 0.361 wave, whereas the 90% probability MT function value is greater than 0.208 wave (nominal value is 0.165 wave), which allow to satisfy the above criterion. In conclusion the 30% of WFE is about 25.3 nm using Monte Carlo statistics.

All the compensators which have been used are in Table 5.13.

| Compensators: | | | |
|----------------------|---------------------|--------------|------------------|
| Type | Surface | Value | Tolerance |
| TTHI [mm] | Lens 7-Image plane | -692.403 | ± 20 |
| TTHI [mm] | Lens 5-Lens 6 | -90.049 | ± 20 |
| TUTX [deg] | Lens 1 | -12.601 | ± 0.005 |
| TUTX [deg] | Lens 2 | 17.678 | ± 0.005 |
| TUDY [mm] | LGS-M1 | -242.294 | ± 1 |
| TTHI [mm] | LGS-M1-Lens 4 | 102.648 | ± 20 |
| TTHI [mm] | Lens 3-LGS-M1 | -649.561 | ± 20 |
| TUTX [deg] | Lens 3 | -1.902 | ± 0.005 |
| TTHI [mm] | Lens 4-LGS-M2 | 380.371 | ± 20 |
| TUTX [deg] | LGS-M1 | -17.031 | ± 0.005 |
| TTHI [mm] | Lens 2-Lens 3 | -66.139 | ± 20 |
| TTHI [mm] | Lens 1-Lens 2 | -2055.782 | ± 20 |
| TTHI [mm] | LGS Dichroic-Lens 1 | -144.509 | ± 20 |

Table 5.13: The chosen compensators used for tolerancing. "Surface" refers to the optical design in Figure 5.1.

The chosen manufacturing tolerances are listed in Table 5.14, except some tighten and loosen tolerances which are listed in Tables 5.15 and 5.16 respectively.

| Parameter | Tolerance |
|------------------------|---------------------------------------|
| Curvature radius | $\pm 0.1\%$ |
| Center thickness | $\pm 0.15mm$ |
| Conic constant | $\pm 0.05\%$ |
| Sag of flat surfaces | $\pm 0.442\mu m$ |
| Wedge | ± 50 micro-rad (± 0.003 deg) |
| Glass refractive index | $\pm 5e-4$ |
| Glass Abbe number | $\pm 1\%$ |

Table 5.14: The chosen LGS Objective optical elements manufacturing and material tolerances.

| Tighten tolerances: | | | |
|----------------------------|----------------|------------------|--|
| Type | Surface | Tolerance | |
| TFRN | LGS-M2 | $-0.29 \mu m$ | |
| TTHI | Lens 1a | ± 0.1 mm | |
| TTHI | Lens 7a | ± 0.1 mm | |

Table 5.15: Tighten tolerances after using the compensators in Table 5.13. "Surface" refers to the optical design in Figure 5.1.

| Loosen tolerances: | | |
|---------------------------|----------------|------------------------|
| Type | Surface | Tolerance |
| TRAD | LGS-M1 | $\pm 0.15 \%$ |
| | Lens 4a | $\pm 0.15 \%$ |
| TIND | LGS Dichroic | $\pm 1e-3$ |
| | Lens 1 | $\pm 1e-3$ |
| | LGS-M1 | $\pm 1e-3$ |
| | LGS-M2 | $\pm 1e-3$ |
| TCON | LGS-M1 | $\pm 0.5 \%$ |
| | Lens 1a/b | $\pm 0.15 \%$ |
| | Lens 2b | $\pm 0.15 \%$ |
| | Lens 3a | $+ 0.15 \%$ |
| | Lens 6a/b | $\pm 0.15 \%$ |
| | Lens 7a/b | $\pm 0.15 \%$ |
| TUTX | LGS-Dichroic | $\pm 0.1 \text{ deg}$ |
| TUTX | Lens 3 | $\pm 0.01 \text{ deg}$ |
| TUTX/Y | Lens 4 | $\pm 0.01 \text{ deg}$ |

Table 5.16: Loosen tolerances after using the compensators in Table 5.13. "Surface" refers to the optical design in Figure 5.1.

At the end, the study of tolerancing on the DOF has been carried out. The chosen *DOF tolerances*, which do not cause a change in the MT function greater than 30 nm (by using the above criterion), are listed in Table 5.17.

| Parameter | Tolerance |
|------------------|-------------------------|
| Tilt X and Y | $\pm 0.005 \text{ deg}$ |
| Decenter X and Y | $\pm 0.1 \text{ mm}$ |
| Center thickness | $\pm 0.1 \text{ mm}$ |

Table 5.17: The chosen LGS Objective optical elements mounting tolerances.

These are the precision with whom lenses will be mounted.

Chapter 6

Results

In the first section the performance of the LGS Objective is shown in terms of the nominal RMS WFE over a specific FoV and in terms of the image displacement, in function of the zenith angles. The goal is to optimize the optical quality within a range of zenith angles, that correspond to different Sodium altitude, because it is easier to apply AO in this case. In fact, a WFE as close as possible to be constant over all the zenith angle implies better NCPA calibration and simple lookup tables.

The tolerance analysis has been performed with a limit of WFE degradation of about 30% of the nominal WFE. The results of Monte Carlo realizations have been plotted in the second section.

In the following, RMS WFE has to be considered as the Zernike coefficients RSS excluding the TT and Defocus. In fact the tolerance as well as the optimization have been made respect to the centroid, that is to say that the TT is automatically removed while the defocus is calculated. In order to exclude the defocus, which is an aberration of the system itself, during the Monte Carlo realizations the Zernike coefficient is extracted and then removed. These low-order aberrations (TT and defocus) are measured by the NGSs.

6.1 Performance

The zenith angle effect discussed in Subsection 2.1.5 is another considerable issue for the LGS Objective. Pointing at different zenith angles, the LGS light, which propagates through MAORY post-focal relay optics and the LGS Objective, introduces different aberrations.

So on the LGS Objective focal plane, the nominal WFE of the six LGSs placed over a radius of 45" FoV in function of the zenith angle has been calculated and plotted in Figure 6.1 excluding TT and defocus; the colors correspond to the six

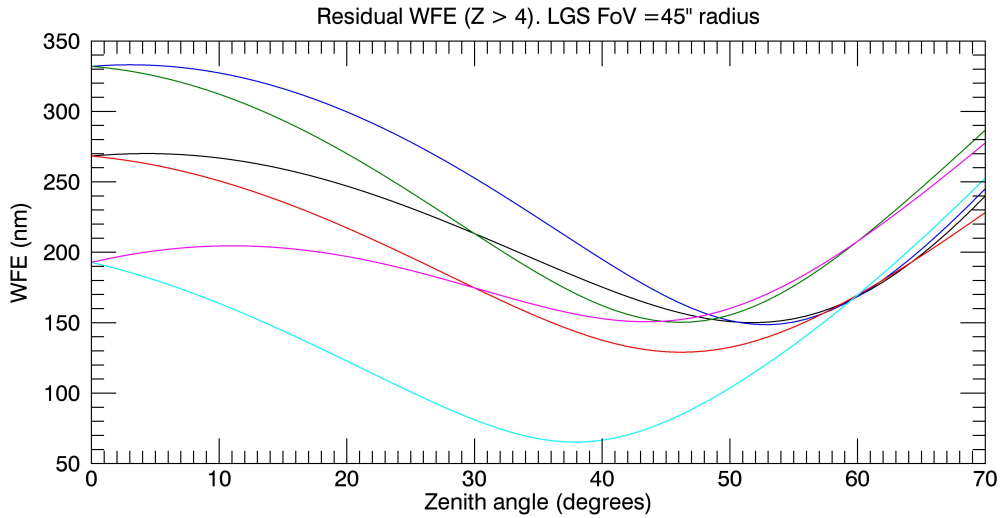


Figure 6.1: The nominal WFE in function of the zenith angle is measured in the LGS Objective focal plane. The TT and defocus are removed. The colors correspond to the six LGSs placed over a radius of 45'' FoV.

LGSs. As far as the discussion of this plot concerned, the WFE values range from about 130 (at $40^\circ \div 50^\circ$ zenith angle) nm to about 330 nm (at 0°). Other efforts will be made in order to keep the WFE value over all the zenith angles as much as possible constant.

The nominal RMS WFE given by the sensitivity analysis is 383 nm and it is the average of the Zernike coefficients RSS over all the Fields (maximum radius of about 1') and within the range of Sodium layer altitude (three Configurations: 80, 160 and 240 Km). So it is obvious that the WFE values in Figure 6.1 are well within 383 nm because it is plotted over a radius of 45'' FoV (as confirmation, see the value in correspondance to 45'' or 0.0125° in Figure 5.5).

In Figure 6.2 a specific case of the previous plot has been reported; only a LGS has been taken into account as example. It has been yet explained that a LGS introduces different aberrations at a specific zenith angle (or height from the primary mirror). So the trend of the WFE in function of the zenith angle has been carried out for each Zernike coefficient Z, from fifth mode to eleventh one. Those greater than eleven have been neglected because their value is about zero. The meaning of this plot is that for a given LGS and zenith angle, each Zernike mode contributes differently to the WFE budget. Furthermore the contribution of a given Z to the WFE budget varies as the zenith angle increases.

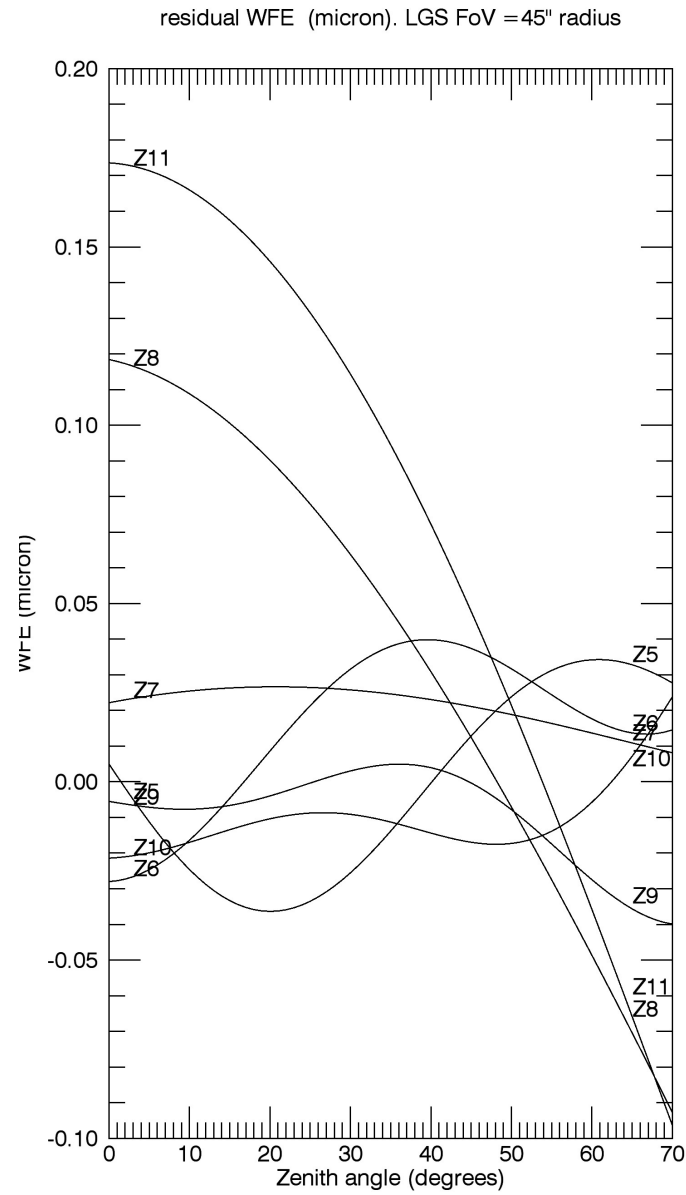


Figure 6.2: The nominal WFE of one LGS in function of the zenith angle is measured in the LGS Objective focal plane. Only $Z > 4$ has been considered.

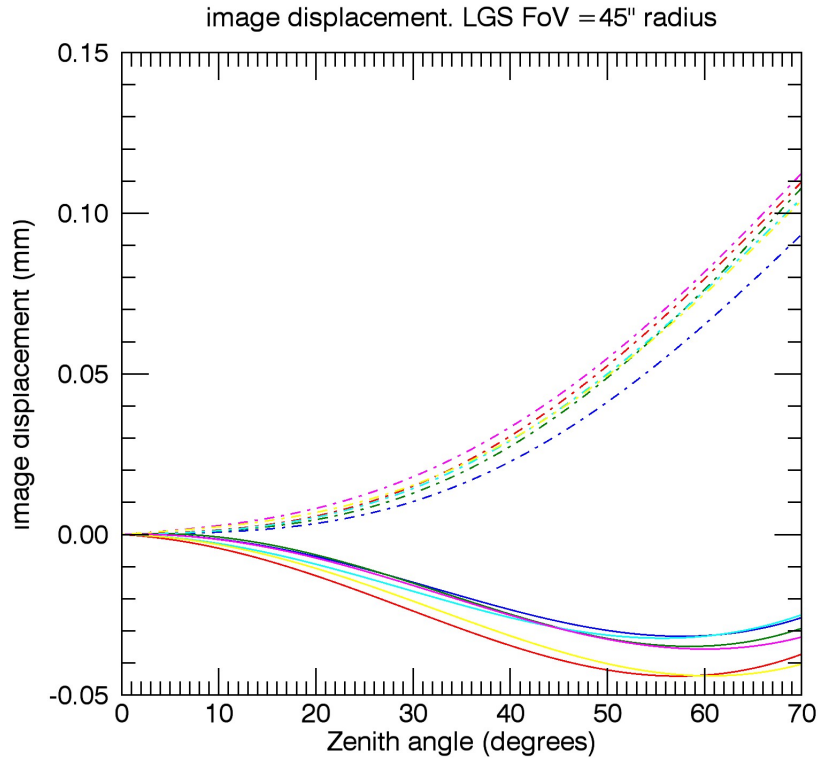


Figure 6.3: Image displacement respect to the mean position at the Objective image plane in function of the zenith angle. The colors correspond to the six LGSs placed over a radius of $45''$ FoV.

In Figure 6.3 the mean image displacement respect to the mean position is plotted for the six LGSs against the zenith angle. This effect is due to distortion (see Section 3.1.4 and Subsection 5.3.3) and corrected with the traslation of the hexapodes (see Figure 4.6).

6.2 Tolerance analysis

After having done the manufacturing tolerances for each of the three Configurations using the Monte Carlo statistics, the residual WFE (see Equation 5.4) in function of the zenith angle is shown in Figure 6.4. The TT and defocus are removed. 100 Monte Carlo trials have been generated for this graphic, 15 zenith angles have been sampled and data extracted for 6 LGSs have been represented by circles. The displayed values are that of 6 LGSs at a radius of $45''$ FoV for each sampled zenith angle and all the Monte Carlo trials. For instance in a specific zenith angle the aberrations have been extracted for each of the six LGSs in this

FoV and for each Monte Carlo files. Then the median of the Zernike coefficients RSS have been plotted. The median values are shown in the right Figure: they stay within -20 and 40 nm. Hence the residual WFE remains mostly constant over all the zenith angles as predetermined. The nominal WFE (see Section 6.1) is about 383 nm (0.65 waves), while the allowable residual WFE is the 30% of the nominal WFE, that means about 115 nm (0.2 waves). Since the TT and Defocus term are excluded, the WFE_{res} could be greater than 115 nm. So the median values are well within this limit.

Figure 6.5 is the real WFE after tolerances. The right Figure is the median values of the left plot: the values stay within 140 and 320 nm. The best performance is around a zenith angle of 50° , while the worst one is around 0° and 70° . The allowable total WFE is about 498 nm (115 plus 383 nm), so these values are well within this limit.

Obviously, until february 2018 (the end of the PDR) other efforts will be made to improve the performance and reduce the residual WFE.

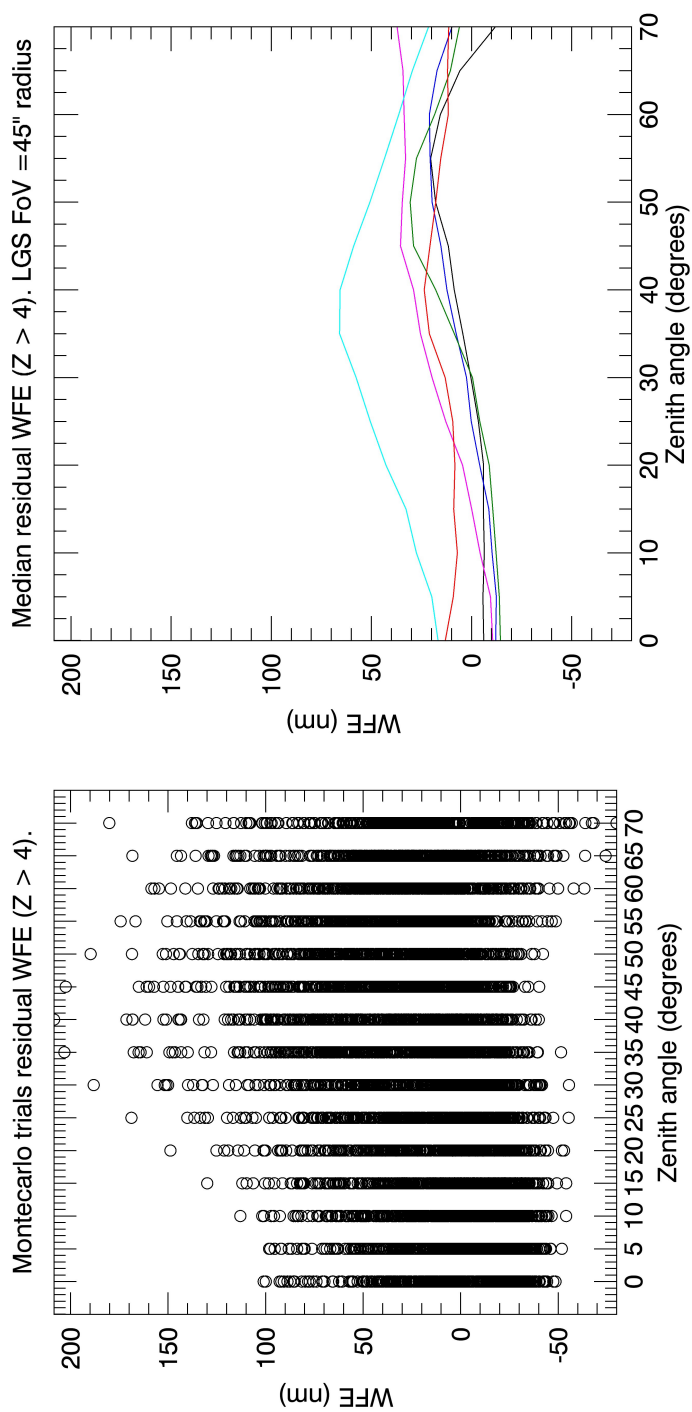


Figure 6.4: Left: Residual WFE at the LGS Objective image plane as a function of the zenith angle. Montecarlo trials for manufacturing errors of the optics. The TT and defocus are removed. Right: Median values of the left plot, different colors correspond to the six LGSs disposed symmetrically over a radius of 45" FoV.

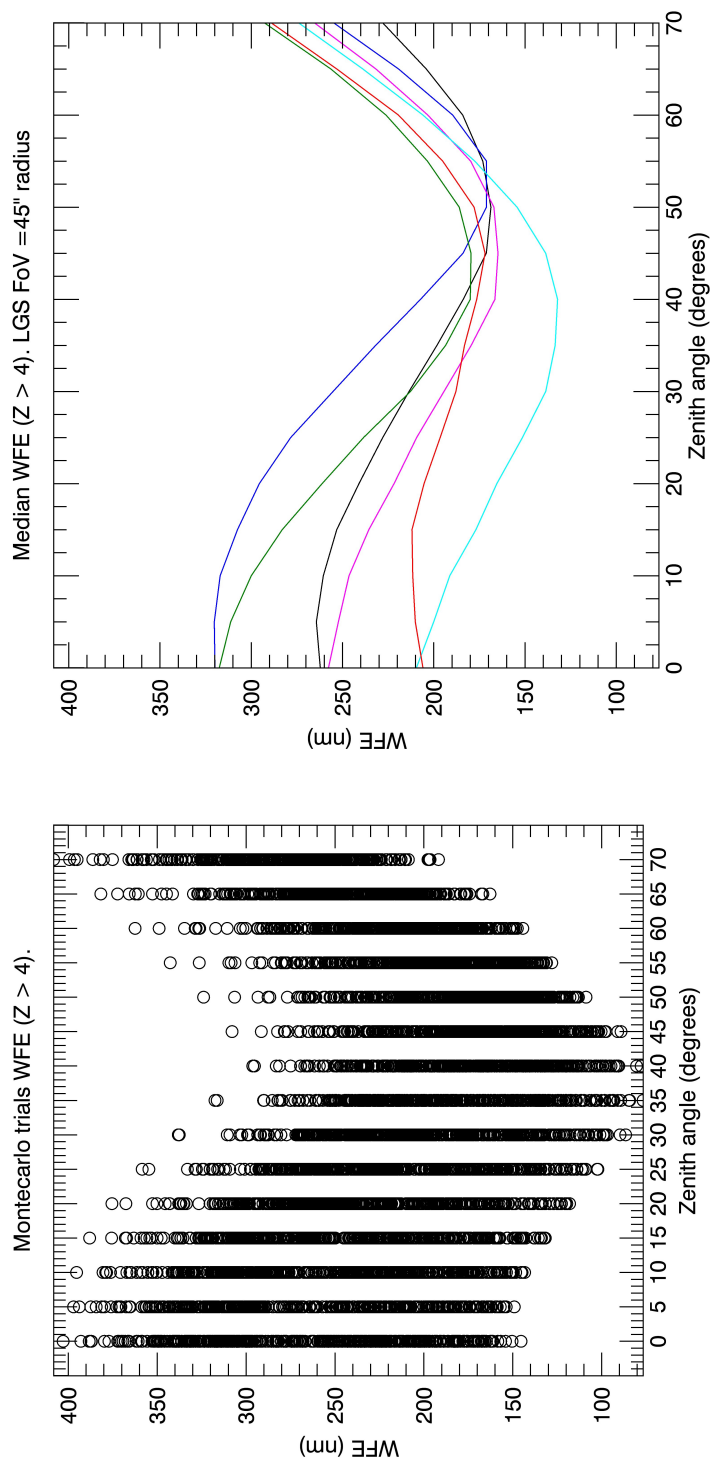


Figure 6.5: Left: The residual WFE plus the nominal WFE in function of the zenith angle is measured on the LGS Objective focal plane. The TT and defocus are removed. Right: Median values of the left plot, the colors corresponds to the six LGSs placed over a radius of 45'' FoV.

Conclusion and future perspective

The first light of European Extremely Large Telescope will be in 2024. This ground-based optical/infrared telescope will have an angular resolution which has never been achieved (about $0.01''$ at band K) allowing detailed studies of subjects including planets around other stars, the first objects in the Universe, super-massive black holes, and the nature and distribution of the dark matter and dark energy which dominate the Universe.

One of its first light instruments working from the optics to the beat IR is MICADO. It will work with the post-focal Multi Conjugated Adaptive Optics Relay, called MAORY, which compensates for atmospheric turbulence by using six laser guide stars launched at a radius of 70° FoV, three natural guide stars for wavefront sensing and two DMs for wavefront correction. The LGS launching angle is a trade-off between the performance on science FoV and the performance on technical FoV for sky coverage. With the use of six LGSs the sky coverage will be increased respect to the case of only NGSs and MAORY will overcome some issues such as anisoplanatism, fratricide effect, cone effect.

The LGS Objective produces a focal plane for the LGS WFSs. Its goal is to reduce the aberrations introduced by the MAORY mirrors M6, M7, M8 and M9. Moreover, during sky tracking the roto-traslational motion of the LGSs launched in the Sodium layer makes the six LGSs at a specific altitude will focus on different points respect to LGSs located at other distances. Since those with a shorter focal length will have a greater aberration and those with a longer one the reverse, the LGS Objective has been designed such that the wavefront error, WFE, would be nearly constant and low over all zenith angles not to affect the wavefront reconstruction. The design has been optimized keeping satisfied the client achievements: $f/5$ for the different altitudes, exit pupil at infinity, it must be $1/10$ of sub-aperture with a round image. The number of optical surfaces has been minimized, the mechanical constraints have been taken in account and the residual aberrations of the LGSs have been kept as small as possible in order to reach the performance requirements of MAORY. The project is not over here, it has to be kept in account

that some other advancements will be made to reduce as much as possible the number of lenses and their dimensions, not forgetting the requirements asked and the available budget.

In addition to the optimization, a study about the tolerances has been carried out: manufacturing errors and alignment precision (Degree Of Freedom) have been calculated. The tolerance analysis has been performed with a limit of wavefront error degradation of about 30%, that is about 115 nm RMS (the nominal WFE is of about 380 nm). Considering the WFE of the nominal design and the manufacturing errors, the total wavefront error is well within the predetermined limit.

Until february 2018 (the end of the Preliminary Design Review) other efforts will be made to improve the performance and reduce the residual wavefront errors.

Appendix A

Worst Offenders

| Worst Offenders: | | | | |
|------------------|---------------|--------|-----------|--------|
| Type | Element | Value | Criterion | Change |
| TUTY | Lens 1 | -0.005 | 0.373 | 0.323 |
| TUDY | Lens 5 | 0.1 | 0.333 | 0.276 |
| TUDX | Lens 5 | -0.1 | 0.327 | 0.268 |
| TUDX | Lens 5 | 0.1 | 0.325 | 0.266 |
| TUDY | Lens 5 | -0.1 | 0.324 | 0.265 |
| TUDY | Lens 6 | -0.1 | 0.272 | 0.198 |
| TUDX | Lens 6 | 0.1 | 0.267 | 0.191 |
| TUDX | Lens 6 | -0.1 | 0.265 | 0.189 |
| TUDY | Lens 6 | 0.1 | 0.264 | 0.186 |
| TUTX | Lens 2 | -0.005 | 0.243 | 0.156 |
| TUTY | Lens 1 | 0.005 | 0.235 | 0.142 |
| TTHI | Lens 5-Lens 6 | -0.1 | 0.228 | 0.131 |
| TUTX | Lens 5 | 0.005 | 0.215 | 0.107 |
| TUTY | Lens 5 | 0.005 | 0.213 | 0.103 |
| TUTY | Lens 5 | -0.005 | 0.212 | 0.101 |
| TUTX | Lens 5 | -0.005 | 0.211 | 0.099 |
| TUDY | LGS-M1 | 0.1 | 0.210 | 0.097 |
| TUDY | Lens 2 | -0.1 | 0.197 | 0.064 |
| TUTX | Lens 1 | 0.005 | 0.196 | 0.06 |
| TUTY | Lens 2 | 0.005 | 0.196 | 0.059 |

Table A.1: The first twenty Worst Offenders with mounting tolerances set in Table 5.3. Criterion and Change are in wavelength unit and for an explanation of their meanings see Section 3.4.

The following tables show the Worst Offenders after having tighten or loosen the tolerance ranges. These ranges are reported in each caption. Hereafter Criterion and Change are in wavelength unit. "a" refers to the front surface of the optical element, while "b" to the rear surface. TUTX and TUTY are used to model a wedge.

| Worst Offenders: | | | | | |
|-------------------------|----------------|--------------|------------------|---------------|--|
| Type | Element | Value | Criterion | Change | |
| TRAD | Lens 5a | -0.258 | 0.901 | 0.886 | |
| TRAD | Lens 1a | 3.102 | 0.894 | 0.878 | |
| TRAD | Lens 1b | -3.163 | 0.87 | 0.854 | |
| TRAD | Lens 1a | -3.102 | 0.85 | 0.833 | |
| TRAD | Lens 1b | 3.163 | 0.821 | 0.804 | |
| TRAD | Lens 5b | 0.189 | 0.821 | 0.804 | |
| TRAD | Lens 5a | 0.258 | 0.739 | 0.720 | |
| TRAD | Lens 5b | -0.189 | 0.661 | 0.641 | |
| TCON | Lens 5b | -0.001 | 0.489 | 0.46 | |
| TRAD | Lens 3a | -3.59 | 0.400 | 0.364 | |
| TRAD | Lens 3a | 3.589 | 0.392 | 0.356 | |
| TIND | Lens 3 | -0.001 | 0.385 | 0.348 | |
| TIND | Lens 3 | 0.001 | 0.375 | 0.336 | |
| TRAD | Lens 6b | -0.744 | 0.351 | 0.310 | |
| TUTY | Lens 5 | 0.006 | 0.340 | 0.298 | |
| TUTY | Lens 5 | -0.006 | 0.339 | 0.296 | |
| TCON | Lens 5 | 0.001 | 0.334 | 0.290 | |
| TUTX | Lens 5 | 0.006 | 0.330 | 0.286 | |
| TUTX | Lens 5 | -0.006 | 0.318 | 0.271 | |
| TIND | Lens 7 | -0.001 | 0.317 | 0.271 | |

Table A.2: The first twenty Worst Offenders with manufacturing tolerances set in Tables 5.5, 5.6 and 5.7. The estimated change in the criterion is 1.899 wave.

| Worst Offenders: | | | | | |
|-------------------------|----------------|--------------|------------------|---------------|--|
| Type | Element | Value | Criterion | Change | |
| TRAD | Lens 1b | -3.163 | 0.87 | 0.854 | |
| TRAD | Lens 1b | 3.163 | 0.821 | 0.804 | |
| TRAD | Lens 5a | -0.194 | 0.703 | 0.683 | |
| TRAD | Lens 1a | 2.327 | 0.674 | 0.653 | |
| TRAD | Lens 5b | 0.142 | 0.640 | 0.618 | |
| TRAD | Lens 1a | -2.327 | 0.631 | 0.609 | |
| TRAD | Lens 5a | 0.193 | 0.542 | 0.517 | |
| TRAD | Lens 5b | -0.142 | 0.489 | 0.460 | |
| TCON | Lens 5a | -0.001 | 0.489 | 0.46 | |
| TRAD | Lens 3a | -2.692 | 0.321 | 0.275 | |
| TRAD | Lens 3a | 2.692 | 0.312 | 0.265 | |
| TCON | Lens 5b | 0.001 | 0.297 | 0.247 | |
| TRAD | Lens 6b | -0.558 | 0.292 | 0.241 | |
| TRAD | Lens 6a | 0.744 | 0.291 | 0.24 | |
| TCON | Lens 5a | 0.001 | 0.287 | 0.235 | |
| TIND | Lens 6 | 0.001 | 0.279 | 0.225 | |
| TIND | Lens 6 | -0.001 | 0.272 | 0.216 | |
| TUTY | Lens 5 | 0.004 | 0.266 | 0.209 | |
| TUTY | Lens 5 | -0.004 | 0.265 | 0.207 | |
| TRAD | Lens 2b | -9.295 | 0.265 | 0.207 | |

Table A.3: The first twenty Worst Offenders after tightening some tolerances: the tolerance values of curvature radius of Lens 1a, 3a, 5a, 5b is $\pm 0.15\%$ and Lens 6b is -0.15% , the conic constant of Lens 5a is -0.06% , the index of refraction of Lens 3 is $\pm 5e-4$, Lens 7 is $-5e-4$, the wedge about Y-axis of Lens 5 is $4e-3$ deg and about X-axis of Lens 5 is $\pm 4e-3$ deg. The estimated change in the criterion is 1.563 wave.

| Worst Offenders: | | | | | |
|-------------------------|----------------|--------------|------------------|---------------|--|
| Type | Element | Value | Criterion | Change | |
| TRAD | Lens 1b | -2.372 | 0.655 | 0.634 | |
| TRAD | Lens 1b | 2.372 | 0.611 | 0.589 | |
| TRAD | Lens 5a | -0.129 | 0.507 | 0.479 | |
| TRAD | Lens 5b | 0.094 | 0.463 | 0.433 | |
| TRAD | Lens 1a | 1.551 | 0.459 | 0.428 | |
| TRAD | Lens 1a | -1.551 | 0.420 | 0.386 | |
| TCON | Lens 5b | -0.0006 | 0.401 | 0.365 | |
| TRAD | Lens 5a | 0.129 | 0.352 | 0.311 | |
| TRAD | Lens 5b | -0.094 | 0.322 | 0.277 | |
| TCON | Lens 5a | 0.0006 | 0.265 | 0.207 | |
| TUTX | Lens 5 | 0.004 | 0.261 | 0.202 | |
| TUTX | Lens 5 | -0.004 | 0.249 | 0.187 | |
| TIND | Lens 2 | -0.001 | 0.249 | 0.187 | |
| TRAD | Lens 3a | -1.795 | 0.248 | 0.186 | |
| TRAD | Lens 6a | 1.495 | 0.248 | 0.185 | |
| TIND | Lens 3 | -0.0006 | 0.243 | 0.178 | |
| TRAD | Lens 6a | -1.495 | 0.241 | 0.176 | |
| TRAD | Lens 3a | 1.795 | 0.240 | 0.174 | |
| TRAD | Lens 6b | -0.372 | 0.237 | 0.171 | |
| TRAD | Lens 6b | 0.557 | 0.236 | 0.169 | |

Table A.4: The first twenty Worst Offenders after tightening some tolerances: the tolerance values of curvature radius of Lens 1a, 3a, 5a, 5b are $\pm 0.1\%$, Lens 6b is -0.1% , Lens 1b is $\pm 0.15\%$, Lens 2b, 6b are $+0.15\%$, the conic constant of Lens 5a is -0.05% , Lens 5b is $\pm 0.06\%$, the index of refraction of Lens 6a is $\pm 5e-4$, the wedge about Y-axis of Lens 5 is $\pm 3e-3$ deg. Some tolerances have been loosen: the sag tolerance value is ± 1.5 fringes, the centre thickness is ± 0.15 mm, the index of refraction of the front surface of the LGS Dichroic, Lens 1a, LGS-M1, LGS-M2 is ± 0.001 , the Abbe number is $\pm 1\%$, the conic constant of Lens 1, 2b, LGS-M1 is $\pm 0.1\%$, the wedge about X-axis of LGS Dichroic, Lens 2, 3, Lens 4 is ± 0.01 and wedge about Y-axis of Lens 1 and 4 is ± 0.01 . The estimated change in the criterion is 1.152 wave.

| Worst Offenders: | | | | | |
|-------------------------|----------------|--------------|------------------|---------------|--|
| Type | Element | Value | Criterion | Change | |
| TCON | Lens 5a | -0.006 | 1.182 | 1.170 | |
| TUTX | Lens 2 | -0.1 | 1.081 | 1.069 | |
| TUTX | Lens 2 | 0.1 | 1.009 | 0.995 | |
| TUTY | Lens 3 | -0.1 | 0.704 | 0.684 | |
| TUTY | Lens 3 | 0.1 | 0.704 | 0.684 | |
| TUTX | Lens 3 | 0.1 | 0.676 | 0.655 | |
| TUTX | Lens 3 | -0.1 | 0.582 | 0.558 | |
| TUTX | Lens 7 | 0.1 | 0.571 | 0.546 | |
| TUTY | Lens 7 | 0.1 | 0.569 | 0.545 | |
| TUTY | Lens 7 | -0.1 | 0.568 | 0.543 | |
| TUTX | Lens 7 | -0.1 | 0.557 | 0.532 | |
| TUTY | Lens 2 | -0.05 | 0.532 | 0.506 | |
| TUTY | Lens 2 | 0.05 | 0.532 | 0.506 | |
| TRAD | Lens 5a | -0.129 | 0.507 | 0.479 | |
| TRAD | Lens 5b | 0.094 | 0.463 | 0.433 | |
| TRAD | Lens 1a | 1.551 | 0.458 | 0.428 | |
| TRAD | Lens 1b | -1.581 | 0.446 | 0.415 | |
| TUTY | LGS Dichroic | -0.1 | 0.439 | 0.407 | |
| TUTY | LGS Dichroic | 0.1 | 0.439 | 0.407 | |
| TRAD | Lens 1a | -1.551 | 0.420 | 0.386 | |

Table A.5: The first twenty Worst Offenders after tightening some tolerances: the tolerance values of curvature radius of Lens 1b is $\pm 0.1\%$, the conic constant of Lens 5b is 0.05 %. Some tolerances have been loosen: the conic constant tolerance value of Lens 1, 2b, 3a, LGS-M1, Lens 4, 6 and 7 is $\pm 0.5\%$, of Lens 5a is 0.5 %, the wedge about X and Y-axis of LGS Dichroic, Lens 3, 4, 7 is ± 0.1 , wedge about X-axis of Lens 2 is ± 0.1 , wedge about Y-axis of Lens 2 is ± 0.1 and of Lens 2 is ± 0.05 . The estimated change in the criterion is 2.173 wave.

| Worst Offenders: | | | | | |
|-------------------------|----------------|--------------|------------------|---------------|--|
| Type | Element | Value | Criterion | Change | |
| TUTX | Lens 3 | 0.1 | 0.676 | 0.655 | |
| TUTX | Lens 7 | -0.1 | 0.557 | 0.532 | |
| TRAD | Lens 5a | -0.129 | 0.507 | 0.479 | |
| TRAD | Lens 5b | 0.094 | 0.463 | 0.433 | |
| TRAD | Lens 1a | 1.551 | 0.458 | 0.428 | |
| TRAD | Lens 1b | -1.581 | 0.446 | 0.415 | |
| TRAD | Lens 1a | -1.551 | 0.420 | 0.386 | |
| TRAD | Lens 1b | 1.582 | 0.409 | 0.375 | |
| TCON | Lens 5b | -0.0004 | 0.357 | 0.317 | |
| TRAD | Lens 5a | 0.129 | 0.352 | 0.311 | |
| TUTY | Lens 2 | -0.03 | 0.345 | 0.303 | |
| TUTY | Lens 2 | 0.03 | 0.345 | 0.303 | |
| TRAD | Lens 5b | -0.094 | 0.322 | 0.277 | |
| TCON | Lens 5a | 0.0006 | 0.265 | 0.207 | |
| TUTY | LGS Dichroic | -0.05 | 0.262 | 0.203 | |
| TUTY | LGS Dichroic | 0.05 | 0.262 | 0.203 | |
| TIND | Lens 2a | -0.001 | 0.249 | 0.187 | |
| TRAD | Lens 3a | -1.795 | 0.249 | 0.186 | |
| TIND | Lens 3a | -0.0005 | 0.243 | 0.178 | |
| TRAD | Lens 3a | 1.795 | 0.240 | 0.174 | |

Table A.6: The first twenty Worst Offenders after tightening some tolerances: the tolerance values of curvature radius of Lens 2b is $\pm 0.1\%$, Lens 6a is $\pm 0.15\%$, Lens 6b, 7a is 0.15% , the conic constant of Lens 5a is 0.1% , Lens 5b is 0.05% , wedge about X-axis of Lens 2, about Y-axis of Lens 3 is ± 0.01 deg, about X-axis of Lens 3 is -0.01 deg, about X-axis of Lens 7 is 0.03 deg, about Y-axis of Lens 2, 7 is ± 0.03 deg, about Y-axis of LGS Dichroic is ± 0.05 deg and about X-axis of Lens 5 is ± 0.003 deg. The estimated change in the criterion is 1.265 wave.

Another compensator has been added: the decentering about Y-axis of the LGS-M1 with tolerance range of ± 1 mm.

| Worst Offenders: | | | | | |
|-------------------------|----------------|--------------|------------------|---------------|--|
| Type | Element | Value | Criterion | Change | |
| TUTY | Lens 1 | -0.1 | 2.936 | 2.932 | |
| TUTY | Lens 1 | 0.1 | 2.817 | 2.812 | |
| TUTY | Lens 2 | -0.05 | 0.532 | 0.505 | |
| TUTY | Lens 2 | 0.05 | 0.532 | 0.505 | |
| TRAD | Lens 5a | -0.129 | 0.506 | 0.478 | |
| TRAD | Lens 5b | 0.094 | 0.462 | 0.432 | |
| TRAD | Lens 1a | 1.551 | 0.414 | 0.380 | |
| TRAD | Lens 1b | -1.581 | 0.409 | 0.374 | |
| TRAD | Lens 1a | -1.551 | 0.403 | 0.368 | |
| TRAD | Lens 1b | 1.581 | 0.397 | 0.361 | |
| TCON | Lens 5b | -0.005 | 0.357 | 0.317 | |
| TRAD | Lens 5a | 0.129 | 0.351 | 0.309 | |
| TRAD | Lens 5b | -0.094 | 0.321 | 0.275 | |
| TUTY | Lens 7 | 0.05 | 0.319 | 0.273 | |
| TUTY | Lens 7 | -0.05 | 0.317 | 0.271 | |
| TUTX | Lens 7 | 0.05 | 0.316 | 0.269 | |
| TUTX | Lens 7 | -0.05 | 0.293 | 0.243 | |
| TCON | Lens 5a | 0.0006 | 0.265 | 0.207 | |
| TRAD | Lens 3a | -1.795 | 0.245 | 0.181 | |
| TIND | Lens 3 | -0.0005 | 0.239 | 0.173 | |

Table A.7: The first twenty Worst Offenders after tightening some tolerances: the tolerance values of curvature radius of Lens 6a, 6b, 7a is $\pm 0.1\%$, Lens 7b is $\pm 0.15\%$, Lens 4a is 0.15% and -0.1% , the conic constant of Lens 4b is $\pm 0.1\%$, Lens 5a is 0.05% , Lens 5b is -0.05% , wedge about X-axis of Lens 3 is 0.01 deg, about X-axis of Lens 7 and about Y-axis of Lens 2, 7 is ± 0.05 deg, wedge about X-axis of Lens 1, 6, about Y-axis of LGS Dichroic and Lens 6 is ± 0.003 deg, the index of refraction of Lens 2, 4 and 5 is ± 0.0005 . The estimated change in the criterion is 3.088 wave.

| Worst Offenders: | | | | | |
|-------------------------|----------------|--------------|------------------|---------------|--|
| Type | Element | Value | Criterion | Change | |
| TRAD | Lens 5a | -0.129 | 0.506 | 0.478 | |
| TRAD | Lens 5b | 0.094 | 0.462 | 0.432 | |
| TRAD | Lens 1a | 1.551 | 0.414 | 0.380 | |
| TRAD | Lens 1b | -1.581 | 0.409 | 0.374 | |
| TRAD | Lens 1a | -1.551 | 0.403 | 0.368 | |
| TRAD | Lens 1b | 1.581 | 0.397 | 0.361 | |
| TCON | Lens 5b | -0.0005 | 0.357 | 0.316 | |
| TRAD | Lens 5a | 0.129 | 0.351 | 0.309 | |
| TRAD | Lens 5b | -0.094 | 0.321 | 0.275 | |
| TCON | Lens 5a | 0.0006 | 0.265 | 0.207 | |
| TRAD | Lens 3a | -1.795 | 0.245 | 0.181 | |
| TIND | Lens 3a | -0.0005 | 0.239 | 0.173 | |
| TRAD | Lens 6b | -0.372 | 0.237 | 0.170 | |
| TRAD | Lens 3a | 1.795 | 0.234 | 0.166 | |
| TIND | Lens 3a | 0.0005 | 0.228 | 0.157 | |
| TUTY | Lens 5 | 0.003 | 0.228 | 0.157 | |
| TUTY | Lens 5 | -0.003 | 0.227 | 0.155 | |
| TIND | Lens 7 | -0.0005 | 0.216 | 0.139 | |
| TUTX | Lens 5 | 0.003 | 0.214 | 0.137 | |
| TUTX | Lens 5 | -0.003 | 0.213 | 0.135 | |

Table A.8: The first twenty Worst Offenders after tightening some tolerances: the tolerance values of curvature radius of Lens 4b is 0.1 %, Lens 7b is $\pm 0.1\%$, the conic constant of Lens 4b is $\pm 0.05\%$, wedge about X-axis of Lens 7, about Y-axis of Lens 1, 2 and 7 is ± 0.003 deg. The estimated change in the criterion is 0.937 wave.

| Worst Offenders: | | | | | |
|-------------------------|----------------|--------------|------------------|---------------|--|
| Type | Element | Value | Criterion | Change | |
| TRAD | Lens 5a | -0.129 | 0.506 | 0.478 | |
| TRAD | Lens 5b | 0.094 | 0.462 | 0.432 | |
| TRAD | Lens 1a | 1.551 | 0.414 | 0.380 | |
| TRAD | Lens 1b | -1.581 | 0.409 | 0.374 | |
| TRAD | Lens 1a | -1.551 | 0.403 | 0.368 | |
| TRAD | Lens 1b | 1.581 | 0.397 | 0.361 | |
| TCON | Lens 5b | -0.0005 | 0.357 | 0.317 | |
| TRAD | Lens 5a | 0.129 | 0.351 | 0.309 | |
| TRAD | Lens 5b | -0.094 | 0.321 | 0.275 | |
| TCON | Lens 5a | 0.0006 | 0.265 | 0.207 | |
| TRAD | Lens 3a | -1.795 | 0.245 | 0.181 | |
| TIND | Lens 3 | -0.0005 | 0.239 | 0.173 | |
| TRAD | Lens 6b | -0.372 | 0.237 | 0.170 | |
| TRAD | Lens 3a | 1.795 | 0.234 | 0.166 | |
| TIND | Lens 3 | 0.0005 | 0.228 | 0.157 | |
| TUTY | Lens 5 | 0.003 | 0.228 | 0.157 | |
| TUTY | Lens 5 | -0.003 | 0.227 | 0.155 | |
| TIND | Lens 7a | -0.0005 | 0.216 | 0.139 | |
| TUTX | Lens 5 | 0.003 | 0.214 | 0.137 | |
| TUTX | Lens 5 | -0.003 | 0.213 | 0.135 | |

Table A.9: The first twenty Worst Offenders after tightening some tolerances: the tolerance values of curvature radius of LGS-M1, Lens 4a is $\pm 0.15\%$, the conic constant of Lens 1a, 1b, 2b, 4a, 6a, 6b, 7a, 7b is $\pm 0.15\%$, of Lens 3a is 0.15% , center thickness of 1a, 7a is ± 0.1 , sag of LGS-M2 is -1 fringe, wedge about X-axis and Y-axis of Lens 4 is ± 0.01 deg, about X-axis of Lens 2 and about Y-axis of Lens 3 is ± 0.003 deg. The estimated change in the criterion is 0.926 wave.

| Worst Offenders: | | | | | |
|-------------------------|----------------|--------------|------------------|---------------|--|
| Type | Element | Value | Criterion | Change | |
| TRAD | Lens 5a | -0.129 | 0.407 | 0.372 | |
| TRAD | Lens 5b | 0.094 | 0.355 | 0.315 | |
| TCON | Lens 5b | -0.0005 | 0.339 | 0.297 | |
| TCON | Lens 5a | 0.0006 | 0.257 | 0.197 | |
| TUTY | Lens 5 | 0.003 | 0.227 | 0.157 | |
| TUTY | Lens 5 | -0.003 | 0.226 | 0.155 | |
| TUTX | Lens 5 | 0.003 | 0.206 | 0.124 | |
| TUTX | Lens 5 | -0.003 | 0.206 | 0.124 | |
| TRAD | Lens 6b | -0.372 | 0.204 | 0.120 | |
| TRAD | Lens 5a | 0.129 | 0.203 | 0.119 | |
| TRAD | Lens 1a | -1.551 | 0.197 | 0.108 | |
| TRAD | Lens 1 | 1.581 | 0.195 | 0.106 | |
| TUTX | Lens 1 | 0.003 | 0.182 | 0.079 | |
| TUTX | Lens 1 | -0.003 | 0.181 | 0.077 | |
| TRAD | Lens 4b | -0.922 | 0.179 | 0.072 | |
| TRAD | Lens 1a | 1.551 | 0.176 | 0.063 | |
| TRAD | Lens 1b | -1.581 | 0.175 | 0.059 | |
| TUTY | Lens 6 | 0.003 | 0.173 | 0.053 | |
| TIND | Lens 6 | 0.0005 | 0.173 | 0.052 | |
| TUTY | Lens 6 | -0.003 | 0.172 | 0.051 | |

Table A.10: The first twenty Worst Offenders after adding the following compensators: the tolerance on the distance from Lens 3 and LGS-M1 and from LGS-M1 and Lens 4 is of ± 20 , while the tilt about X-axis of Lens 3 is ± 0.005 deg. The estimated change in the criterion is 0.546 wave.

| Worst Offenders: | | | | | |
|-------------------------|----------------|--------------|------------------|---------------|--|
| Type | Element | Value | Criterion | Change | |
| TRAD | Lens5a | -0.129 | 0.240 | 0.208 | |
| TUTY | Lens5 | 0.003 | 0.196 | 0.154 | |
| TRAD | Lens5b | 0.094 | 0.195 | 0.154 | |
| TUTY | Lens5 | -0.003 | 0.195 | 0.153 | |
| TCON | Lens5b | -0.0004 | 0.187 | 0.143 | |
| TUTX | Lens5 | -0.003 | 0.171 | 0.121 | |
| TUTX | Lens5 | 0.003 | 0.169 | 0.119 | |
| TRAD | Lens1a | 1.551 | 0.151 | 0.092 | |
| TRAD | Lens1b | -1.581 | 0.15 | 0.089 | |
| TCON | Lens5a | 0.001 | 0.145 | 0.081 | |
| TUTX | Lens1 | -0.003 | 0.143 | 0.078 | |
| TUTX | Lens1 | 0.003 | 0.143 | 0.078 | |
| TRAD | Lens1a | -1.551 | 0.141 | 0.074 | |
| TRAD | Lens1b | 1.582 | 0.14 | 0.071 | |
| TUTY | Lens6 | 0.003 | 0.131 | 0.052 | |
| TUTY | Lens6 | -0.003 | 0.131 | 0.051 | |
| TCON | Lens5b | 0.0004 | 0.128 | 0.044 | |
| TUTY | Lens1 | -0.003 | 0.127 | 0.0419 | |
| TCON | Lens3a | 0.005 | 0.127 | 0.042 | |
| TUTY | Lens1 | 0.003 | 0.126 | 0.0393 | |

Table A.11: The first twenty Worst Offenders after adding the following compensators: the tolerance on the distance from Lens 4 and LGS-M2 is of ± 20 , while the tilt about X-axis of LGS-M1 is ± 0.005 deg. The estimated change in the criterion is 0.341 wave.

Acknowledgements

I would like to thank Bruno Marano to have introduced me to the MAORY team and to have supervised my dissertation, Emiliano Diolaiti for the possibility he gave me to be part of the MAORY team and for having devoted his time to teach me Zemax. I would like to thank from the bottom of my heart Matteo Lombini for supporting me throughout the preparation of my dissertation and Mauro Patti who transmitted to me his knowledge about tolerancing. Last but not least, I would like to thank my family and love who, even though they worked constantly behind the scenes, they have been essential to reach my master thesis.

List of Figures

| | | |
|-----|---|----|
| 1.1 | Astronomical seeing: image formation by a telescope in a turbulent atmosphere. (a) In a short exposure, WF distortions caused by variations in refractive index in the atmosphere produce interfering Airy patterns. In (b) turbulent motion in the atmosphere during a long exposure moves the individual maxima around the image plane to produce a large seeing disk. | 2 |
| 1.2 | A C_n^2 profile shows the amount of air turbulences over height above the ground telescope in Mt. Graham. The strongest turbulences are close to the ground. (Figure by E. Masciadri, INAF) | 3 |
| 1.3 | 20×20 arcseconds region nearby the centre of the globular cluster Omega Centauri. The image on the left was obtained in K-band by ISAAC and has an average FWHM of 0.6 arcseconds. The right-hand image was obtained at the same wavelength by MAD with MCAO correction. In the latter case the FWHM is often below 0.1 arcsecond, a remarkable value taking into account that the closest GS is $\simeq 1$ arcmin away. | 4 |
| 1.4 | A schematic of a practical AO system. | 5 |
| 1.5 | Anisoplanatism effect leading to a degradation of the correction. . . | 6 |
| 1.6 | Contactless DM. | 9 |
| 1.7 | The Shack Hartmann sensor. | 11 |
| 1.8 | The principle of MCAO. Several WFSs and DMs are combined in order to optimize the adaptive correction in a larger FoV. | 13 |
| 2.1 | The typical magnitudes of GSs and their distances from the object as restricted by anisoplanatism for various photometric bands. The labeled curves show the probability to find a suitable GS at medium Galactic latitude, while dashed line at Galactic pole. | 17 |
| 2.2 | The operating principle of the LGS. | 18 |
| 2.3 | TT indetermination. | 19 |
| 2.4 | (a) Cone effect, (b) MCAO with LGSs | 20 |
| 2.5 | The launching angle. | 21 |

| | | |
|------|---|----|
| 2.6 | The description of the LGS parallactic effect on the off-axis sub-apertures of a SHWS, the red circle indicates a telescope with side launch of the LGS. | 22 |
| 2.7 | Parallactic effect: a sub-aperture with a given FoV at a distance r from the laser launcher and centered at H_m , sees the LGS inside two edge heights H_{min} and H_{max} that are at different distances from H_m | 23 |
| 2.8 | Sodium layer profile in function of time. (Paul Hickson, Department of Physics and Astronomy, University of British Columbia.) | 24 |
| 3.1 | Diagram (a) shows rays through the center of curvature and vertex V. Diagram (b) locates points P, V, and B in the plane of the aperture when looking down the optical axis. In this diagram, the distance b is related to the angle θ ($b = R\sin\theta$), that is, it measures how far the source is from the axis. The circular coordinates ϕ and ρ locate the intersection of the test ray and the aperture. | 26 |
| 3.2 | Third-order monochromatic aberrations. | 26 |
| 3.3 | A simple converging lens with undercorrected SA. The rays farther from the axis are brought to a focus nearer the lens. | 27 |
| 3.4 | In the presence of coma, the rays through the outer portions of the lens focus at a different height than the rays through the center of the lens. | 28 |
| 3.5 | Astigmatism: tangential and sagittal image. | 29 |
| 3.6 | (a) Pincushion distortion of an object that has a square outline centered on the optical axis. (b) Barrel distortion of the same object. The sides of the image are curved because the amount of distortion varies as the cube of the distance from the axis. Thus, in the case of a square, the corners are distorted $2\sqrt{2}$ as much as the center of the sides. | 30 |
| 3.7 | Qualitative appearance of images of a point source in optical systems with a single aberration present. In the diagram, "focus" means the best compromise on-axis focus, which may differ from the Gaussian focus. | 31 |
| 3.8 | Two dimensional plots of Zernike polynomials. | 33 |
| 3.9 | Double-index Zernike polynomial describing optical aberrations up to the sixth order coefficients. | 34 |
| 3.10 | Representation of the RMS WFE. | 38 |
| 3.11 | Sagitta. | 40 |
| 3.12 | The tolerance guidelines for prototype optics. | 41 |
| 4.1 | Nasmyth configuration of E-ELT. | 44 |

| | | |
|------|---|----|
| 4.2 | The Strehl ratio value as a function of the off-axis for two different seeing values. Data are shown for different wavelength. | 45 |
| 4.3 | MAORY post-focal relay optical design. Red rays: optical beam from telescope focal plane to exit port for MICADO, for scientific purpose. The orange circles are the projection of the design volumes for the LGS WFS and for MICADO. | 47 |
| 4.4 | A schematic view of a LGS launched in the Sodium layer at different zenith angle, that is, at different distances from the telescope primary mirror. The minimum distance is 80 km, the maximum allowable one is 240 km. | 48 |
| 4.5 | The roto-traslational motion of the LGSs launched in the Sodium layer: ξ is the zenith angle and the z-axis represents the altitude. | 48 |
| 4.6 | LGS WFS baseline current design. | 50 |
| 5.1 | The optical design of the LGS Objective. Table 5.2 describes the specifics of each elements. | 54 |
| 5.2 | The RMS WFE vs. Field after the LGS Dichroic for Configuration 1. | 58 |
| 5.3 | The RMS WFE vs. Field after the LGS Dichroic for Configuration 2. | 59 |
| 5.4 | The RMS WFE vs. Field after the LGS Dichroic for Configuration 3. | 60 |
| 5.5 | The RMS WFE vs. Field in the focal plane of Configuration 1. | 63 |
| 5.6 | The RMS WFE vs. Field in the focal plane of Configuration 2. | 64 |
| 5.7 | The RMS WFE vs. Field in the focal plane of Configuration 3. | 65 |
| 5.8 | Distortion at the focal plane of the LGS Objective for Configuration 1 (80 km or zenith angle of 0°) and Field 1 ((0,0)deg). The scale is 100x for a better visualisation. | 68 |
| 5.9 | Distortion at the focal plane of the LGS Objective for Configuration 2 (160 km or zenith angle of 60°) and Field 1 ((0,0)deg). The scale is 100x for a better visualisation. | 69 |
| 5.10 | Distortion at the focal plane of the LGS Objective for Configuration 3 (240 km or zenith angle of 70°) and Field 1 ((0,0)deg). The scale is 100x for a better visualisation. | 70 |
| 6.1 | The nominal WFE in function of the zenith angle is measured in the LGS Objective focal plane. The TT and defocus are removed. The colors correspond to the six LGSs placed over a radius of $45''$ FoV. | 77 |
| 6.2 | The nominal WFE of one LGS in function of the zenith angle is measured in the LGS Objective focal plane. Only $Z > 4$ has been considered. | 78 |
| 6.3 | Image displacement respect to the mean position at the Objective image plane in function of the zenith angle. The colors correspond to the six LGSs placed over a radius of $45''$ FoV. | 79 |

| | | |
|-----|---|----|
| 6.4 | Left: Residual WFE at the LGS Objective image plane as a function of the zenith angle. Montecarlo trials for manufacturing errors of the optics. The TT and defocus are removed. Right: Median values of the left plot, different colors correspond to the six LGSs disposed simmetrically over a radius of 45'' FoV. | 81 |
| 6.5 | Left: The residual WFE plus the nominal WFE in function of the zenith angle is measured on the LGS Objective focal plane. The TT and defocus are removed. Right: Median values of the left plot, the colors corresponds to the six LGSs placed over a radius of 45'' FoV. | 82 |

Bibliography

- [1] Frederick R. Chromey, "To Measure the Sky. An introduction to Observational Astronomy", (2011) Cambridge University Press
- [2] John W. Hardy, "Adaptive Optics for Astronomical Telescopes", (1998) Oxford University Press
- [3] Marchetti E. et al, "On-sky Testing of the Multi-Conjugate Adaptive Optics Demonstrator", (2007) The Messenger 129
- [4] R. Biasi,a, D. Gallieni, (Microgate and A.D.S. International), "Contactless large deformable mirrors: ELT AO corrector technology available now"
- [5] R. Biasi et all, "E-ELT M4 adaptive unit final design and construction: a progress report"
- [6] S. Thomas et al, "Comparison of centroid computation algorithms in a Shack-Hartmann sensor"(2006) Astron. Soc. 371, 323336
- [7] J. E. Greivenkamp, "Field Guide to Geometrical Optics", (2004) SPIE Press, Bellingham, WA.
- [8] Matteo Lombini, "Laser Guide Star Wavefront Sensors for the E-ELT", (2011) PhD Thesys
- [9] M. Patti, "Integration of a prototype of wavefront sensor for laser guide stars", (2014) Master Thesys
- [10] Daniel Malacara, Manuel Servn, Zacarias Malacara, "Interferogram Analysis for Optical Testing", (2005) Taylor & Francis Group
- [11] Warren J. Smith, "Modern Optical Engineering, The Design of Optical Systems", (2000) McGraw-Hill
- [12] Haiyin Sun, "Lens Design: A Practical Guide", (2016) CRC Press

- [13] M. Dekker, "Encyclopedia of Optical Engineering", (2003) New York
- [14] Haiyin Sun, "Lens Design: A Practical Guide", (2016) CRC Press
- [15] Hongzhang Ma, "Tolerancing optical systems", (2013) Opti 521
- [16] Ramsay, Suzanne, "ESO-254311-1 MAORY (E-ELT MCAO) Technical Specification", Confidential Document
- [17] E. Diolaiti, "E-MAO-000-INA-RER-001", (2016) Review Report
- [18] Patrick Rabou, "E-MAO-IL0-IPA-DER-001-01D9 LGS WFS Probes Design and Analysis Report", (2017) Review Report
- [19] ZEMAX Development Corporation, "Optical Design Program. User's Manual", (2010)

Sitography

[20] www.eso.org

[21] www.maory.oabo.inaf.it